Design of a Freeze Plug for the Molten Salt Fast Reactor(MSFR)

Parth Swaroop

Master Thesis Report [1]

in partial fulfillment of the requirements for the degree of

Master of Science
in Sustainable Energy Technology

at the Delft University of Technology,
to be defended publicly on Wednesday 31st August, 2016 at 10:00 AM.

Student number:	4412826
Supervisor:	Dr. ir. M. Rohde
Thesis committee:	Dr. ir. M. Rohde
	Prof. Dr. ir. Jan Leen Kloosterman
	Prof. Dr. ir. C. R. Kleijn

[1] An electronic version of this thesis is available at http://repository.tudelft.nl/.

ABSTRACT

In this report the design of a freeze plug, which is one of the safety component in generation IV Molten Salt Fast Reactor (MSFR), is studied. The freeze plug is placed in between the reactor core and the drain tank inside a pipe. From the experience of Fukushima-Daiichi nuclear power plant disaster, an additional safety criteria has been put forth. It is required to remove the decay heat from the reactor core, passively i.e without mechanical or electrical assistance. In the old MSRE design [45], the freeze plug was melted by electrical heaters i.e non passively. The inputs for the current freeze plug design calculations are velocity and temperature profile inside the core along with the response time of the system. The velocity and the temperature profiles are adopted from [33] while the response time for the system is obtained from [12]. The rest of the engineering aspects of the freeze plug with respect to the current MSR design is unknown. These aspects include 1) Sizing the freeze plug system (length, diameter and depth), and 2) Selecting a suitable material for the freeze plug. The physics of the melting process is modelled using a deformed geometry method in COMSOL. The different aspects of models which were implemented are verified using the analytical solution of Stefan problem [38], numerical simulations from [10, 39] and from the experimental results of [25]. This is followed by the results pertaining to the unknown parameters of the design. Based on the current mathematical model, it was concluded that the current concept could not satisfy the required response time of 600 seconds.

ACKNOWLEDGEMENT

Firstly, I would like to thank Dr. ir M. Rohde and Prof.Dr.ir.Jan Leen Kloosterman for giving me the opportunity to work on this project. I enjoyed working on it with you. Secondly, I would like to thank Comsol for their support. I also highly appreciate the efforts of Matteo Gamarino and Marco Tiberga, PhD students of the group, for giving me an elaborate feedback on my report. Lastly, I would like to thank the research group for making my time very memorable.

CONTENTS

List of Figures vii

List of Tables viii

1 INTRODUCTION 1
1.1 Overview of MSR . . . 1
1.2 History of Freeze Plug Design . . . 2
1.3 Current Design . . . 4
1.3.1 EVOL configuration . . . 4
1.4 Failure scenarios . . . 6
1.4.1 Power Outage . . . 6
1.4.2 Heat exchanger failure . . . 7
1.4.3 Pump Failure . . . 7
1.5 Research Questions . . . 8
1.6 Outline . . . 8

2 MELTING BY CONDUCTION 10
2.1 Mathematical Formulation: . . . 11
2.1.1 Analytical Solution . . . 12
2.2 Mesh selection . . . 14
2.3 Results . . . 14

3 MELTING BY LID DRIVEN CAVITY 17
3.1 Lid Driven Cavity . . . 18
3.1.1 Isothermal Lid Driven Cavity . . . 18
3.1.2 Lid driven cavity with stratification . . . 19
3.2 Guidelines for Material Selection . . . 21

4 TURBULENCE MODELLING 26
4.1 2D approximation: . . . 27
4.2 Selection of turbulence model . . . 28
4.3 Algebraic yPlus Model . . . 30
4.4 Boundary conditions . . . 32
4.5 Cases . . . 33
4.6 Mesh Selection: . . . 34

5 RESULTS 35
5.1 Verification of Turbulence Model . . . 35
5.1.1 Velocity profile . . . 35
5.1.2 Qualitative Comparison with Experiment . . . 37
5.2 Results for Melting . . . 39
5.2.1 Effect of Temperature Rise . . . 39
5.2.2 Effect of Geometry . . . 42

5.2.3 Steady State 47
5.2.4 Effect of Temperature Distribution 50

6 CONCLUSION AND RECOMMENDATION 54
6.1 Recommendation 55

A APPENDIX: 57
A.1 Material Properties 57
A.2 Wall functions 57
A.2.1 Law of the Wall 58
A.2.2 Thermal Wall Functions: 59
A.3 Implementation in Comsol 60
A.3.1 Selection of Method 61
A.3.2 ALE Method 62
A.3.3 Weak Form 63
A.3.4 Parameter Study 65
A.3.5 Solver Settings 65

LIST OF FIGURES

Figure 1 A schematic representation of typical MSR design (Generation IV Forum in 2002)[4]. 2
Figure 2 In figure (2), A final configuration of one of freeze valve component which connected the reactor core and drain pipe in MSR design of ORNL is shown [45]. 3
Figure 3 In figure (3), a schematic layout of experimental setup with one of the heater configuration is shown. [44]. 3
Figure 4 The melting time of freeze plug is plotted against power inputs for different type of heater configuration (4a). The heat transfer coefficient (h) measured as function of air flow, for cooling the freeze plug, is plotted in (4b). Experimental results from [44] 4
Figure 5 2D geometry of the reference EVOL MSFR congifuration. In fig (5a), a simplified scale vertical scheme of reactor core system included the heat exchangers are shown. Figure (5b) 5
Figure 6 In figure (6a), the simulation results of the average velocity profile of flow field is shown. In figure(6b), a simplified layout of the freeze plug represented where D, is the depth of location of plug, W is the width, L is the length along-with the control volume represented by the dotted line 5
Figure 7 Figure (7a) represents an increase in the average temperature of the fuel at the inlet and outlet of the reactor due to the decay heat. In figure (7b), the mean velocity profile of the salt after 130s of pump failure. [33] 6
Figure 8 Figure (8) represents the total fission power profile and average temperature as function of time during a heat exchanger failure scenario. [33] 7
Figure 9 Figure 9 represents the total fission power profile and average temperature as function of time during a pump failure scenario. [33] . . 8
Figure 10 A Work flow diagram of this thesis work 9
Figure 11 2-D layout of the freeze plug; D, is the depth of location of plug, B is the width, L is the length 10
Figure 12 Analytical Model: Melting due to conduction with constant temperature at y=0 and $t > 0$. 12
Figure 13 Distribution of quadrilateral mesh for cavity and freeze plug. 14
Figure 14 Time snapshot of temperature distribution over the distance y, for COMSOL simulation. 15
Figure 15 Comparison of simulation result between COMSOL and analytical. 15
Figure 16 Simplified layout of Lid Driven Cavity with some characteristic features. 17
Figure 17 A simplified layout of the Lid Driven Cavity with stratification. Adopted from [25] 19

Figure 18 In figure(18a) normalized average depth as function of Ri for fixed Re vs non-dimensionalised time is plotted. In figure(18b) Log-Log plot of Entrainment rate E vs Ri for flows with Re= 10,000 is plotted. Results of [25] 20
Figure 19 Energy content of various material, suitable for freeze plug, versus melting temperature 23
Figure 20 Figure (20a) represents the cooling curves of different types of compounds. Here A to B represent liquid state, B to C represent phase change and C to D represent solid. Adopted from [46]. Figure (20b) represents the equilibrium phase diagram of LiF- CsCl with eutectic point at (626 °C). Adopted from[35] 24
Figure 21 Span-wise streamlines of cubical lid driven cavity. Adopted from [27] 28
Figure 22 Quadrilateral mesh , Default, Mixed (respectively) 34
Figure 23 Comparison of normalised averaged velocity profiles for Reynolds Number =10,000 of algebraic yplus turbulence model with literature results of [10] and SST and SA model of [39] 36
Figure 24 Development of Flow : Figures (24a , 24c & 24e) represents Comsol simulation for the following parameters: Re = 40,000 D= 0.3m, B =0.3m $\Delta T = 32K$ Ri =0.64, Figures (24b, 24d & 24f) represent the experiment results performed by [25] for the following parameters: Re = 10,000 D= 0.15m, B =0.15m $\Delta T = T_{hot} - T_{cold} = 9°C$ Ri =0.53 38
Figure 25 Figures (25a & 25b), shows temperature profile at the interface, and time averaged velocity profile in the cavity, similar to figure(23), for quadrilateral and triangular meshes respectively at time t =0 for melting simulation. Parameter Setting : Re =60,000 , Ri = 0.085, D=B= 0.2m 40
Figure 26 Time snapshots of the melting due to temperature increase at the moving wall. Parameter Setting : Re =60,000 , Ri = 0.085, D=B= 0.2m 41
Figure 27 The above graph shows the heat flux values at the interface for time t= 20s, 50s and 100s as f(x) for quadrilateral and triangular meshes. 42
Figure 28 In figure(28a), heat flux is evaluated for Mesh B and Mesh C at time t= 0. In figure(28b), heat flux is time averaged at each on the node at the interface for Mesh B and Mesh C. Parameter Setting : Re =40,000 , Ri = 0.19, D=B= 0.2m 43
Figure 29 Development of melting: time snapshot at t=100s and t=600s for square cavity A=1 D=B=0.2m. Note the change in scale for temperature labels for cavity and freeze plug. 44
Figure 30 Comparison of time averaged heat flux (total heat flux in figure(30a) and heat flux from the freeze plug figure(30b)) with respect to respective heat flux at time t=0. 44
Figure 31 Root-Cause Analysis performed to determine the cause of spikes in the heat flux values. 45
Figure 32 Initial condition inside the cavity for melting considering different dimensions. This correspond to time t= 2000s for step 1. 49
Figure 33 In fig(33a & 33b), the initial condition of temperature distribution is cavity and freeze plug and the velocity profile in cavity is shown. 51

Figure 34 In fig(34a & 34b), the temperature distribution inside the cavity and the freeze plug and the velocity profile in cavity is shown along-with the melted freeze plug at t= 600s. Note the change in scale for temperature labels for cavity and freeze plug. 51
Figure 35 The above graph shows the time averaged heat flux values as a function of non dimensional distance 'x/B' for the two different temperature distribution cases considered. 52
Figure 36 Temperature response based expansion valve. Adopted from [49] . 56
Figure 37 Wall function approximation of turbulence models using analytical expression developed for turbulence over flat plate. Adopted from [6] 58
Figure 38 Computational domain joining wall and the logarithmic layer at distance δ_w 59

LIST OF TABLES

Table 1 Thermal properties of CsCl and LiF – ThF_4 25
Table 2 Turbulence model available in COMSOL 29
Table 3 Properties of Material within temperature range of 600-700 °C . . . 57

1 INTRODUCTION

In 2011, the Fukushima-Daiichi nuclear power plant suffered from the natural disaster of the Great East Japan Earthquake, subsequently followed by a 15-metre high tsunami. Although the reactors were designed to be protected against emergency situations, based on previous scientific data available [23], the natural disaster still managed to inflict a significant damage to the power plant.

After the earthquake, due to the loss of external power source, the reactors units were shutdown. Despite shutdown, the reactor cores were still be producing about a few percent of their nominal thermal power, from fission products decay [55]. The external cooling circuit, which includes the cooling pumps and the heat exchanger, dumped the reactor heat into the sea. This system was running on back-up generators to remove the residual heat from the core during the external power loss. Earthquake was followed by tsunami, which eventually submerged the back-up power system, leading to the failure of the auxiliary cooling system. Ultimately, it isolated the reactor cores from their heat sink, causing the reactor core to melt.

This incident has been translated into an important safety requirement for the future nuclear reactor power plants. These power plants would have to incorporate a safety system which would be passive and effectively remove the decay heat during electrical/mechanical power system failure. The system evaluated in the generation IV Molten Salt Fast Reactor (MSFR) for this purpose, among other features, is a so-called freeze plug. This idea is partially carried forward from the old MSR configuration developed by ORNL in 1960s. A freeze plug was the choice of flow control valve because a proven and reliable mechanical valve suitable for the application was unavailable during that time [44]. It will be placed in the pipe which connects the reactor core and the emergency drain tanks. In the current intended design, the plug will melt due the temperature difference between the reactor core and the melting temperature of the material, consequently allowing the fuel to be drained in these tanks, in this emergency situation. This report studies the design of such a freeze plug for the Molten Salt Fast Reactor (MSFR).

1.1 OVERVIEW OF MSR

MSRs are referred to a class of nuclear fission reactors in which the fissile material is dissolved in the molten salt. This fuel is typically fissile material such as UF_4, PuF_3, minor actinides fluorides and/or fertile elements as ThF_4, depending on the desired application (breeder reactor, actinides burner, etc), dissolved in molten fluoride salt such as LiF or BeF_2 etc [18].

The physical properties of the salt also allow MSRs to run at high temperature which range from (700°C to 750°C) [12] and operate at near atmospheric pressure. MSRs have large negative temperature feedback coefficients. Temperature feedback is the change in the reactivity of the core with some perturbation in temperature. Since the reaction coefficient is negative it allows the reactor to be shut down due to expansion of the fuel salt when temperature increases beyond design limits. These salts are, also relatively inert substances

with no rapid reaction with air or water. Hence there is neither fire nor explosion hazard for this fuel.

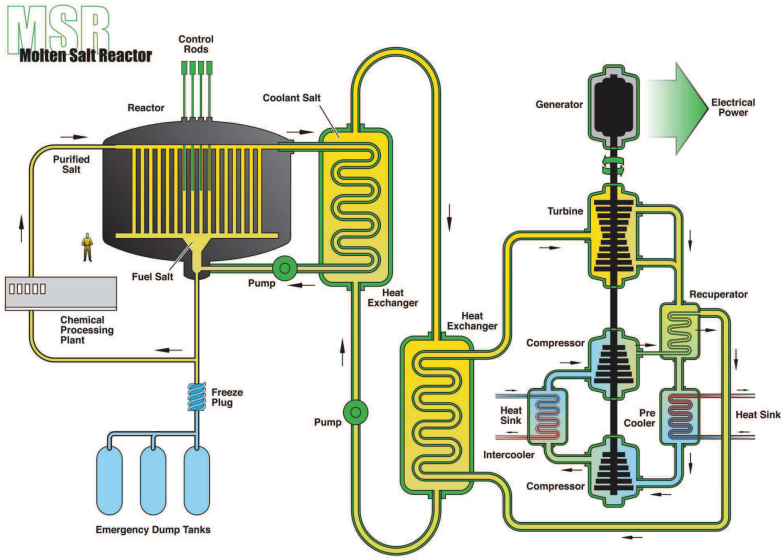

Figure 1: A schematic representation of typical MSR design (Generation IV Forum in 2002)[4].

In MSRs, fission reactions occur within the mixture of molten salt. This fuel can be transported between the reactor core and external heat exchangers with the help of a pump and piping system. The heat produced during the reaction is transferred to a secondary liquid-salt coolant from the primary molten salt. This configuration is depicted in figure(1). It also consists of a circuit which connects the core volume to the emergency drain tanks through a freeze plug. A freeze plug acts like a valve and is expected to be a compound of solid state of the fuel salt. In normal operating condition, the solid plug will be cooled with the help of external fan(s) (this is not shown in the figure). During the pump failure (or any other critical scenario in which reactor needs to be stopped), the solid plug begins to melt due the decay heat from the reactor core. After the complete melting of the solid salt, it is possible to drain the fuel salt through gravity. Hence, there are two functions that the freeze plug should satisfy:

1. It should prevent the flow of the fuel-salt mixture to the drain tank (i.e avoid leakage) in the normal operating condition

2. It has to allow fuel-salt mixture to be drained when required.

1.2 HISTORY OF FREEZE PLUG DESIGN

As mentioned before, evaluation of "freeze plug" as a valve was undertaken during development of MSR by ORNL. Their requirement was to use a flow control valve for draining, filling and processing systems. A flow control valve regulates the flow of fluid. The plug was melted directly or indirectly using external electrical heaters, thus non passively(This primary change now demands redesigning of the plug!) To freeze the plug, a stream of gas or air was passed through it. The concept was developed through extensive testing with arrangements of heaters and coolers to attain the require freezing and

thawing times. The concept was also tested for vertical and horizontal orientations.The section in between where salt was frozen, was a flattened section of the continuous pipe.

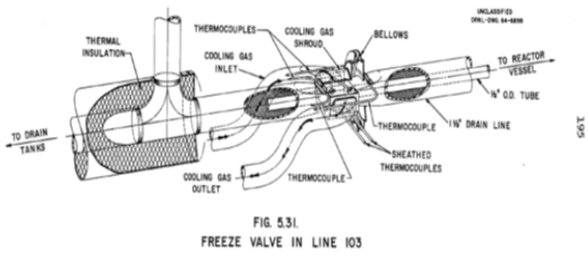

Figure 2: In figure (2), A final configuration of one of freeze valve component which connected the reactor core and drain pipe in MSR design of ORNL is shown [45].

Further, very long plug lengths were avoided in order achieve uniform heating and thawing in the center along with the edges of the plug. Extensive report of design of freeze valve is provided in [44] and [45]. The cooling design could be more understood with the figure below (fig 2). The cooling gas is allowed to flow across the freeze plug via a secondary piping line. The opening to the freeze plug for the air flow, can be visualized as rectangular shape on the side of the main pipe line.

In the experiment conducted in [44], the freeze valve undergoes constant freezing and thawing cycles. The material composition used for testing the valve is:

Wt % :

U: 5.45 Th : 6.21 Li : 9.74 Be : 4.61 Zr : 13.3 F : 60.69

The operation of experiment is simple. The experimental system comprised of containing two tanks (head tank and sump tank) placed at the bottom and at a height connected by pipe as shown in figure(3). The total volume of the system was 5.6 gal with volume of the sump and head tank amounting to 2.2 gal each.[1]. A pressure difference was maintained between the two tanks. Under various valve test conditions, the molten salt that was filled into the system, was maintained between temperatures 1100 °F to 1200 °F. Cooling gas flows perpendicular to this pipe over a fixed area to freeze the salt. The length of the plug used, was around 6 inches[2]. The melting temperature of the salt was measured to be between 800 °F to 850 °F [3]. The flow of air was lowered to maintain the plug at this temperature. Electric heaters are also placed within this area to melt the plug. By applying an electric power, the plug was melted. The melting time of different heaters used, is shown in figure(4a). But there was no clear definition of melting time.

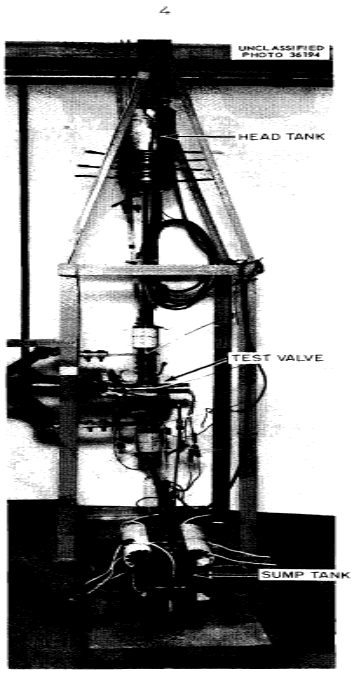

Figure 3: In figure (3), a schematic layout of experimental setup with one of the heater configuration is shown. [44].

[1] 1 US gallon = $3.785 \cdot 10^{-3}$
[2] 6 inch = 15.24 cm
[3] 800 °F = 425 °C

Since the heating element was wrapped around the plug, in this vertical set-up, it is thus possible that the melted salt begins to lose contact from the walls of pipe and falls down.

The coolant used during the experiment for freezing was room air. It was of interest to improve the heat transfer along the ends of the plug (concave design for the opening is shown in figure 2). From the experiment data, heat transfer coefficient h[4] is plotted for volumetric air flow. With a flow of cooling at 50-60 scfm [5] the time required to freeze the valve was 10 to 15 mins. The temperature difference between the molten salt and frozen salt was $\sim$ 400 °F . It required a very high heat transfer coefficient and high temperature difference to freeze the plug. A gas flow of 3 to 7 scfm is required to maintain the salt at 850 °F. Further, these cooling gas flow uniformly across the length of plug.

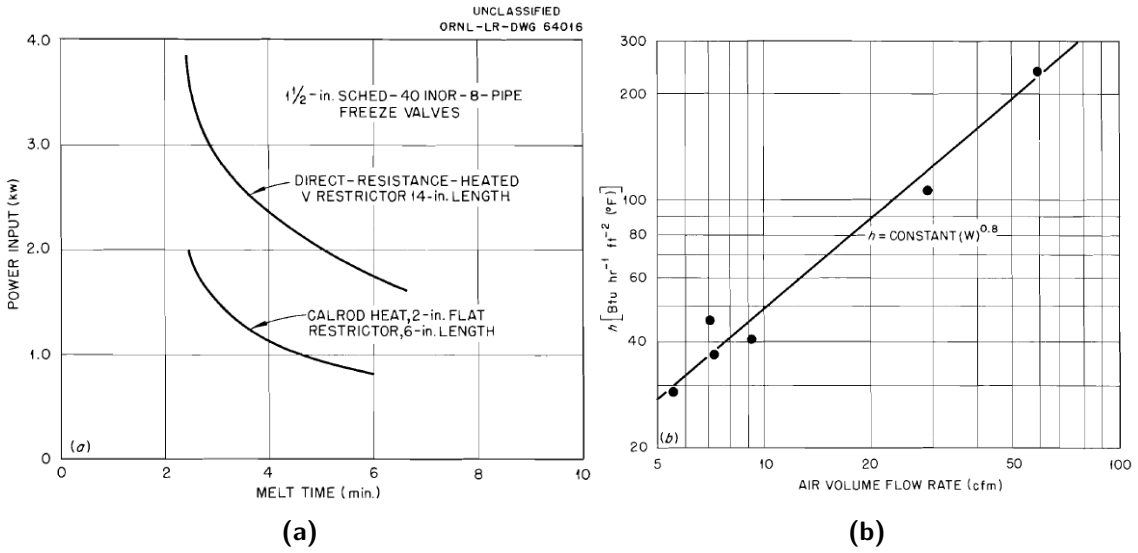

Figure 4: The melting time of freeze plug is plotted against power inputs for different type of heater configuration (4a). The heat transfer coefficient (h) measured as function of air flow, for cooling the freeze plug, is plotted in (4b). Experimental results from [44]

1.3 CURRENT DESIGN

1.3.1 EVOL configuration

The reactor configuration used for the present thesis is taken from [12]. It uses thorium, which is a fertile material, dissolved in molten salt LiF in 78% -22 % molar ratio ($LiF-ThF_4$. Thorium (^{232}Th) is converted into fissile uranium (^{233}U) using neutron in the fast thermal spectrum, thus the reactor is known as Molten Salt Fast Reactor (MSFR). The geometry consists of four distinct regions, fuel (yellow), fertile blanket (red) , neutron absorber(blue) and structural material. The volume of the fuel is evenly distributed in the yellow region shown in fig(5a), while the reactions occur in the core region. The fertile blanket also consists of thorium, in order to use up the neutrons which leaks from the core, thus improving neutron economy. The reflector protects the surrounding materials and components from the neutrons released during the fission events. The core is connected to the drain system via pipes below the reflector (not shown in the figure). In this current design, the placement of the freeze plug with respect to reactor geometry is still unknown.

[4] BTU $ft^{-}2$ h °F : A unit of heat transfer coefficient. 1 BTU $ft^{-}2$ h °F = 5.68 W/m^2K [15]
[5] scfm : standard cubic feet per min (volumetric flow). 1scfm = $4.72 \cdot 10^{-4} m^3/s$ [15]

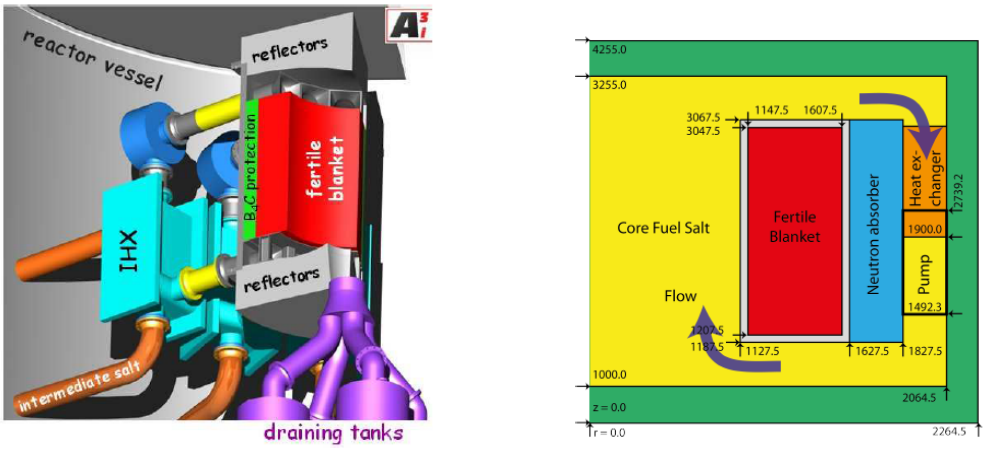

(a) Layout of the Reactor **(b)** Geometry used for the simulation

Figure 5: 2D geometry of the reference EVOL MSFR congifuration. In fig (5a), a simplified scale vertical scheme of reactor core system included the heat exchangers are shown. Figure (5b) represent the geometry considered for simulation due to symmetrical design.

Normal operating conditions represent the steady state of the reactor. The fuel salt which enters the core has a temperature of $T_{in} = 950$K while the fuel salt which flows out of the reactor towards the heat exchanger has a temperature $T_{out} = 1021K$. The temperature distribution and the velocity profile around the core region is determined by HEAT solver, described in [33], according to a RANS-model. The flow in the core is of turbulent regime. Thus, in fig (6a) time averaged velocity are plotted.

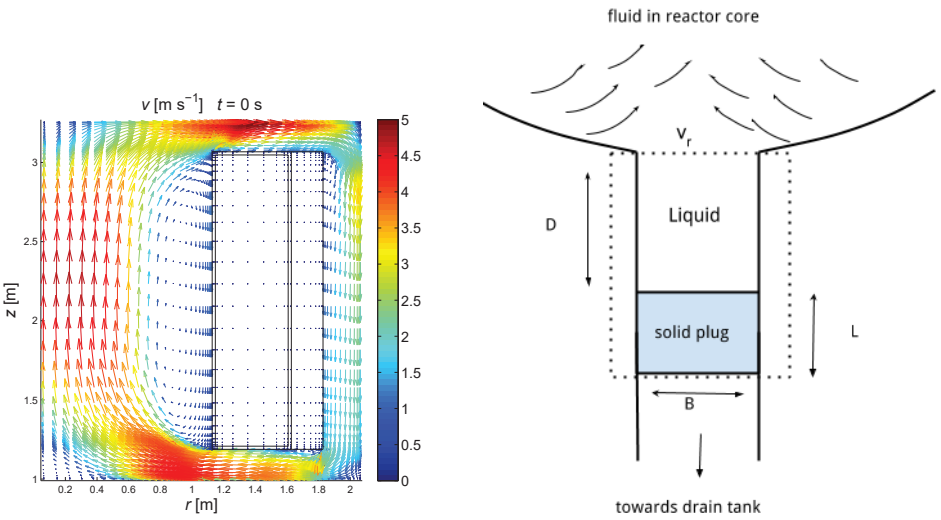

(a) Normal operating conditions **(b)** Simplified layout of the plug

Figure 6: In figure (6a), the simulation results of the average velocity profile of flow field is shown. In figure(6b), a simplified layout of the freeze plug represented where D, is the depth of location of plug, W is the width, L is the length along-with the control volume represented by the dotted line

1.4 FAILURE SCENARIOS

There are several accident scenarios that is considered while designing a nuclear reactor. For the freeze plug, these cases acts as an input for the required response time. The response time is time frame within which the plug should melt so as to mitigate this situation. Some of the possible cases which should be taken into account based on for safety scenarios according to [8, 56] are as follows:

1. Failure of Pump
2. Failure of Heat exchanger
3. Fuel salt leak accident
4. Power Outage

Out of these situations, cases(i and ii) are considered in [33] and case (iv) is considered in [12]

1.4.1 Power Outage

Power Outage is the scenario when no external electricity is available. Based on simulations in [12], it was predicted that decay heat will be initially 4.3% of the nominal power of the reactor. Since this decay heat is not removed, the reactor core temperature will increase with time which is shown in figure(7a). Although the salt boiling point is 2028 K, the damage to the reactor system occurs at an earlier temperature of 1473 K which indicates the melting temperature of steel. Hence a safety system is required to drain the fuel before this point is reached. Based on the results, the damage point is reached in approximately 11 minutes, while the boiling point is reached after 30 minutes. Within these 11 minutes, the freeze plug has to be melted with the available decay heat and all the molten salt has to be drained into the emergency drain tank. Since it does not rely on external electrical or mechanical source , the system is called passive Decay Heat Removal(DHR).

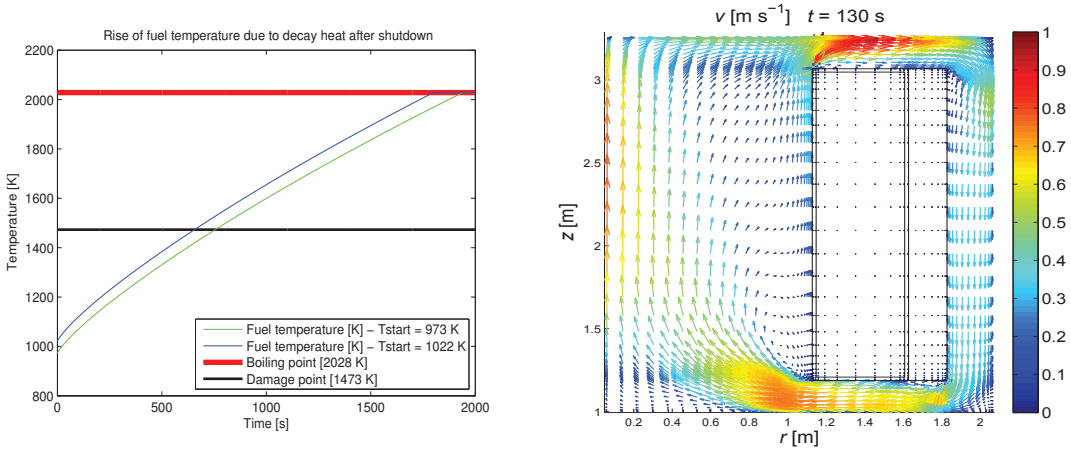

(a) Adopted from [12]

(b) Adopted from [33]

Figure 7: Figure (7a) represents an increase in the average temperature of the fuel at the inlet and outlet of the reactor due to the decay heat. In figure (7b), the mean velocity profile of the salt after 130s of pump failure. [33]

1.4.2 Heat exchanger failure

For the heat exchanger failure scenario, a heat sink for the power produced in the reactor no longer functions. Since the heat loss due to the walls are also not taken into account in [33], no heat can be extracted from the system. In this simulation, the decay heat produced was 0.3 % of the starting power (P(t=0) as shown in figure(8), which is much less than it was predicted in [12]. This was due to fact that delayed fission heat was not taken in account. As a result, the temperature increase due heat exchanger failure never reaches the damage point of the steel as experienced in power outage scenario. According to [33], at this lower power production, the internal feedback mechanism of change in the reaction coefficient and the Doppler effect are sufficient to mitigate the temperature increase in the reactor.

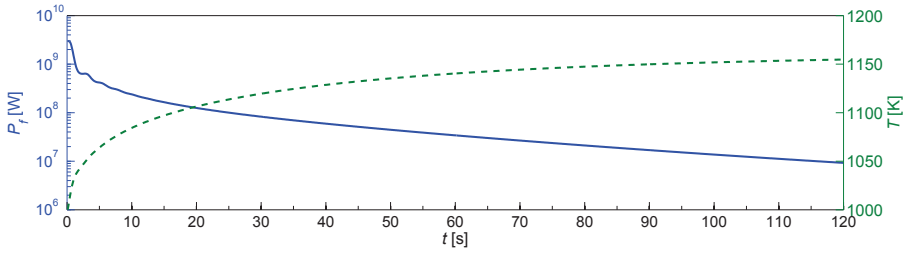

Figure 8: Figure (8) represents the total fission power profile and average temperature as function of time during a heat exchanger failure scenario. [33]

1.4.3 Pump Failure

In the pump failure scenario, the external driver (i.e. pump) for the fluid flow no longer functions. Due to the presence of fuel inside the reactor core, there are still fission events which produce heat. The heat removal rate of the heat exchanger was independent of the flow rate of fuel salt. It was modelled as:

$$S_{sink} = h_{HX}(T - T_{res})$$

where, S_{sink} is the heat sink term [W m^{-3}], $h_{HX} = 8.31 \cdot 10^5$ [W m^{-3} K^{-1}] is the heat transfer coefficient and $T_{res} = 773K$ is the temperature of the fluid in the secondary loop. Since, this heat transfer coefficient is constant, just after the pump failure, conditions are very similar with respect to the heat exchanger, such that it keeps extracting heat at the same rate. Initially the fluid flow is driven by inertia. After a certain point of time, new steady state is established where the fluid motion is driven by density difference. This gives a equilibrium velocity profiles after 130 secs of pump failure as shown in fig (7b). The average temperature increase in this situation is much lower than failure of heat exchanger which can be observed in figure (9).

Due to the assumption involved in the computations, it is difficult to gauge which serves as worst case scenario: failure of heat exchanger or power outage. Unfortunately, the failure of heat exchanger and the failure of pump was not modelled in [12]. This is very important since these simulations serve as initial conditions for modelling of freeze plug. Since in none of the other cases reaches the damage point, it will be assumed that the power outage serves as a worst case scenario.

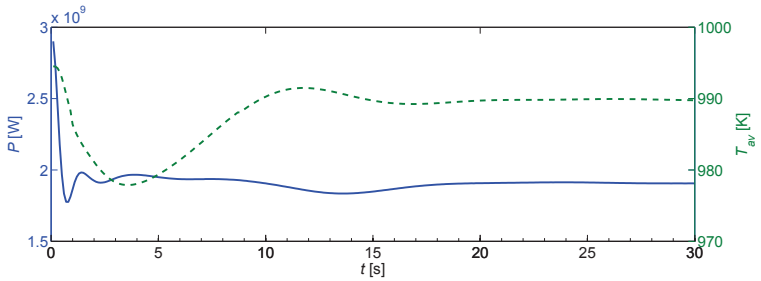

Figure 9: Figure 9 represents the total fission power profile and average temperature as function of time during a pump failure scenario. [33]

1.5 RESEARCH QUESTIONS

Based on the comparison of the old design of the freeze plug and with the new requirements of the plug, the functional requirements and operating conditions are found to be very different. The old design incorporates the melting of the plug due external heaters, whereas a new safety requirement implies this freeze plug should also have the capability to be melted solely from the decay heat. This will require a selection of salt material suitable for freeze plug, modeling of the heat transfer depicting melting of the plug and calculations of the geometric parameters. Further, during the normal operating conditions, it is required that the plug is maintained below T_m. This cooling requirements is not studied as a part of this thesis work.

The most fundamental question that this thesis will look to answer would be :

Is the concept of freeze plug melting based on decay heat, feasible?

Here, feasibility indicates the function freeze plug is expected to perform, i.e melt fast enough in an emergency situation. The aim of this thesis is to either establish a proof of concept or eliminate the iterations which will not be feasible based on this framework. Now, the functionality has to be now related to the unknown design parameters:

i What can be a framework for the selection of material suitable for freeze plug?

ii What is the influence of liquid layer in between the reactor and freeze plug?

iii What is the affect of the dimension of i.e width and depth, on the process of melting?

1.6 OUTLINE

This section is intended to provide with a brief outline which serves as a guideline to the reader on how the chapters are structured. The backbone of this thesis to establish a proof of concept for the freeze plug design. Since the proof of concept leads into iterative methodology, there will be results in certain chapters based on which conclusions will be drawn in the iteration performed. Flow chart in figure(10) provides a connection to all the aspects connected to this thesis work.

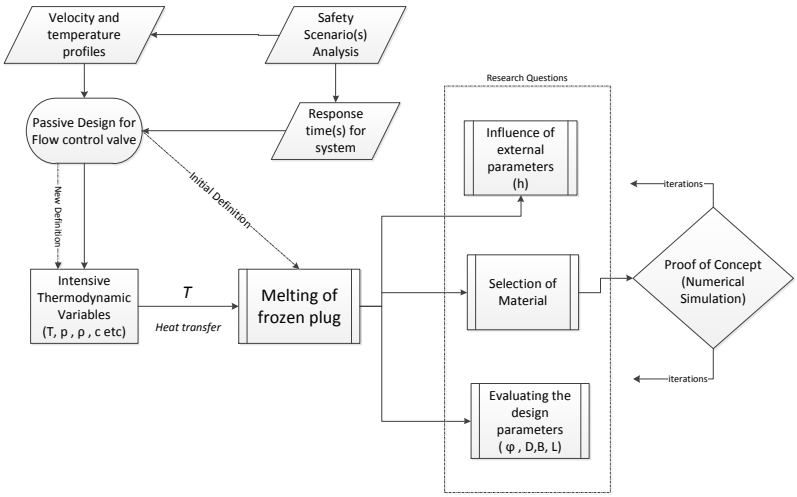

Figure 10: A Work flow diagram of this thesis work

Chapter 2 will introduce to the physics of the conduction based melting. This chapter serves two purpose: 1) It is a design iteration which serves as the worst case scenario to melt the freeze plug and 2) An analytic solution for melting is available in [38] which will help us evaluate comsol's implementation of the physics.

In order to improve on this worst-case scenario, Chapter 3 will put forth the theory of convection driven melting. This theory also provides us with a framework for the selection of the material, because the convective heat transfer is governed by certain non dimensional parameters. A part of this non dimensional parameters can be controlled by the selection of material. Thus, this chapter answers one of the sub questions : What can be a framework for the selection of material suitable for freeze plug? Hence, the answer to this question is dependent on the process in the liquid layer above.

In the convection driven heat transfer, the flow regime is in the turbulence region. Chapter 4 will look into turbulence models which would be most suitable to the modelling of melting due the convective heat flux in COMSOL. It will also incorporate the cases introduced as a parametric study to elaborate on the sub-question (iii).

Finally, Chapter 5 will first provide results pertaining to the theory of Chapter 3. The selected turbulence model will be compared with literature results of [10, 39] and experimental results of [27]. Then the results related to the cases introduced in Chapter [4] will be explained.

In the Appendix, section A.3 will provide an introduction to the modelling of melting in COMSOL. This section will answer the questions : (i) What is the best approach to model the physics of melting related to the material selected in Chapter 3? and (ii) What are the parameters in COMSOL that affects this model? In the main content, only the meshing used for different cases considered for different simulation will be introduced when required.

2 MELTING BY CONDUCTION

This chapter will establish the physics of the melting due to conduction. Since the placement of the pipe which connects the drain tank and reactor core is also not fixed, it is first assumed that it will be placed in the middle. When this is assumed, the melting of the freeze plug is purely driven by conduction. As it will be shown in the results at the end of the chapter, this serves as a worst case condition for melting.

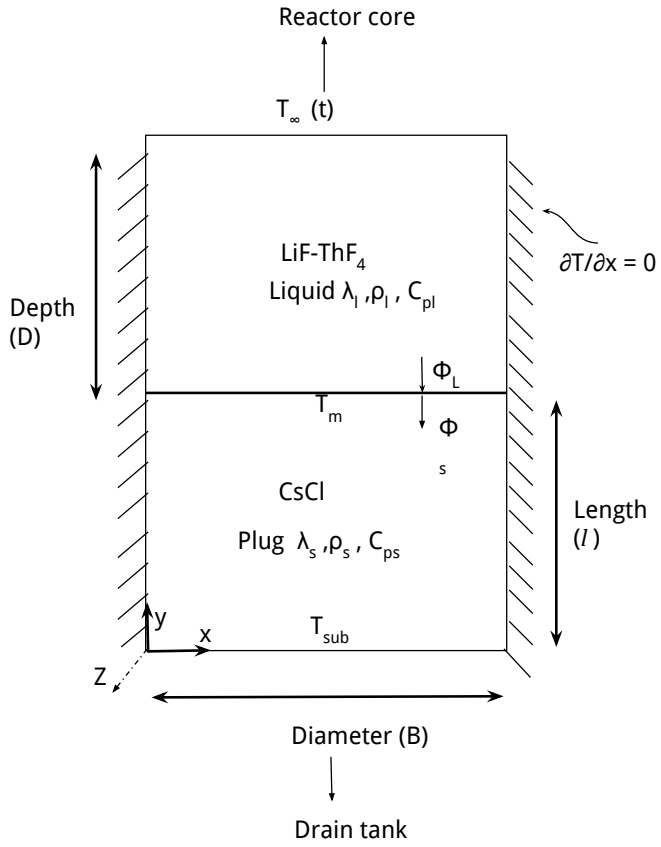

Figure 11: 2-D layout of the freeze plug; D, is the depth of location of plug, B is the width, L is the length

The figures (7b & 6a) represent the simulation result of the velocity profile for different operating conditions in the reactor. Since, these represent axis symmetrical geometry, the other half can be visualized as mirror image of this result. The velocity of the fuel salt near the edge (z=1 m, r=0 m) is close to zero, indicating presence of a stagnation region. Thus if the pipe is placed in the middle, the liquid region above will be stationary, and the heat transfer mechanism will be pure conduction. The layout of this plug is represented in figure(11). In order to begin with some design values, the length of the freeze plug is fixed at 20 cm. This length is slightly longer than the length of plug used in the MSRE experiment[1]. Once the plug is melted, the flow rate of the fuel-salt will be determined by the diameter of the pipe. Based on [12] drain calculation, the diameter of plug was

[1] The length used in the MSRE was 6 inches which amounts to 15.24 cms

chosen as 20 cm since it would lower the time to drain out the salt after melting. Later, the influence of these values will be studied based on the modelling of heat transfer due fluid motion above. The effect of simplifying it to a 2D geometry will be explained in later chapters.

2.1 MATHEMATICAL FORMULATION:

This section provides an mathematical formulation of the equations which governs the melting due to conduction and its implementation in COMSOL. In section (2.1.1), an analytical model will be introduced in order to verify the method of COMSOL.

The temperature (T) distribution for the melting, in each phase, is governed by the conduction equations:

$$\rho_s C_{p_s} \frac{\partial T_s(x,y,t)}{\partial t} = \lambda_s \nabla^2 T_s(x,y,t) \tag{1}$$

$$\rho_l C_{p_l} \frac{\partial T_l(x,y,t)}{\partial t} = \lambda_l \nabla^2 T_l(x,y,t) \tag{2}$$

In general, the subscript s represents the solid phase, while l represents the liquid phase. Here, ρ is the density [kg/m^3], C_p is the heat capacity[J/kg $\cdot$ K], λ is the thermal conductivity [W/m $\cdot$ K] and the x,y is the coordinates as shown in figure(11).

Initial conditions:

It is assumed that the liquid layer above the plug, in absence of fluid motion, will achieve a steady state such that it will be at T_∞ and the plug is maintained at a sub cooled temperature(10°C below its T_m)

$$T_l(x,y,0) = T_\infty \tag{3}$$

$$T_s(x,y,0) = T_{sub} = T_m - 10 \tag{4}$$

This is also represented in figure(11).

Boundary conditions for melting:

The data for boundary conditions for the model is obtained from the work of [33]. As established previously, due to power outage, there will be an increasing temperature distribution in near the inlet and the outlet of core as shown in figure(7a). Near the stagnation point of the reactor core, an linearly increasing temperature profile is assumed as:

$$T(0,t) = T_\infty(t) = T_\infty(0) + \frac{T_{600} - T_\infty(0)}{t(600) - t(0)} t = 950 + 0.75 \cdot t \tag{5}$$

where $T_{600} = 1400K$ is the temperature at time $t = 600s$ and $T_\infty(0)$ is the initial temperature based on figure(7a).

The speed of the melting is obtained by the heat balance at the interface. This interface is identified by the melting temperature of solid. Mathematically it can represented as:

$$T_s(x,y,t) = T_l(x,y,t) = T_m \tag{6}$$

By applying conservation of energy principle at the interface, we obtain:

$$\phi_{in} - \phi_{out} + \text{Production} = 0$$

$$\rho_s v_n \Delta H_{fus} = \Phi_l \cdot \hat{n} - \Phi_s \cdot \hat{n} \tag{7}$$

where $\Phi \cdot \hat{n}$ is the heat flux at the interface along the outward normal vector at any arbitrary location pointing towards the solid region. v_n is the velocity of the boundary at that location in the direction n̂ and ΔH_{fus} is the latent heat of fusion of freeze plug [J/kg][40]. Here, Φ_s is due to conduction. It will be zero if the plug is maintained at T_m. But this could be hard to achieve in reality, thus a sub-cooled temperature difference of 10K with respect to T_m is considered in the solid plug.

Equation (7), in COMSOL, is modelled using deformed geometry method. A detailed explaination and its working principle of the method is provided in section (A.3, & A.3.2) of the Appendix.

In all the simulation during melting, the side walls and the bottom wall as shown in fig(11), are always assumed to be insulated. For side walls and bottom wall:

$$\Phi = 0 \tag{8}$$

The properties of materials is provided in Table[1]. If only the plug is considered as a control volume, then an analytical solution is available for melting which is driven by only conductive heat flux. Before comparing the results of both the cases, the analytical model will be explained in the next section. This comparison achieves two purposes : 1) It serves as a validation for COMSOL and 2) It helps us compare the influence of the presence of the liquid layer and increasing temperature as a boundary condition. For this particular scenario, the depth of the liquid layer (D), is taken as 0.01m.

2.1.1 Analytical Solution

i Here, the initial area of freeze plug is assumed to be the control volume. A constant temperature (T_∞) is applied at time t=0 at y =0. Since this is a 1D approximation, the heat is transferred only in y-direction as shown in the figure(12). Further, conduction is the only transport mechanism in both solid and liquid.

ii The position of the interface, at any point of time t, is determined by the parameter $\delta(t)$ as shown.

iii The solid plug is a semi-infinite medium with $y \to \infty, T(y,t) = T_{sub}$.

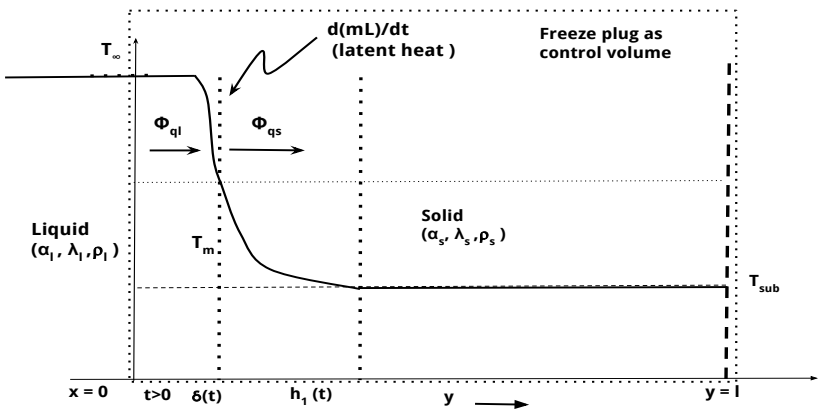

Figure 12: Analytical Model: Melting due to conduction with constant temperature at y=0 and $t > 0$.

The equation governing this transport mechanism is given by equation (9) and (10)

$$\frac{\partial T(y,t)}{\partial t} = \alpha_s \frac{\partial^2 T(y,t)}{\partial y^2} \tag{9}$$

$$\frac{\partial T(y,t)}{\partial t} = \alpha_l \frac{\partial^2 T(y,t)}{\partial y^2} \tag{10}$$

The boundary conditions for this situation can be summed as below:

$$T_l(y,0) = T_1 \tag{11}$$

$$\lim_{y\to\infty} T_s(y,t) = T_2 \tag{12}$$

Common boundary conditions for liquid-solid interface ($y = \delta(t)$) are:

$$T_s = T_l = T_m \tag{13}$$

The energy balance at this interface:

$$\lambda_l \frac{\partial T(y,t)_s}{\partial y}\bigg|_{y=\delta(t)} + L\rho_s \frac{d\delta}{dt} = \lambda_s \frac{\partial T(y,t)_l}{\partial y}\bigg|_{y=\delta(t)} \tag{14}$$

when compared with equation(7), it can be seen that

$$\Phi_l = \lambda_l \frac{\partial T(y,t)_s}{\partial y}$$

$$\Phi_s = \lambda_s \frac{\partial T(y,t)_l}{\partial y}$$

The solution to this problem can be found in [38]. The liquid phase temperature turns out to be :

$$T_l(y,t) = T_1 + \frac{(T_m - T_1)\,\mathrm{erf}\left(\frac{y}{2\sqrt{\alpha_l t}}\right)}{\mathrm{erf}(p)} \tag{15}$$

where erf is the error function which is defined as:

$$\mathrm{erf}(z) = \frac{2}{\sqrt{\pi}} \int_0^z e^{-y^2} dy$$

The equation for the solid phase is,

$$T(y,t)_s = T_2 - (T_2 - T_m)\frac{\mathrm{erfc}\left(\frac{y}{2\sqrt{\alpha_s t}}\right)}{\mathrm{erfc}\left(p\sqrt{\frac{\alpha_l}{\alpha_s}}\right)} \tag{16}$$

where erfc is the complementary error function, defined as:

$$\mathrm{erfc}(z) = 1 - \mathrm{erf}(z)$$

The position of interface as a function of time is given by :

$$\delta(t) = 2p\sqrt{\alpha_l t} \implies \delta(t) = F\left(\sqrt{t}\right) \tag{17}$$

where p is a constant. It is defined by the following transcendental equation:

$$\lambda_l \left(\frac{T_m - T_1}{\sqrt{\pi \alpha_l}} \frac{\exp(-p^2)}{\operatorname{erf}(p)} \right) + L\rho_s (p\sqrt{\alpha_l}) = \lambda_s \left(\frac{T_2 - T_m}{\sqrt{\pi \alpha_s}} \frac{\exp\left(-p^2 \frac{\alpha_l}{\alpha_s}\right)}{\operatorname{erfc}\left(p\sqrt{\frac{\alpha_l}{\alpha_s}}\right)} \right) \tag{18}$$

The heat flux at the interface is given by :

$$\Phi"_l = -\lambda_l \left. \frac{\partial T_l}{\partial y} \right|_{y=\delta} = -\lambda_l \frac{T_m - T_1}{\operatorname{erf}(p)} \frac{1}{\sqrt{\pi \alpha_l t}} \exp(-p^2) \implies F\left(\frac{1}{\sqrt{t}}\right)$$

$$\Phi"_s = -\lambda_s \left. \frac{\partial T_s}{\partial y} \right|_{y=\delta} = -\lambda_s \frac{T_2 - T_m}{\operatorname{erfc}\left(p\sqrt{\frac{\alpha_l}{\alpha_s}}\right)} \frac{1}{\sqrt{\pi \alpha_s t}} \exp\left(-p^2 \frac{\alpha_l}{\alpha_s}\right) \implies F\left(\frac{1}{\sqrt{t}}\right)$$

2.2 MESH SELECTION

There are some fundamental differences between COMSOL and analytical model. Firstly, in the analytical model, initially only the freeze plug is present and a temperature higher than T_m is applied at (x=0). In COMSOL, the control volume consist of the depth of 0.01 m of liquid layer along-with the freeze plug and an increasing temperature is applied at the liquid wall as per equation (5) as shown in fig (11). Secondly, analytical solution exists only for constant temperature and infinite boundary. In COMSOL, the bottom wall (y=0 in figure(11)) is assumed to be at T_{sub}. Since the model in COMSOL is 2D and the analytical result is only available for a 1D model, the boundary for side walls, equation (8), is replaced by a periodic boundary condition [37]. The mesh distribution used for the simulation is shown in figure(13). The number of elements in each direction is the same. A grid independent result is obtained when the number of elements is 75x75.

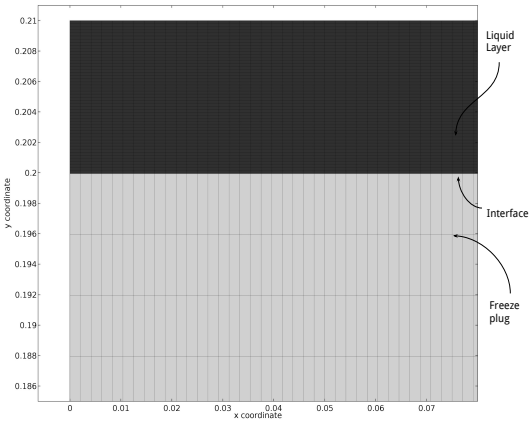

Figure 13: Distribution of quadrilateral mesh for cavity and freeze plug.

2.3 RESULTS

Let the analytical situation be represented by Case A and simulation of freeze plug by COMSOL be represented by Case B.

For case B, in fig(14),time snapshots of temperature distribution at x= 0.1 are plotted as a function of y. Here, Temperature profiles are plotted only up to y=0.02m (this is not the bottom wall of the freeze plug), while here y=0 corresponds to the top wall as shown in 11

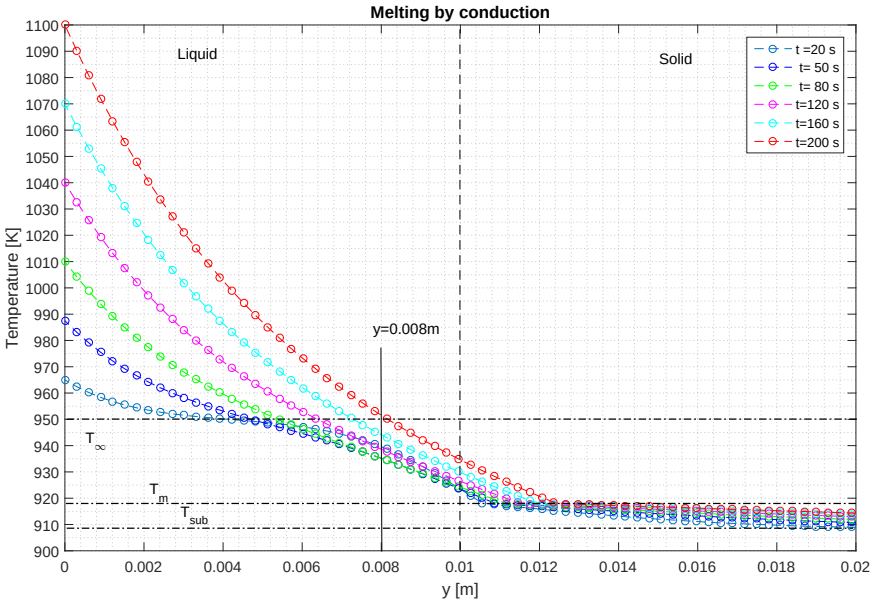

Figure 14: Time snapshot of temperature distribution over the distance y, for COMSOL simulation.

The region, y>0.01 represents the freeze plug region and y<0.01 is the liquid layer at time t=0 as shown in the figure. Two isotherms, $T = T_\infty$ and $T = T_m$ are plotted as a reference lines. The temperature distribution is plotted at t= 20s, 50s, 80s,120s ,160s and 200s as shown in the legend. The intersection of these temperature curves with the isotherm $T = T_{melt}$ indicates the position of the interface. The temperature at y=0 increases linearly in time due to imposed boundary condition as per equation (5).

In the graph (15a), the velocity of the interface is plotted on y axes for both analytical and COMSOL versus time while similarly in the graph(15b), heat flux is plotted versus time. The heat flux values evaluated in COMSOL is at the point x =B/2 on the interface. Both graphs will be referenced with fig(14) to have a clear explanation.

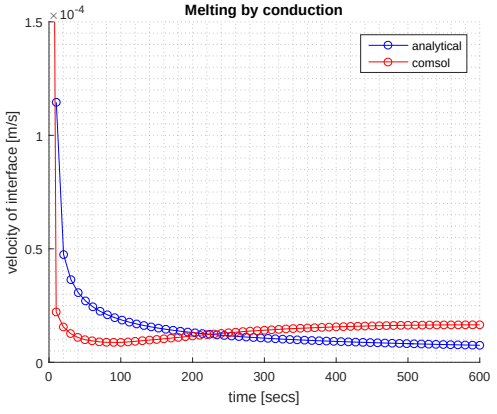

(a) Velocity (v_n) of the interface (m/s)

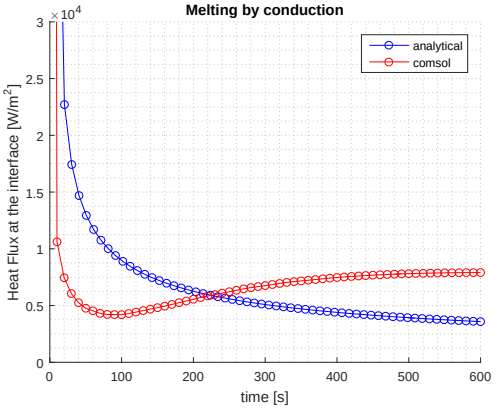

(b) Heat flux (Φ) at the interface [W/m^2]

Figure 15: Comparison of simulation result between COMSOL and analytical.

In fig(15a), at time $t > 0$, for both the cases, a non-zero interface velocity is observed i.e. Melting starts as soon as constant temperature is applied as along as the below criteria is satisfied (based on equation (7)):

$$\Phi(0)_l > \Phi(0)_s \implies |v(0)_n| > 0$$

In fig(15b), for both the cases, the heat flux at the interface decrease as a function of time (for case B , up to t = 200 secs). Thus, the corresponding interface velocity also decreases. Physically, this means that the melting of freeze plug by conduction, will progress slower and slower in time due to decrease in heat flux.

In fig(15b), it can also be observed that :

$$\Phi_A > \Phi_B \quad \forall \ t < 200s$$

As observed in fig(14), up to distance y=0.08m for $t < 200s$, the temperature in the liquid layer is lower than the initial temperature $T_\infty(0)$. In case A, the temperature at y=0, is maintained at $T_\infty(0)$, and thus an higher heat flux is observed in case A. After $t > 200s$, due to the increase temperature as a boundary condition, a higher heat flux at this depth is realized. Two conclusions can be drawn from this:

i Melting of freeze plug is affected by the local temperature (heat flux) values i.e very near to the interface. In the case, this distance is found to be 0.002m.

ii It is interesting to compare the two penetration(of heat) depth [15] here. First is the penetration depth (D_{p1}) in the liquid layer due to an increasing temperature, and the other due to melting(D_{p2}). Based on the fig(14), it can be observed that penetration of heat is much faster than the distance travelled by the interface. At the end of time t= 200s, (D_{p1}) is equal to 0.08m while (D_{p2}) 0.002m

Based on the maximum heat flux achieved in case A, a quick estimation of time can be made here by some approximation

$$\Phi \backsim 3 \cdot 10^4$$

$$\rho \cdot \Delta H_{fus} \equiv 10^3 \cdot 10^5$$

$$\therefore \ v_n \equiv \frac{3 \cdot 10^4}{10^3 \cdot 10^5}$$

$$l = 0.2 \implies t \equiv \frac{0.2 \cdot 10^3 \cdot 10^5}{3 \cdot 10^4 \cdot 60} \equiv 12 \,\text{mins}$$

But in order to achieve this, the freeze plug has to be placed extremely close to the reactor core. This design can be considered as extremely impractical because other auxiliary components for cooling around this freeze plug.

In conclusion, in order to drive faster melting, it is important to maintain the heat flux at the melting interface. This could be achieved by placing the plug below the region of fluid flow represented in figure(6a) i.e eccentric placement of the drain pipe. The phenomena introduced by fluid flow in liquid region would be then similar to lid driven cavity which is explained in the next chapter.

3 MELTING BY LID DRIVEN CAVITY

For an non symmetric placement of drain pipe (r=1m), a simplified layout of freeze plug with boundary conditions are drawn in fig(16). According to figures (5a & 5b), at this point, the velocity of fluid in steady state is equal to 4 m/s which drops to 0.6 m/s after t= 130s for the case of pump failure. The fluid velocity is in the horizontal direction, which is indicated by U_{lid}, as shown in the figure (16) and the process is known as lid driven cavity. This chapter is aimed at establishing the fundamental physics behind this process through understanding the experiments carried out in the literature [25, 27]. This chapter will end with a set of restrictions that should be placed on the material selection in order to drive faster melting.

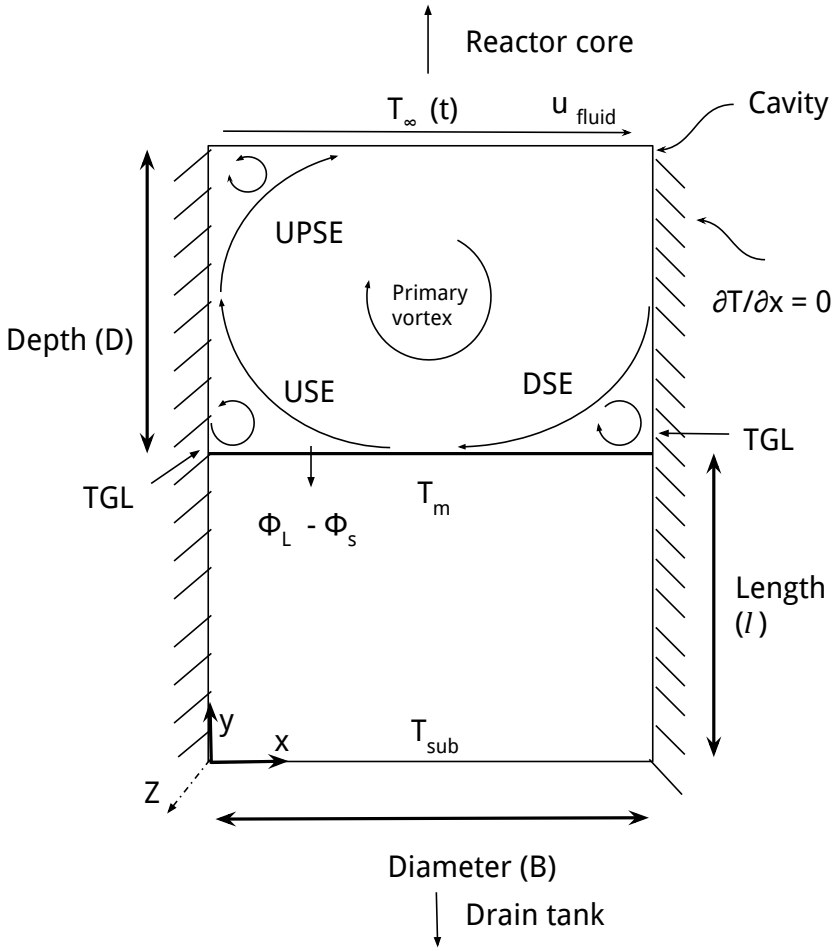

Figure 16: Simplified layout of Lid Driven Cavity with some characteristic features.

3.1 LID DRIVEN CAVITY

In this section, a detailed physics of isothermal lid driven cavity and the effects of the temperature boundary conditions is explained. The primary relevance in understanding the physics in detail is because it forms as selection criteria's for the turbulence model which is explained in the section (4.2).

3.1.1 Isothermal Lid Driven Cavity

The main characteristics to the isothermal ($\Delta T = T_\infty - T_m$=0) lid driven cavity can be understood from the experimental work of [27, 26]. These characteristics are listed below:

i Velocity of the lid : The top wall of the cavity is given a sliding motion which translates into a shear force on the top layer of liquid. Due to this shear force, the liquid is set into a recirculation motion. The flow pattern consists of a large primary eddy, two flow separation regions at the bottom of the cavity represented as downstream secondary eddy and upstream secondary eddy as described in the fig(16). There also exist vortices known as Taylor-Görtler like vortices (TGL), near the corners of the cavity and at high Reynolds number at the left hand top corner of the cavity. The Reynolds number for this process is defined as:

$$\mathrm{Re} = \frac{BU_{lid}}{\nu}$$

ii The fluid is dragged in the direction of motion of the lid due to the shear force. This develops a high pressure region the top right corner and from there flow is then pushed down due the side wall. It decelerates as it flows towards the bottom of the lid due to friction. This cause the separation of flow leading to a down stream secondary eddy(DSE). In case of an isothermal lid driven cavity, the primary eddy depth is the point where upward the buoyancy force by the lower fluid balances the downward momentum flux generated by the lid.

iii After this, flow returns upwards, forming an upstream secondary eddy (USE). Due to the flow separation at the corners of the cavity, TGL vortices' are formed. The velocity at the center of the cavity is zero and also at the end walls, due to the no slip condition. Hence, there must exist a point where the velocity is maximum with large gradients leading to higher shear stress. Thus these vortices' are induced to wall effects. Further, the size of these vortices' are a function of Re.

iv Turbulence effects in the cavity, are observed near the downstream secondary eddy region. The velocity fluctuations observed for Re =3200 are of low magnitude, and hence considered as unsteady laminar flow. The transition from laminar to turbulence occurs in the region of $6000 < Re < 8000$. The maximum Reynolds shear stress was measured at the DSE region. The fluctuations are largest near the DSE and go on reducing in intensity along flow from the bottom wall towards the secondary upstream eddy. The flow in the secondary upstream eddy, near the lid, shows laminar features for Re upto 8000. This is attributed to the fact that the recirculation forms a convex walls (of fluid layer) near the lid. A convex surface thus formed, stabilizes the flow , and delays the onset of turbulence. Therefore, it is quite possible that the effects of turbulence are localized and that a larger part of the flow retains laminar unsteadiness like features.

The velocity based on fig (6b) is 0.6 m/s which corresponds to a Re of $6.6 \cdot 10^4$. Thus, the flow in the cavity region is in the turbulent regime.

3.1.2 Lid driven cavity with stratification

From the isothermal lid driven cavity, the effects of maintaining the temperature at the end walls can be understood from another experiment of [25, 5]. In our case, the moving wall is kept at a higher temperature T_∞ while the bottom wall is kept at lower temperature T_m.

i As understood in the isothermal lid driven cavity, the maximum depth is achieved when the momentum flux is balanced by the buoyancy force. In case of stratification, the higher density of the fluid is at the bottom end of the cavity. This results in larger buoyancy force which induces a counteracting stability mechanism to the perturbation obtained by the lid. This opposing effect plays an important role in mixing of layers, temperature profiles and eventual heat transfer. The effective strength of stratification is determined by the bulk Richardson Number(Ri)

$$\mathrm{Ri}_b = \frac{\mathrm{Gr}}{\mathrm{Re}^2} = \frac{gD^3}{B^2 U_{lid}^2}\beta(T_\infty - T_m) \tag{19}$$

If $Ri_b \gg 1$, the strength of natural convection is much higher than forced convection. This increase in strength of natural convection decreases the size of primary eddy. From the experiments it was observed that the number of secondary re-circulation is related to the bulk Richardson number. When $Ri_b > 1$, at least two secondary circulation were observed. In between $0.5 < Ri_b < 1$ only one secondary cell is observed. The consequence of such phenomena is that velocity and temperature fields stabilized. Near the bottom wall, the magnitude of velocity is zero and isothermal lines are horizontal in nature. This means that the heat transfer at the bottom will be due to conduction. If $Ri_b \ll 1$ implies forced convection dominates the process. The velocity field are then similar to the physics of isothermal lid driven cavity and the temperature distribution field will follow this [14].

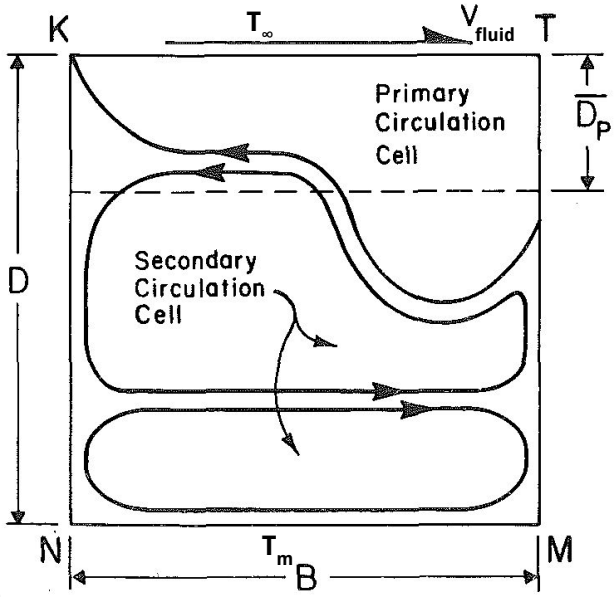

Figure 17: A simplified layout of the Lid Driven Cavity with stratification. Adopted from [25]

ii The size of this primary recirculation is shown in fig (18a) as a function of Ri. In the experiment, different Ri values was obtained by keeping Re constant at 10,000 but by varing ΔT from 1.2 °C to 9 °C. For a Ri = 0.53 the penetration depth of the primary recirculation was observed to be about 0.5D while for Ri> 0.2 it was greater than 0.7D. Since the flow in the secondary eddy is of much weaker strength when compared to primary eddy, the heat transfer at the interface is likely to be driven by conduction. Based on the conclusions of chapter[2] in section (2.3), conduction based melting should be avoided, which implies penetration depth should be greater than 0.8D and Ri > 0.15.

iii Further, stratification delays the onset of turbulence. In the experiment, it was observed that flow at Re=10,000 was only partially turbulent for Ri < 0.15. The critical Richardson number, above which turbulence is suppressed, lies in the range of 0.05 to 0.3 .

iv Another important parameter associated with the mixing process is the entrainment rate. Entrainment rate is defined as the extent to which turbulent flow mixes with the non turbulent flow. Thus, it can be understood as the vertical transport of momentum and temperature under the influence of stratification. The entrainment rate calculated in the experiment is defined as :

$$E = \frac{U_e}{U_{lid}} = \frac{1}{U_{lid}} \frac{dD_p}{dt}$$

This penetration depth considered, is not the maximum penetration depth, as shown in the figure(17), but calculated as by dividing area of the mixed layer (the area is calculated at a vertical plane along the span wise direction of the cavity) by the width (B).

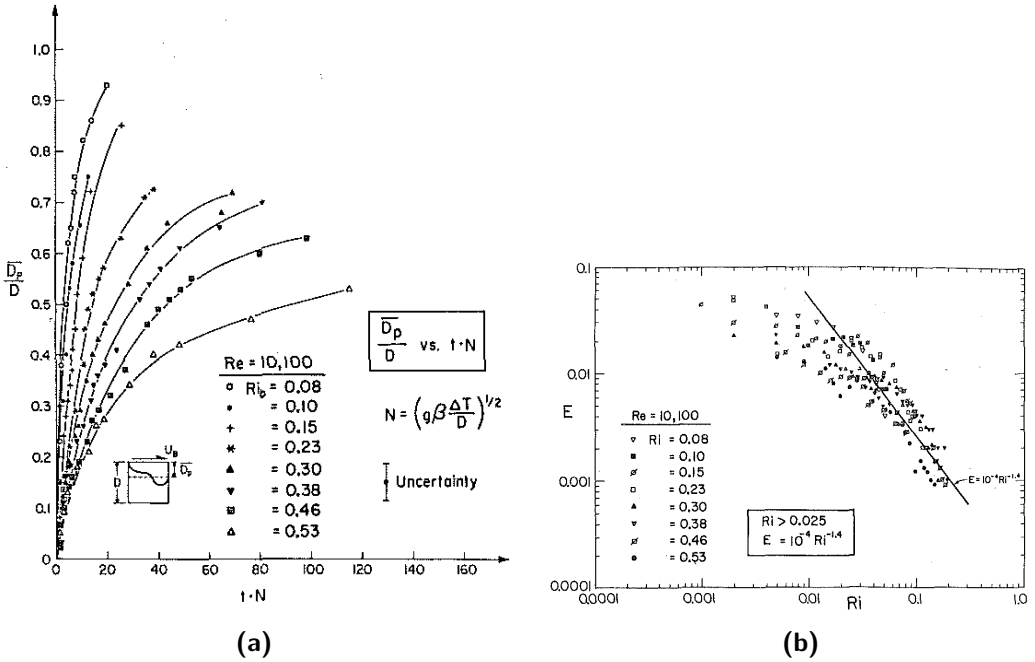

Figure 18: In figure(18a) normalized average depth as function of Ri for fixed Re vs non-dimensionalised time is plotted. In figure(18b) Log-Log plot of Entrainment rate E vs Ri for flows with Re= 10,000 is plotted. Results of [25]

v From the data plot in figure(18b) it is established that $E \propto Ri^{-1.4}$. Since in the experiment a 3D dimensional geometry is considered, this entrainment rate could be in span wise and vertical direction. The mixing mechanism is likely to depend on the shear stress between the layers and turbulence in the primary eddy. Further, it was observed that there is presence of vortices' between the primary circulation layer and the secondary circulation layer, which enhances this mixing rate.

vi In this experiment, a remark had been made that belt induced motion induced shear stress may have a different behaviour than the fluid induced shear. This might be different due to several possible reasons. Firstly,the boundary condition implied by the velocity of the moving wall may not take into the mixing process due to fluid interactions at this boundary. Secondly, it is quite possible that the shear stress will be of different magnitude due to fluid-wall and fluid-fluid interaction. Thirdly, it may not take turbulence effects of fluid flow into account. Nevertheless, in this study, simulations will be performed assuming moving wall induced flow.

3.2 GUIDELINES FOR MATERIAL SELECTION

$LiF-ThF_4$ serves as an ideal material for the design of freeze plug since it avoids reprocessing and potential other problems due to unknown chemistry that one has to take into account for other materials. But the melting temperature of $LiF-ThF_4$ is 838 K while the reactor core is at 950 K. If the Re =60,000, D= 0.2m, B=0.2m, based on the properties given in table(1), corresponding $U_{lid} = 0.81$ m/s. For this Re, bulk Richardson number can be evaluated as :

$$\mathrm{Ri}_b = \frac{gD^3}{B^2U_{lid}^2}\beta(T_\infty - T_m) = 0.3$$

This implies, based on figure(18a), the penetration depth (D_p) will $0.7 \cdot D$, which should be avoided. Thus, selection of $LiF-ThF_4$ will work against the mechanisms which can enhance the heat transfer. If, we desire to achieve Ri < 0.1 at Re $= 60{,}000$, then the required melting temperature of the material :

$$Ri < 0.1, Re = 6 \cdot 10^6 D = 0.2m, B = 0.2m, \implies T_m > 910K$$

This will be considerably lower the heat flux compared if a material with lower melting temperature was chosen. In conduction driven melting, it was established that the magnitude of heat flux is governed by the local temperature difference near the interface (point(i) in section (2.3)). Hence, a $Ri < 0.1$ is a condition that is imposed in order to ensure that the penetration depth of flow is up to the interface (refer to figure(18a)). Thus a compromise would be needed between high heat flux and lower Richardson number. Hence, a material with 930 K $<T_m <$900 K will be chosen for simulation such that Ri < 0.1 at Re close to $6 \cdot 10^4$. Based on the experience of MSRE experiment introduced in section (1.2), some of the other requirements which should be considered for the material, is also listed :

i Based on equation (7), the material should have a low product of $\rho \cdot \Delta H_{fus}$ (product is the energy content per unit volume [J/m^3]) in order to facilitate faster melting.

ii The thermal properties of the material in solid state should be available so as to have a predictable behaviour for the design of the plug.

iii The solubility of the material should be extremely low in $LiF-ThF_4$ in the operating conditions so as to keep the length of the plug constant. If the solubility of the material is high, this will cause erosion of the plug due to fluid flow. In the MSRE experiments, this was not noticeable, since the fuel and the plug were of the same material.

iv For binary eutectic type compounds, it would be necessary to maintain the plug at the eutectic composition, in order to have the phase change at a constant temperature.

v The duty cycle used to the test the freeze valve was 100 times freezing and thawing cycles to ensure the durability of their system. Now, if a different material other the fuel-salt is used, then it would be necessary to refreeze the plug conveniently every-time. Further, it should be also possible to separate this material from the fuel salt, in order to decontaminate the fuel.

vi The material should be non toxic and environmentally friendly.

Quite a lot of research for phase change materials has been done in the solar thermal application[1]. Here materials are being researched as a potential for thermal energy storage. There is a list of molten salt materials presented in [21] and for metallic alloys in [32] which could be used as high temperature phase change material. Using these, in figure (19), a list of potential materials, with 950 K $< T_m <$ 850 K, is plotted. The energy content of the material during phase change, is calculated as:

$$E = \rho \cdot \Delta H_{fus} \ \ [\mathrm{J/m^3}]$$

The latent heat data for all the compounds, except for the metal alloys, is available. For $Mn-Al\,(92.3-7.7)$, since the percentage of Aluminium is quite low, ΔH_{fus} and ρ of Mn is assumed, while for $NiAl_3$, this is interpolated based on the composition fraction (x). Thus it is calculated as :

$$\Delta H_{fus_{\mathrm{mix}}} = x_{Ni} * \Delta H_{fus_{\mathrm{Ni}}} + x_{Al} * \Delta H_{fus_{\mathrm{Al}}}$$

In the binary and ternary salt materials for which the density is not available, the mixed salt density is evaluated based on ideal mixing [50] (non volume change due to formation of components) :

$$\rho_{\mathrm{mix}} = \frac{M_{\mathrm{mix}}}{V_{\mathrm{mix}}}$$

where,

$$M_{\mathrm{mix}} = \Sigma x_i M_i$$

$$V_{\mathrm{mix}} = \Sigma x_i V_i$$

thus,

$$\rho_{\mathrm{mix}} = \frac{\Sigma x_i M_i}{\Sigma x_i V_i}$$

The same principle is also applied for some molten salts and numerical data of the graph is provided in table(3).

[1] But the material requirements are complementary in nature, for example storage material require high energy content per unit volume, in order to store more energy [1]

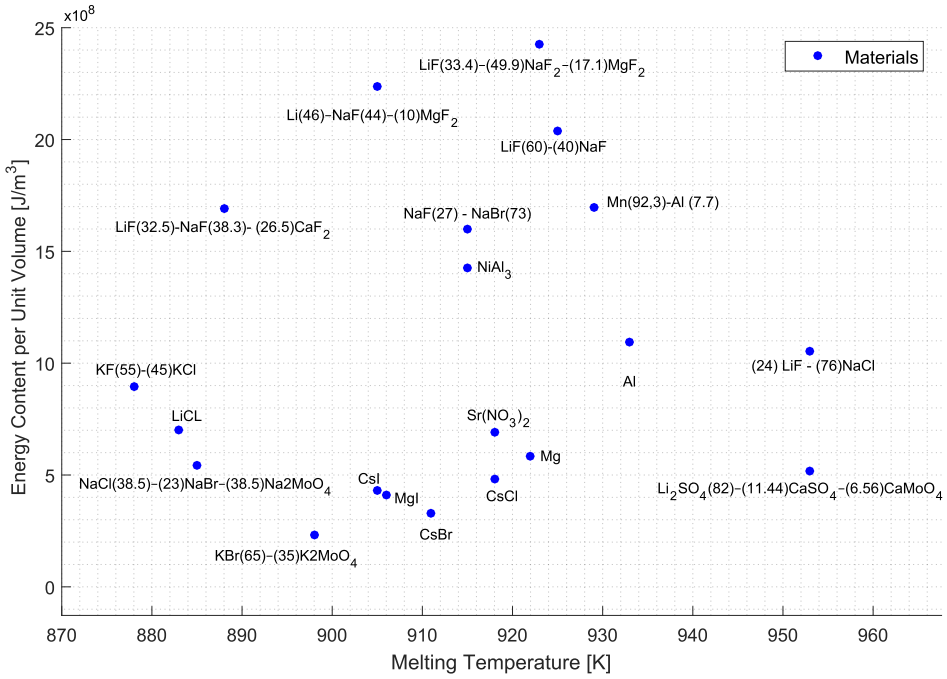

Figure 19: Energy content of various material, suitable for freeze plug, versus melting temperature

Based on point (i), one should select the material with as low energy content per volume as possible and 930 k $< T_{melt} <$900 K (this is only applicable for this stratified lid driven cavity process). Cesium salts comply with this aspect. Metallic alloy have extremely high thermal conductivity, nevertheless it is not a suitable material because, eventually λ_l and Φ_l are the limiting factors. Thus, CsCl is selected as the material for the freeze plug. Before continuing the study of heat transfer, brief focus on the phase diagram is touched, mainly to elaborate on points (iii) and (iv) mentioned above.

Phase Change

For a chemical compound, a phase, is defined as a homogeneous but mechanically separable state of the material, for a given chemical composition. It is a function of both pressure and temperature. The process of phase change behaviour is different for pure crystalline substance and binary compounds. A binary system is a homogeneous mixture of two different substances and their phase changes depends on the solubility of these substance in each other in different phases. Phase diagrams for different compounds can be used to study their phase stability as a function of temperature, pressure and composition. It can also be viewed as a solubility diagram for the mixture of compounds in equilibrium condition and constant pressure.

- For a pure substance like MgI, CsBr, CsCl etc, phase change occurs at constant temperature. The process is depicted in the curve(a) of fig(20a). Initially heat is removed from a liquid state which results in gradual temperature decrease, until the point B. It is at this point at which first crystals are formed and further removal of heat, equivalent to the latent heat, results in complete solidification (point C) at constant temperature. This latent heat required is equal to the enthalpy difference at points B and C.

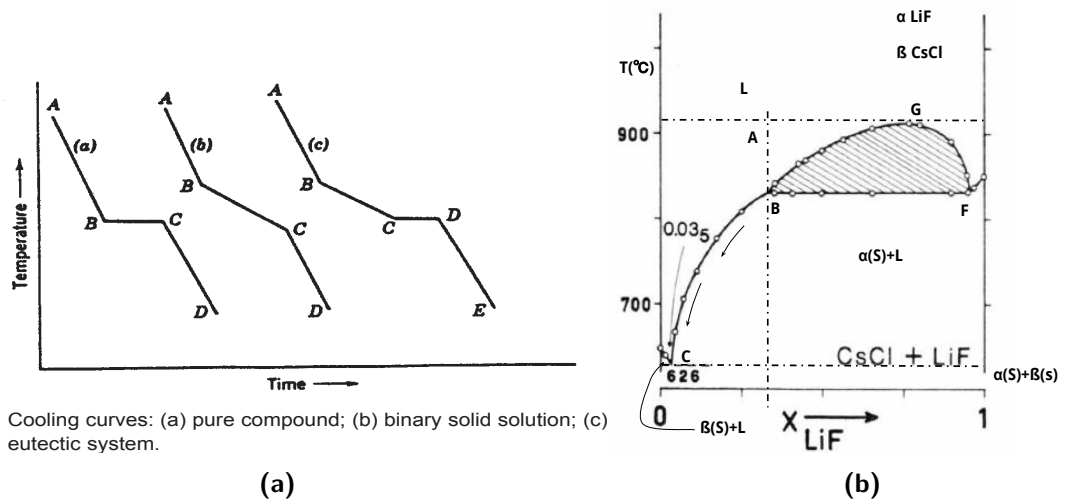

Figure 20: Figure (20a) represents the cooling curves of different types of compounds. Here A to B represent liquid state, B to C represent phase change and C to D represent solid. Adopted from [46]. Figure (20b) represents the equilibrium phase diagram of LiF- CsCl with eutectic point at (626 °C). Adopted from[35]

- Further, the curve(b) of fig(20a) shows the cooling process of a binary system in which are both the substance are soluble in the liquid as well as in the solid phases. This melting range for the binary substance is attributed to the fact that there are changes in the composition of the two substances in the solid and liquid phase.

- The curve(c) of fig(20a) shows the cooling of two substance which are completely soluble in liquid state while non-soluble in solid state(α and β phase as shown in fig(20b)). CsCl-LiF mixture is an example of such mixture for which the phase diagram of CsCl- LiF is shown in fig(20b). The curve joining the temperature points T_m of CsCl to 626 °C (point C) to points B-F line is the liquidus curve. Thus, the region above the curve represents liquid phase while the isotherm 626 °C is the solidus line. The point in graph at 626 °C is the eutectic point, where all the three phase α, β and liquid coexist. Assume an initial composition of the mixture corresponding to point A. From points A-B represents the cooling of this, while crystallisation starts at point B , where the component with excess composition starts to solidify. At C, the mixture has reached a composition where both the components starts to solidifying simultaneously from the liquid solution and temperature remains constant [46].

- It can also be seen that, for a pure substance latent heat of fusion is a unique characteristic, which is the enthalpy change for from B and C whereas for binary mixture, especially eutectic compounds, exhibit different enthalpy changes for phase change transformation due difference in composition. Thus, the assumption of constant T_m and ΔH_{fus} during melting, is valid only for a pure substance or melting at a eutectic composition.

- It can observed in the fig (20b) that addition of ThF_4 lowers the melting temperature of LiF [2]. Thus, this phase diagram would not be very representative to study the solubility of CsCl in the fuel salt. Further, this phase diagram is drawn for an equilibrium temperature and for a closed system, whereas the situation in freeze plug is non equilibrium, because the fluid is constantly being recirculated (at a different

[2] T_m of LiF is 845 °C

temperature). In more general terms, it would be of interest to characterise solubility, diffusion or reaction rates of CsCl due to interactions with LiF – ThF_4. This would be helpful in determining the erosion of solid due liquid interaction, which indicates whether the plug can be maintained at a constant length.

Thus, the governing physics has given certain criterion within which the material should be selected. In addition to this, phase stability should also be incorporated but in this thesis not further researched. The focus is on modelling the melting part of the design of the freeze plug. Hence, here an iteration for stratified lid driven cavity melting with CsCl as the freeze plug material will be performed.

The temperature dependence of thermal properties for LiF – ThF_4 :

$$\rho(T) = 4.094 - 8.82 \cdot 10^{-4} \cdot (T - 1008) \qquad \left[\frac{g}{cm^3}\right]$$

$$\nu(T) = 5.54 \cdot 10^{-8} \cdot \exp\left(\frac{3689}{T}\right) \qquad \left[\frac{m^2}{s}\right]$$

$$\lambda(T) = 0.928 + T \cdot 8.397 \cdot 10^{-5} \qquad \left[\frac{W}{m \cdot K}\right]$$

$$C_p(T) = (-1.111 + 0.00278 \cdot T) * 10^3 \qquad \left[\frac{J}{kg \cdot K}\right]$$

The thermal properties of CsCl and fuel salt LiF – ThF_4 evaluated at T= 950K is given below in the table:

Table 1: Thermal properties of CsCl and LiF – ThF_4

Sr No	Properties	CsCl	LiF – ThF_4	Units
1	Density ρ	3988.0	4124.8	(kg/m^3)
2	Thermal Conductivity λ	1.3	1.0	(Wm/K)
3	Heat Capacity C_p	450.4	1530.0	(J/KgK)
4	Latent heat of Fusion ΔH_{fus}	$1.21 \cdot 10^5$	$1.71 \cdot 10^5$	(J/kg)
5	Melting Temperature (T_m)	918	838	K

The properties of fuel and fertile salt are measured for the salt 78% LiF4- 22% ThF4 (ISTC Project No.3749)[12]
The latent heat of fusion for the salt is calculated by weighted average (based on molar mass percentage) of individual components LiF4 and ThF4 [3]
The properties of CsCl obtained from [16, 21, 47]

It is not necessary to introduce all the properties as a function of temperature in the simulation but more important to incorporate density as a function of temperature, since buoyancy force governs convective heat transfer. In order to model for stratification, Boussinesq approximation to model volume force will be used. As mentioned previously the density which varies linearly for LiF – ThF_4 with temperature, can also be expressed as:

$$\rho(T) = \rho_0 - \beta\rho_0\Delta T$$

which can rewritten as

$$\frac{\rho(T) - \rho_0}{\rho_0} = \beta\Delta T$$

this can be replaced in the volume force (section (4.3)) as

$$V_f = \rho_0 g\beta\Delta T \tag{20}$$

4 TURBULENCE MODELLING

Based on point(iv) in section (3.1.1), the flow in the cavity is in the turbulent regime. Turbulence modelling for 3D geometry with a deforming mesh could be too complicated. This chapter will first establish reasonings and influence of the 2D approximation, followed by the selection of the turbulence model. Two important questions to answer here are: 1) What are the consequences of the 2D approximation? and 2) Which turbulence model should be used? After answering these questions, the turbulence model and its approximation will be introduced. In section (4.5 & 4.6), the different cases consider to answer research sub question (ii & iii) will be explained followed by corresponding mesh settings for each of the cases.

The most fundamental characteristic of turbulence is that, velocity($\vec{u}$) and pressure (p) fluctuate at a point, in the domain, with time. Thus, the velocity, at this point, can be divided into two components, mean ($\overline{u}$) and fluctuation (u') about this mean.

$$\vec{u} = u' + \overline{u}$$

All the turbulence models described in COMSOL apply Reynolds Averaged Navier Stokes (RANS) approximation. In RANS models, only the mean flow($\overline{u}$) is modeled while the fluctuations are modeled in the form of turbulence quantities(viz. k, ϵ or ω where k is the turbulent kinetic energy(TKE), ϵ is the dissipation rate and ω is k/ϵ). The detailed transport equation of k and ϵ can be found in [22, 41]. Here, some specific terms of the transport equation which is of utmost interest, is explained below.

TKE is defined in terms of velocity fluctuations:

$$k = \frac{1}{2}\left(\overline{{u_i'}^2 + {u_j'}^2 + {u_k'}^2}\right) \tag{21}$$

here, u_i' represents the ith component of the fluid velocity fluctuation at a point in space $[\vec{x}]$ [1]. The variation of k in time depends on the production rate, dissipation and molecular diffusion. Production P_k is the rate at which TKE is produced from the mean flow. The dissipation ϵ_k is the rate at which TKE is lost as thermal internal energy of the flow [53]. These variables are written as :

$$P_k = \tau_{ij}\frac{\partial \overline{u}_i}{\partial x_j} = -\rho\overline{u_i'u_j'}\frac{\partial \overline{u}_i}{\partial x_j} \tag{22}$$

where τ_{ij} is the Reynolds stress tensor.

$$\epsilon_k = \nu\overline{\frac{\partial u_i'}{\partial x_j}\frac{\partial u_i'}{\partial x_j}} \tag{23}$$

Similar to the Reynolds stress tensor, τ_{ij}, the decomposition and then Reynolds averaging of the energy equation, introduces turbulent heat flux Φ_T, which is defined as :

$$\Phi_T = -\rho C_p\overline{T'u_i'} \tag{24}$$

[1] This notation causes a bit of inconvenience. The symbols used previously for direction was x,y,z. According to the notations followed in literature and standard textbooks, in turbulence equations the subscript of i,j and k would represent directions, which in Cartesian coordinate system is indicated as x,y and z

This turbulent heat flux, as a buoyancy force term, is introduced in the time variation of k as :

$$V_T = \beta g \overline{T' u_i'} = -\beta g \left(\frac{\mu_T C_p}{Pr_T} \frac{\partial \overline{T}}{\partial x_j} \right) \tag{25}$$

In this term, V_T is interpreted as exchange between the turbulent kinetic energy and the potential energy. If $V_T < 0$, the process consists of a stable stratification, indicating that turbulence decreases and potential energy increases. Thus it appears as a sink for k. If $V_T > 0$, the potential energy decreases and turbulent energy increases, thus acting as a source.

In the transport equation of ϵ, the mean temperature gradient appears as :

$$G_\epsilon = 2\beta\nu g \overline{\frac{\partial u_i}{\partial x_j} \frac{\partial T_i}{\partial x_j}} \tag{26}$$

which would indicate the rate of dissipation of TKE due to temperature gradient. These variables helps to understand the consequence of 2D approximation.

4.1 2D APPROXIMATION:

- The most important difference between the experimental results available and our interest of modeling, is the cylindrical geometry. It should be expected that the driven cavity flow in a cylinder would be different than a cubical geometry, because the features of this flow is wall induced and thus curvature of the wall will influence the flow greatly. The full scale modeling of the cylinder geometry greatly increases the computational time due to substantial increase in requirements in number of mesh elements.

- The data available for velocity profile, for the reactor core is in a 2D geometry. Thus 2D geometry will be considered here.

- Further, an important driver for 2D approximation is the modeling for a deformed geometry to simulate melting phenomena. This involves coupling of turbulent fluid flow, heat transfer and a moving mesh. It is of more important interest to first establish an understanding of how this heat transfer affects the progress of melting interface. Having understood this, a 3D dimension simulation could be performed so that effects of the geometry can be study exclusively.

- The nature of turbulence flow is 3D. Further, it was established in the experiment that the streamlines and TGL vortices' are 3D in nature which is shown in figure (21) below. For this figure, the axis system is shown at the bottom of the figure where, the span wise direction is along the z- axis and the direction of lid movement is x axis (into the plane) as shown on the right hand side by the symbol $\odot$. Thus, the figure indicates span wise variation of streamlines for Re = 6000 at two different times. The flow is partially turbulent at Re = 6000.

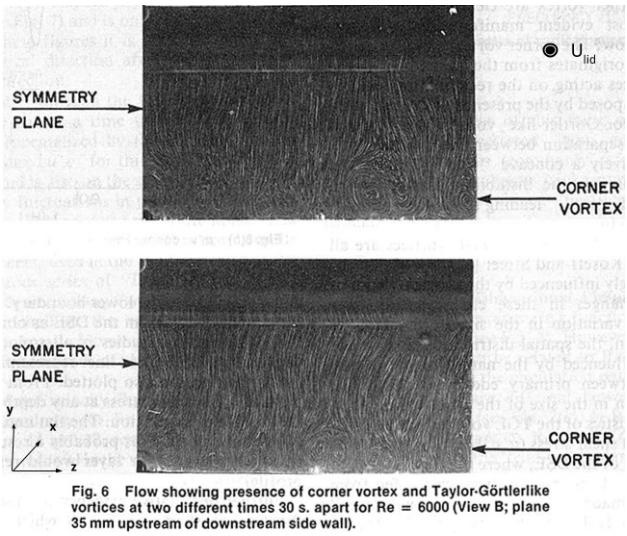

Figure 21: Span-wise streamlines of cubical lid driven cavity. Adopted from [27]

In the above fig (21) it can be observed that the size of the TGL vortices' vary along the span wise direction as well as with time, and hence the turbulent flow is anisotropic. The fluctuations in vertical direction were found to be 25 times higher than fluctuations in horizontal direction but along the span wise direction it was not measured. Based on equations (22, 26 & 23), the approximation from 3D $\rightarrow$ 2D, not only means reducing a dimension, but also changing the production and dissipation rates of the turbulent kinetic energy of the flow. In 3D, this can affect the temperature distribution across the interface.

4.2 SELECTION OF TURBULENCE MODEL

The selection criterion for turbulence model is already put forth in points(ii, iii & iv) of section (3.1.1) and points (i & ii) of section (3.1.2). In brief, the fluid flow is initiated by the wall and the turbulence inside the cavity is present near DSE and USE, while towards the center of the cavity and upper stream eddy, turbulence is decayed and the flow is laminar. Hence this would require turbulence model to capture the evolution of turbulence near the wall along with laminar flow towards the center. Further, it would be needed to incorporate stratification due the temperature difference inside the cavity and would need to provide an accurate computation of heat transfer prediction at the interface.

Various turbulence models in COMSOL differ significantly in two ways: 1) The way these models formulate the τ_{ij}, Reynolds stress tensor (in order to formulate turbulent eddy viscosity μ_t) and 2) The way they resolve the flow near the wall. The list of turbulence models offered by COMSOL is tabulated below:

Table 2: Turbulence model available in COMSOL

Model Name	Eddy Viscosity	Approach near the wall
Algebraic yPlus	$\mu_T = \rho l_{mix}^2 \frac{\partial U}{\partial y}$	no slip
Spalart Allmaras [48]	$\mu_t = \rho \tilde{\nu} f_{v1}$	no slip
$k-\epsilon$ [37]	$\mu_t = \rho C_\mu \frac{k^2}{\epsilon}$	wall functions
$k-\omega$ [54, 2]	$\mu_t = \rho C_\mu \frac{k}{\omega}$	wall functions
$k-\omega$ (SST) [37]	$\mu_t = \frac{\rho a_1 k}{max(a_1\omega, S f_{v2})}$	no slip
Low Reynolds $k-\epsilon$ [37]	$\mu_t = \rho f_\mu C_\mu \frac{k^2}{\epsilon}$	no slip

The standard turbulence models, $k-\omega$ and $k-\epsilon$, instead of resolving the flow near the wall, use analytical expressions derived from the law of the wall and then use this to model for the variables k, ω, ϵ and ν_T. There are two main reasons for using wall functions: firstly, in wall bounded flows, a large number of grid points are required to evaluate to resolve the flow near the wall [19]. Secondly, turbulence models are invalid near the wall region where Reynolds number are low and only the stress exerted on the wall is by viscous effects.[28, 11]. It is because at the walls the fluid velocity is zero, which implies both mean and fluctuations are set to zero.

$$\tau_{ij} = -\rho\overline{u'v'} = 0 \quad \because \bar{u} = 0, \quad u' = 0 \quad \bar{v} = 0, \quad v' = 0$$

A detailed explanation of fluid flow wall function and thermal wall functions used by COMSOL is provided in Appendix (A.2). Here some of the limitations of the wall functions implemented by COMSOL will be discussed :

- Wall functions in COMSOL, computes a vertical distance (δ_w) from the actual wall boundary. This corresponding enclosure is treated as the computational domain for the simulation. This undefined region during heat transfer acts as an isolation layer at all the wall boundaries. Thus, COMSOL may not be able accurately predict the heat flux at the interface.
- The Prandtl(Pr) of LiF–ThF_4 is 16.975, which is $\gg 1$. For a high Pr number, convective transport is much higher than conductive diffusivity. This implies that the derivation of thermal wall function, which assumes that Pr ≈ 1 [2], is not satisfied.
- In simulations for thermal buoyancy driven flows (unstable stratification), [22, 41, 13] and various other authors do not use wall functions.

Further, according to [37], implementation of Low Reynolds $k-\epsilon$ and $k-\omega$ (SST) requires an initial guess from $k-\omega$ and $k-\epsilon$ to achieve convergence. This implies that the success of these models will depend on how accurate the initial guess is. Also, this will increase the computational time due to an increased number of steps, thus the model chosen for further simulation is Algebraic yPlus.

4.3 ALGEBRAIC YPLUS MODEL

As explained previously, the instantaneous velocity can be computed as sum of mean and fluctuation. The RANS equation [53] for the flow mean can be written as:

$$\frac{\partial \rho\overline{u_i}}{\partial t} = -\overline{u_i}\frac{\partial \rho\overline{u_i}}{\partial x_i} + \rho g_i - \frac{\partial \overline{P}}{\partial x_i} + \frac{\partial}{\partial x_j}\left[\mu\left(\frac{\partial \overline{u_i}}{\partial x_j} + \frac{\partial \overline{u_j}}{\partial x_i} - \rho\overline{u_i' u_j'}\right)\right] \tag{27}$$

which indicates that the mean flow is governed by convective flux and the summation of forces acting on the fluid.

$$\Sigma F = \underbrace{\rho g_i}_{\text{gravity force}} - \underbrace{\frac{\partial \overline{P}}{\partial x_i}}_{\text{pressure force}} + \underbrace{\frac{\partial}{\partial x_j}\left[\mu\left(\frac{\partial \overline{u_i}}{\partial x_j} + \frac{\partial \overline{u_j}}{\partial x_i} - \rho\overline{u_i' u_j'}\right)\right]}_{\text{shear stress}}$$

Here, density ρ is a function of temperature, thus the gravity term is modelled according equation(20). Similarly, the equation for the mean temperature [22] can be described by :

$$\frac{\partial \rho\overline{T}}{\partial t} + \underbrace{\overline{u_i}\frac{\partial \rho\overline{T}}{\partial x_i}}_{\text{convective transport}} = \frac{\partial}{\partial x_i}\left[\underbrace{\frac{\mu}{Pr}\frac{\partial \overline{T}}{\partial x_i}}_{\text{conductive transport}} - \underbrace{\rho\overline{u_i' T'}}_{\text{turbulent transport}}\right] \tag{28}$$

where the term $\overline{u_i' T'}$ signifies the transport of energy due to temperature fluctuations.

Thus, in order to solve for the mean flow, mathematical relations has to be found for turbulent shear stress $\overline{-\rho u_i' u_j'}$ and turbulent heat flux $\overline{u_i' T'}$ in terms of known quantities

All the turbulence model in COMSOL, use Bousinessq approximation which models the $\overline{-\rho u_i' u_j'}$ as:

$$-\overline{\rho u_i' u_j'} = \mu_T\left[\frac{\partial \overline{u}_i}{\partial x_j} + \frac{\partial \overline{u}_j}{\partial x_i}\right] - \underbrace{\frac{2}{3}\left[\rho k + \mu_t \frac{\partial \overline{u}_i}{\partial x_i}\right]\delta_{ij}}_{\text{mean normal stress}}$$

Here, the subscript T denotes turbulence. For an incompressible flow ($\nabla.\overline{u} = 0$) this simplifies to:

$$\overline{-\rho u_i' u_j'} = \mu_T\left[\frac{\partial \overline{u}_i}{\partial x_j} + \frac{\partial \overline{u}_j}{\partial x_i}\right]$$

In Algebraic yPlus model, the eddy viscosity is defined as:

$$\mu_T = \rho l_{mix}^2 \frac{\partial \overline{u}}{\partial y} \tag{29}$$

where l_{mix} is the length in y- direction over which the fluid can retain their x-directed momentum [54]

For the turbulent heat flux, the approximation used is [2]:

$$\overline{u_i' T'} = \frac{\mu_T C_p}{Pr_T}\frac{\partial \overline{T}}{\partial x_i} \tag{30}$$

The physical interpretation of the approximation of equations (29 & 30)is that turbulent mixing of momentum and energy is modelled similar to molecular mixing. Thus, the Algebraic yPlus model does not model any fluctuation in the flow.

[2] this approximation is valid for all the turbulence model in COMSOL

Equation(29) can be made non dimensionless by using the following relations:

$$u^+ = \frac{u}{u_\tau} \; y^+ = \frac{yu_\tau}{\nu} \; \nu_T^+ = \frac{\nu_T}{\nu} \tag{31}$$

$$\left(1 + l_{mix}^{+^2} \frac{\partial u^+}{\partial y^+}\right) \frac{\partial u^+}{\partial y^+} = 1 \tag{32}$$

where u_τ is the friction velocity. It is used to scale the velocity of fluid. Since u_τ is interpreted as a scale for velocity, y^+ can be interpreted as a scale for local Reynolds number, such that y is the vertical distance from the wall. Now the model postulates the definition of l_{mix} based on Prandtl mixing length theory, which states that close to the wall mixing length (l_{mix}) is zero (because at the $\mu_T = 0$ and thus viscous effects dominate) and far away from the wall it is proportional to y^+:

$$l_{mix} = \begin{cases} 0 & y^+ < y^* \\ \kappa \cdot y^+ & y^+ \geq y^* \end{cases}$$

Substituting the above formulation in equation (32), and integrating for u^+ :

$$u^+ = \begin{cases} y^+ & y^+ < y^* \\ y^* + \frac{1-\sqrt{1+4\kappa^2(y^+-y^*)^2}}{2\kappa^2(y^+-y^*)} + & \\ \frac{1}{\kappa}\left(ln\left(\left(\sqrt{1+4\kappa^2(y^+-y^*)^2}\right) + 2\kappa(y^+-y^*)\right)\right) & y^+ \geq y^* \end{cases}$$

for large values of y^+, the equation can be rewritten as:

$$u^+ = y^* + \frac{1}{\kappa} log(y^+) + \frac{1}{\kappa}(log(4\kappa) - 1)$$

y^* is determined by comparing the above with equation(42) :

$$y^* = B - \frac{1}{\kappa}\left(ln|4 \cdot \kappa| - 1\right)$$

In order to complete the formulation , it is required to know y^+, which is given by local Re number:

$$Re = \frac{uy}{\nu} = \frac{u}{u_\tau} \cdot \frac{u_\tau y}{\nu} = u^+ y^+$$

$$= \begin{cases} y^{+^2} & y^+ < y^* \\ y^+\left(y^* + \frac{1-\sqrt{1+4\kappa^2(y^+-y^*)^2}}{2\kappa^2(y^+-y^*)} + .. \right. & \\ \left. ..\frac{1}{\kappa}\left(ln\left(\left(\sqrt{1+4\kappa^2(y^+-y^*)^2}\right) + 2\kappa(y^+-y^*)\right)\right)\right) & y^+ \geq y^* \end{cases}$$

This is solved for each node point using the relation:

$$Re = \frac{uy}{\nu}$$

where u is the local velocity, y is nearest distance to the wall.

4.4 BOUNDARY CONDITIONS

The simulation for melting is performed in two steps. The first step involves finding the initial condition in the cavity and the freeze plug. The time of simulation for this step is 2000s. The second step involves solving for the melting problem. The time of simulation for this step is 600s, which is the required response time for the freeze plug.

The boundary condition applied for these studies are:

- Fluid Flow: At the stationary wall:

$$\vec{u} = 0 \tag{33}$$

  At the moving wall:

$$\vec{u}.t = u_{lid} \tag{34}$$

  where t indicates tangential direction.

- Temperature

  For the initial condition, the following boundary conditions are applied:

$$T(x)|_{y=(l+D)} = T_\infty \tag{35}$$

$$T(x)|_{y=l} = T_m \tag{36}$$

$$T(x)|_{y=0} = T_{sub} \tag{37}$$

  At the four side walls, an insulated boundary conditions is applied:

$$\Phi = 0. \tag{38}$$

- Melting

  For this process, the four sides and the bottom wall(y=0), are considered to be insulated:

$$\Phi = 0$$

  At the interface

$$T(x)|_{y=l} = T_m$$

  At the moving wall:

$$T(x)|_{y=(l+D)} = T_\infty(t)$$

  Velocity at the interface.

$$\rho_s v_n \Delta H_{fus} = \Phi_l \cdot \hat{n} - \Phi_s \cdot \hat{n}$$

The crucial part of the implementation of the above set of equation is the interface velocity. As per the recommendation of [37], the standard constraints should not have time derivative. Thus, in order to compute the flux, weak formulation(for more details refer to [34, 20]) is used for the temperature constraint at the interface. Then, the variable T_{lm}

[3] represents the heat flux. In the weak form, the differential equation (27 & 28), to be satisfied at the interface, is converted into a integral equation. This integral equation is satisfied at each node, which implies the constraint is satisfied in an "average" sense. The advantage of implementing weak form of solution is that the heat flux is computed as a part of the solution. Following are the important aspects governing the implementation of weak form:

i The accuracy of the solution depends on the number of integral equation formed i.e number of the node points used for the interface

ii The shape of the solution is defined by the polynomial approximation (linear, quadratic cubic etc) used.

When it is possible to satisfy the constraint everywhere at the boundary then the weak and strong form of constraint would lead to the same result.

4.5 CASES

This turbulence model will be applied to study the research sub question (ii & iii) mentioned in section (1.5). The following cases are applied to basically answer the question at what Ri number would correspond to maximum melting of the freeze plug:

i Effect of Temperature Rise: Since the data from graph (7a) in chapter[1] is not very representative of the temperature rise of the fluid exactly above the cavity, and hence both the conditions of constant temperature and increasing temperature is considered for the geometry with aspect ratio =1 and B =0.2 m

ii Effect of Geometry: This effect is considered in three ways: 1) By keeping the cavity aspect ratio (A) same, where the aspect ratio is defined as follows:

$$A = D/B$$

This aspect ratio is set to 1, i.e the cavity is considered to be a square. 2) The width of the cavity is fixed at 0.2m, and then the depth of the cavity is increased from 0.2m to 0.3m 3) The depth of the cavity is fixed at 0.2m, and then the width of the cavity is increased 0.2m to 0.3m. Thus an aspect ratio from the range of 0.67 to 1.5 is considered.

iii Effect of Initial temperature distribution: This case is required to replicate the fact that initially there will be a flow of cold fluid over the freeze plug in order to maintain it's temperature below T_m. Thus, this changes the boundary conditions applied for side walls of freeze plug as:

$$\Phi = h \cdot (T - T_{air})$$

where T_{air} is the ambient air temperature equal to 298K and h is the heat transfer coefficient. The value of h = 113.6 [W/m^{2}K] for an air flow rate of $0.23 \cdot 10^{-2}$ m^3/s as shown in the graph (4b) in chapter[1].

[3] A due care is required when flux per unit area is evaluated using the weak formulation, for example in case of cylindrical geometry

4.6 MESH SELECTION:

In figure(22), the different types meshing considered for the above cases are shown. In this figure(22b)shows that a boundary layer mesh is used for cavity and a triangular element for freeze plug. A boundary layer mesh implies that, near the wall the elements are rectangular, while away from the wall, elements are triangular [6]. This is also the default mesh proposed by COMSOL when "physics induced mesh" option is chosen.

This was also the initial choice of mesh used for simulation. But the most common warning which occurred during the simulation was " inverted mesh elements near the coordinates.. ". This warning indicates the breakdown of mesh due to deformation such that it is wrapped "inside-out" leading to zero area in 2D. This causes a zero determinant for the jacobian matrix which maps local coordinates to global coordinates (for details refer section (A.3.2). According to COMSOL [37], as such, an occurrence of inverted mesh element do not pose a threat if the solution converges but it was observed that it caused breakdown in iterative solvers. Thus, the problem will be addressed by changing the mesh elements of the domain.

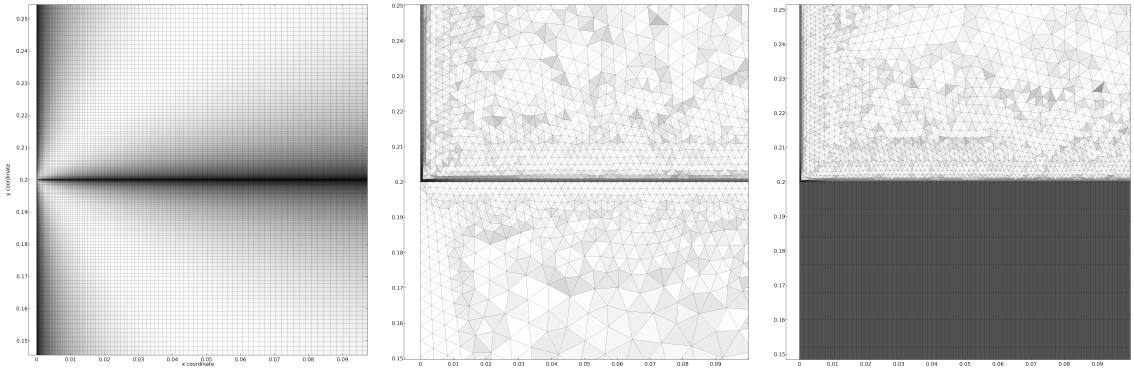

(a) MeshA **(b)** Mesh B **(c)** Mesh C

Figure 22: Quadrilateral mesh , Default, Mixed (respectively)

It is recommended by [37] to start with a mesh that is uniform in distribution. Further, it advices that a quadrilateral elements tends to perform better than triangular elements for deformed geometry. This was the motivation behind choosing option shown in figure (22a & 22c). For the case(i)(Effect of temperature rise), mesh configurations represented in figure (22a & 22b) were tested while for the case (ii), for square cavity with B=0.2, mesh configurations represented in figure (22c & 22b) were examined. For the case(iii) (Effect of temperature distribution), the mesh distribution shown in figure(22b) is used.

Grid dependency test was performed for time averaged velocity profile for isothermal lid driven cavity. These velocity profiles were derived in same way as explained for figure (23) in section (5.1.1). This was achieved for figure (22b) by generating grid choosing extra fine in the default option. The total number of mesh elements, for this option, in the entire domain for is 21281. In order to have a comparison between the meshes, the number of mesh elements for the geometry in figure(22a) is kept at 20,000. The number of elements along the interface for quadrilateral elements based mesh is 100 while the number of elements along the interface for boundary layer mesh is 150. This is an important part of the meshing, since it governs the evaluation of weak formulation.

5 RESULTS

This chapter is organized as follows: in the section (5.1), the turbulence model chosen in section (4.2) will be verified with the simulation results available from literature. The next section (5.2) explains the results of melting. Since the simulation is performed in two steps, in the beginning of the chapter, the initial condition in the cavity are explained. Then, the results based on the cases considered in section (4.5) are put forth.

5.1 VERIFICATION OF TURBULENCE MODEL

In order to benchmark the solution, it will be compared with isothermal lid driven cavity for Re = 10000. Here, comparisons will be drawn with the solution of 2D DNS results from [10] and [39] by comparing time averaged velocity profiles. In [10], a time dependent stream-function and vorticity-function form of the Navier-Stokes (NS) equation is solved with the objective of seeking a steady state solution. These equations are discretized based on finite difference method with pseudo time derivative approach. In [39], turbulence model of Wray-Aggrawal [43], Spalart Allmaras model [48] and SST $k-\omega$ [37] which is a combination of $k-\epsilon$ (away from the wall) and $k-\omega$ (near the wall), is used. All the three turbulence model used in the thesis [39], do not use wall functions. The simulation is carried out in OpenFOAM. This literature also compares its results with [10]. Since Wray-Aggrawal is not part of the RANS models offered by comsol, it will be excluded from the results.

5.1.1 Velocity profile

In figure (23), the time averaged velocity profiles of the turbulence models is shown. The vertical mean velocity vs x/B is plotted with axis marked red, while the horizontal velocity vs y/D is plotted with axis marked blue. The center of the plot is (0,0) and hence represents the center of the cavity. The horizontal velocity values are obtained at a vertical line passing through x=B/2, while the vertical velocities are obtained at a horizontal line at distance y= D/2 [1]. This graph can also be viewed as a qualitative graph which shows the direction change of the velocity components along the four walls of the lid. Thus, horizontal velocity component change direction from right to left when the flow moves from top wall to the bottom wall, while the vertical component change direction from downwards to upwards from the right hand side wall to the left hand side wall, which indicates the recirculation of the flow in the cavity.

[1] for notations of D,B refer figure (17), OF in the figure (23) indicates OpenFOAM.

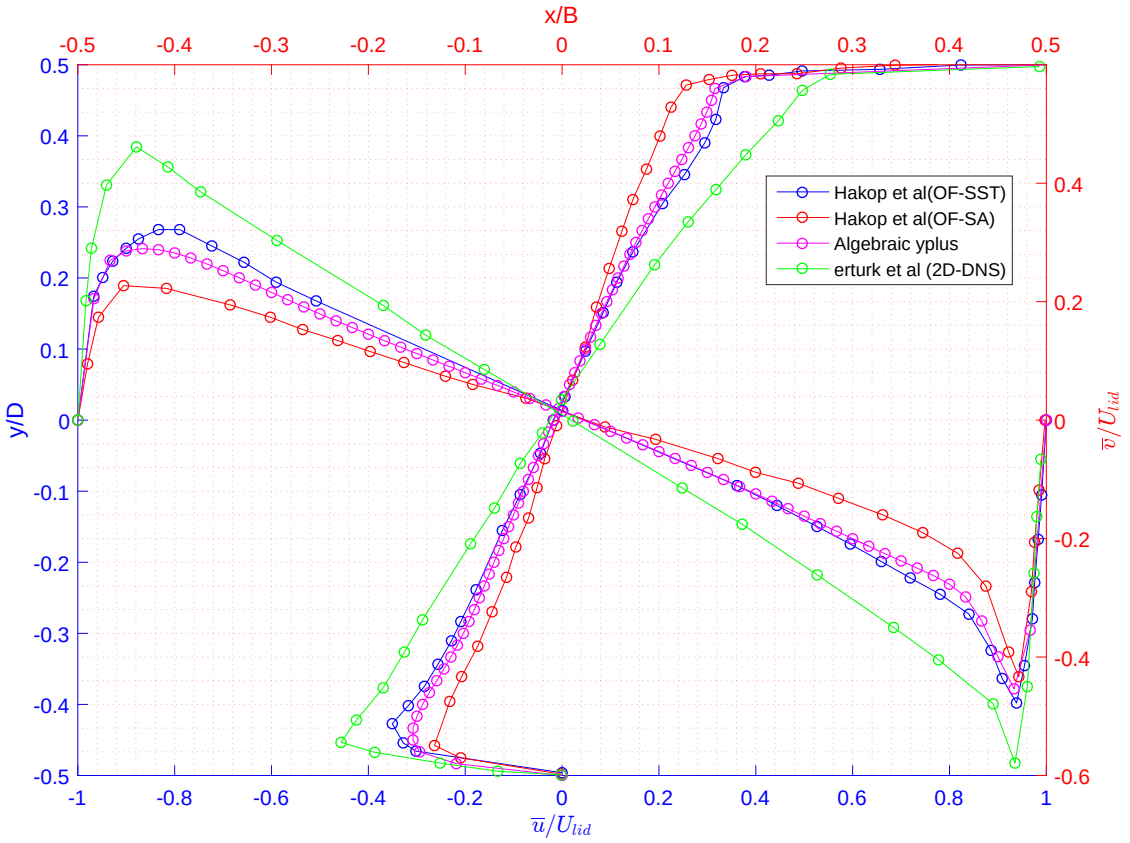

Figure 23: Comparison of normalised averaged velocity profiles for Reynolds Number =10,000 of algebraic yplus turbulence model with literature results of [10] and SST and SA model of [39]

Here, the observations will be divided into two parts : 1)Region near the wall and 2) Region far away from the wall. But the explanation will focus more on detailed understanding of the flow near the wall.

i Region far away from the wall: At the center of the cavity, it can be observed that the velocity predicted by different models is zero. This implies, due to the recirculation of the flow inside the cavity, as one approaches towards the center of the cavity, the fluid decelerates. This gradient of velocity predicted by different turbulence models are slightly different. In terms of the gradient of the velocity, algebraic yplus and SST model exhibit a very good correlation while SA model under predicts. As put forth in point(iv) of section (3.1.1) and above, towards the center of the cavity, the flow reverts to laminar regime. This would imply that the flow can be predicted by mean quantities. SA is a unique turbulence model because it derives a transport equation for ν_t [48]. It can be concluded that from above plot and table [2] that the viscosity value predicted by the SA model during the transition could be different than SST and Algebraic yplus model.

ii Region near the wall: In figure (23), this region is the part of the graph very close to the axes. In all the four near wall regions, a sharp gradients of horizontal (top and the bottom wall) and vertical(side walls) velocity components can be observed. The gradient close to wall predicted by the various turbulence models are in good agreement. These models use the exact boundary condition of no slip. As expressed in points (ii & iii) in section(3.1.1) of chapter [3], the features of lid driven cavity is due to no slip boundary at the wall.

But the most interesting aspect of this result is the comparison with the numerical simulation of [10]. In order to understand this, it will be emphasized again that turbulence by nature is 3D, and thus 2D turbulence, in most cases, is a purely mathematical concept. Thus in order to understand the deviation, it is important to understand what is the mathematical difference between both simulation.

Mathematically there are three possibilities for a solution [9]:

i The solution is steady i.e independent of time

ii The solution is unsteady but independent of time (i.e the flow is choatic)

iii The solution is unsteady and time dependent (i.e flow is periodic)

The solution of the equation of isothermal lid driven cavity cannot be of type (iii), because the boundary conditions applied are independent of time.

In literature[10], stream and vorticity forms of NS equation (written below) are modelled with the aim of seeking a numerical steady state solution, i.e solution of type(i).

$$\rho\left(\frac{\partial u_i}{\partial t}+u_j\frac{\partial u_i}{\partial x_j}\right)=\rho g-\frac{\partial p}{\partial x_i}+\mu\frac{\partial}{\partial x_j}\left(\frac{\partial u_i}{\partial x_j}+\frac{\partial u_j}{\partial x_i}\right)$$

where u is the magnitude of instantaneous velocity vector and subscript i,j indicate direction. At higher Reynolds numbers, the solutions of these equations are achieved by mesh refinement. Mathematically, the flow is not allowed to be chaotic [9].

In RANS simulations, it is assumed that the flow is unsteady but independent of time. This is indicated by the facts that the time averaged fluctuations are zero and the boundary conditions are independent of time. Thus this thesis, seeks a solution of type (ii). Here is the fundamental difference between both the flows. This difference can been observed by comparing the above equation with equation (27). Although, the time average of fluctuation is zero, its presence still affects the mean flow due to the contribution of Reynolds stress tensor. This effect in flow is accounted as shown in the mean flow equation (27). Now, comparing the solution of [10] and turbulence models in (23), it can be observed that near the side walls and the bottom wall, the following relation holds true :

$$|\vec{u}|_i > |\vec{u}|_{ii}$$

where i indicate the solution of [10] and ii indicate the solution of the algebraic turbulence model. Thus effect of $\overline{u_i'u_j'}$ in the mean flow equation (27) is to redistribute momentum [53].

For this thesis, the flow near the wall is of primary importance. An important conclusion from figure(23) is that, for lid driven cavity, the simple algebraic yplus model performs equivalent to a more complex SST model near the wall.

5.1.2 Qualitative Comparison with Experiment

In order to verify the algebraic model for stratification, a qualitative comparison of development of the flow with the experiment results of [25] is shown in figure(24) for time t= 10s, 20s and 40s. Since the experiment result is 3D while simulation is 2D, the flow is assessed qualitatively.

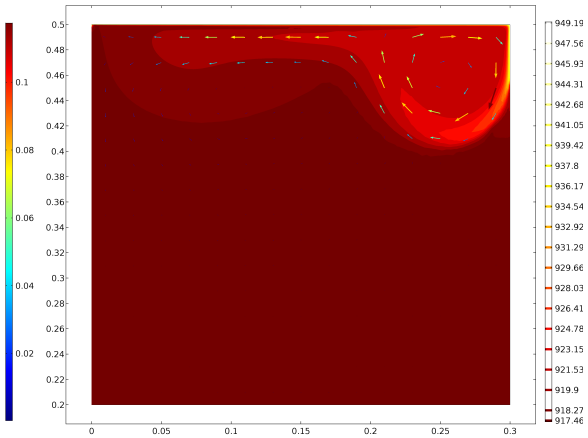

(a) Algebraic yplus: t=10s

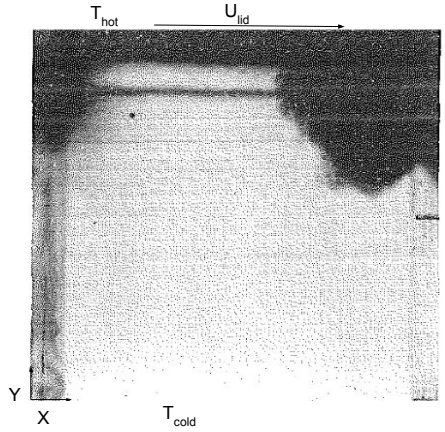

(b) Exp: t=10s

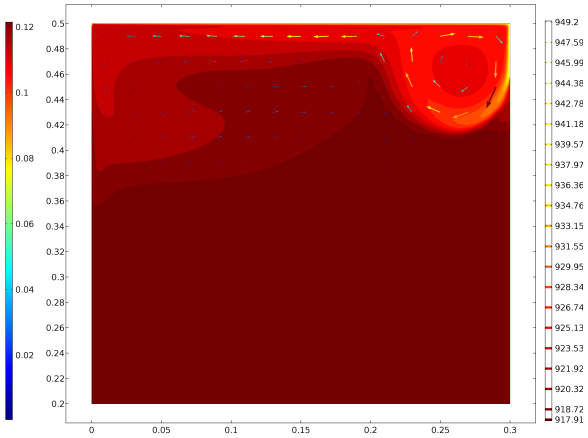

(c) Algebraic yplus: t=20s

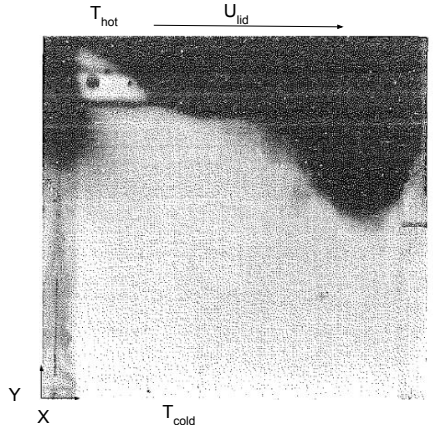

(d) Exp: t=20s

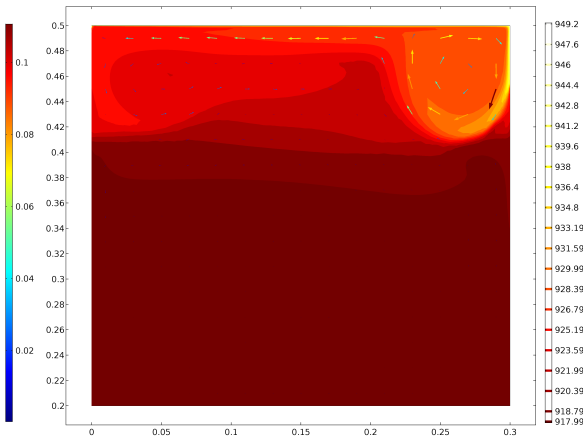

(e) Algebraic yplus: t=40s

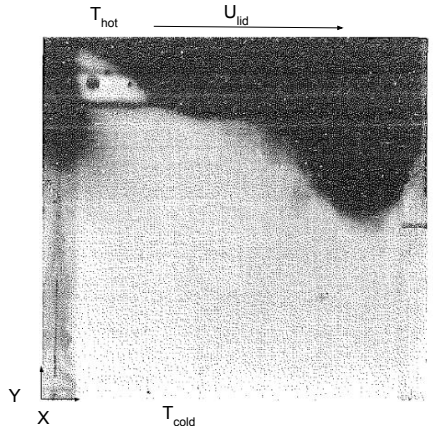

(f) Exp: t=40s

Figure 24: Development of Flow : Figures (24a , 24c & 24e) represents Comsol simulation for the following parameters: Re = 40,000 D= 0.3m, B =0.3m $\Delta T = 32K$ Ri =0.64, Figures (24b, 24d & 24f) represent the experiment results performed by [25] for the following parameters: Re = 10,000 D= 0.15m, B =0.15m $\Delta T = T_{hot} - T_{cold} = 9°C$ Ri =0.53

In figure (24a , 24c & 24e), the direction of the velocity is indicated by arrow plot and the magnitude is represented by the rainbow colour code. Inside the cavity temperature distribution is described using contour plots indicated by thermal colour code. For the graph pertaining to the experiment results (24b , 24d & 24f), the result shown at the symmetry plane (along the spanwise length (z)) of the cubical cavity. The direction of the

moving wall is indicated by U_{lid} and the temperature applied is indicated by T_{hot} and T_{cold}. The black region (thymol blue dye) traces the fluid flow in the cavity.

In figure(24a & 24b), it can be observed that initially, the flow is restricted in the vertical direction near DSE[2]. Further, there is a large temperature gradient from the top right corner of the cavity along direction of the flow. This is indicated by shift in colour from yellow → orange → red. Due to this temperature difference, the flow experiences a large buoyancy force and thus restricting further penetration into the cavity. Due to this effect, the flow directed in the horizontal direction which is indicated by direction of arrow velocity plot. This convection and the depth of penetration (D_p) of fluid flow is higher in figure(24b), possibly due to a lower Ri value.

In figure(24c), the temperature increase near DSE of the flow is now more prominent. The depth of penetration is the same when compared to t=10s. However, the flow has been directed completely towards the right hand side of the cavity, which is visible with a presence of a distinct isotherm when compared with figure(24a).There are two distinct differences between the comsol and the experimental results. Firstly, the profile of interface as depicted in figures (24a , 24c & 24e) is comparatively smoother than in figures (24b, 24d & 24f). Secondly, it can be observed in figures (24d & 24f), that the extent over which the flow is dispersed in the vertical direction, as one moves from right to left of the cavity when compared with figures (24c & 24e), is much larger. This specifically corresponds to region between 0.1 <x< 0.2 in figure (24c), the corresponding scale for the experimental results in not present. This dispersion is not predicted(qualitatively) by algebraic yplus model. This due to the fact that, there is no mean flow in this region, as observed from the velocity arrow plot. Thus, the turbulent viscosity in the near region, according to equation (29), is negligible. As a result of this, in figure (24c), the temperature near this vicinity is still closer to the initial conditions. Due to negligible fluid flow, the strength of buoyancy force is much higher than momentum.

In conclusion, from figure(24), the algebraic yplus will be able to model stratification. For Ri< 0.2, the physics of the flow is similar to isothermal lid driven cavity as explained in section(3.1.2). For isothermal lid driven cavity, from figure(23) it can concluded that the algebraic yplus model performs equivalent to a more complex SST model near the wall.

5.2 RESULTS FOR MELTING

The generic plot labelling for all the figure in this sections is as follows : - for the cavity: the contour plots of temperature is indicated by a thermal colour code along with the arrows plots of velocity vectors indicated by rainbow colour code. The relative sizes of these arrows indicate the comparative magnitude of the velocity. The purpose of the arrow plots is to show the relative strength of the flow field inside the cavity. The temperature distribution in the freeze plug is indicated by a surface plot of thermal colour code. It should be noted that these scales might be different for different result. The simulations are performed for a fixed Re= 40,000, expect for temperature rise which is performed for Re = 60,000.

5.2.1 Effect of Temperature Rise

The velocity profile shown in figure (25a) is plotted in a similar way as explained in the previous section, for two meshes(figures (A - 22a & B -22b)), considered for this simulation.

[2] DSE - Downstream Eddy , USE- Upstream eddy as shown in figure(16)

It can be seen that the velocity profile for both the mesh types A and B coincide with each other.

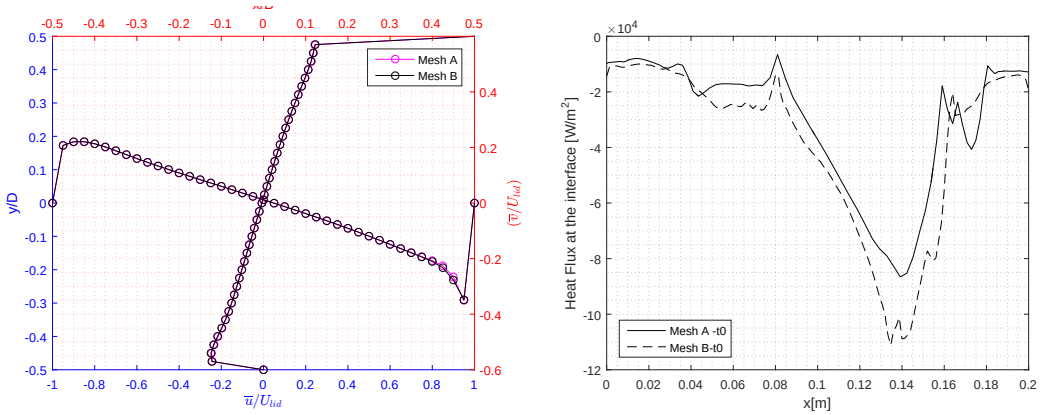

(a) velocity **(b)** Temperature

Figure 25: Figures (25a & 25b), shows temperature profile at the interface, and time averaged velocity profile in the cavity, similar to figure(23), for quadrilateral and triangular meshes respectively at time t =0 for melting simulation. Parameter Setting : Re =60,000 , Ri = 0.085, D=B= 0.2m

An interesting result can be observed for the heat flux values plotted in figure (25b). Here, the heat value at time t=0, i.e initial condition for melting, is shown against x (the length of the interface). The peak values do not coincide as one would expect, since the velocity profile for the cavity coincides. As explained before in section (4.6), in order to have a comparison between the meshes, the number of mesh elements in Mesh A and Mesh B is kept almost the same. However, the number of nodes along the interface for Mesh A is 100 while the number of nodes along the interface for Mesh B is 150. The effect of this difference can be understood by referring to the implementation of weak form in section(4.4). In weak form of constraint, the equation is evaluated at each node point in order to satisfy transport equations (27 & 28) with given the constraint($T = T_m$). For the Mesh A setting, the number of elements is symmetrically distributed in such a way that, as one proceeds to towards the center from the corner, the number of elements gradually decreases.The initial ideology behind this was to capture strong gradients of the flow on the side. However, this reduces the number of mesh nodes towards the center of the cavity. This also implies that the Mesh A setup by using mapped option, would require more number of elements to compute the heat flux at the interface when compared to default physics induced extra fine mesh (Mesh B).

Figure (26), represent time snapshots of melting of freeze plug at t=20s, 50s, 100s, 150s, 200s and 500s. In graphs (26a & 26b), it can be observed that the velocity profile still follow the features of lid driven cavity mentioned in section (3.1.1). This is due to the fact that initial (at t=0) Ri = 0.085. But the magnitude of velocity, near the center of the interface (between $0.08 < x < 0.12$), decreases from 0.15 m/s to 0.1 m/s from t =20s to t=50s. Thus, in this case, the fluid starts to decelerates as the melting progresses. In graphs (26c & 26d), it can be observed the penetration depth of the fluid flow decreases as time progresses. In graphs (26e & 26f), the flow is completely stratified, and the melting progresses because of conduction.

From the temperature contour plots of (26a ,26c, 26d & 26b), it can be observed that, although the temperature rise along the fluid flow (Downstream eddy DSE and Upstream secondary eddy USE) is very predominant, the temperature near the right hand bottom

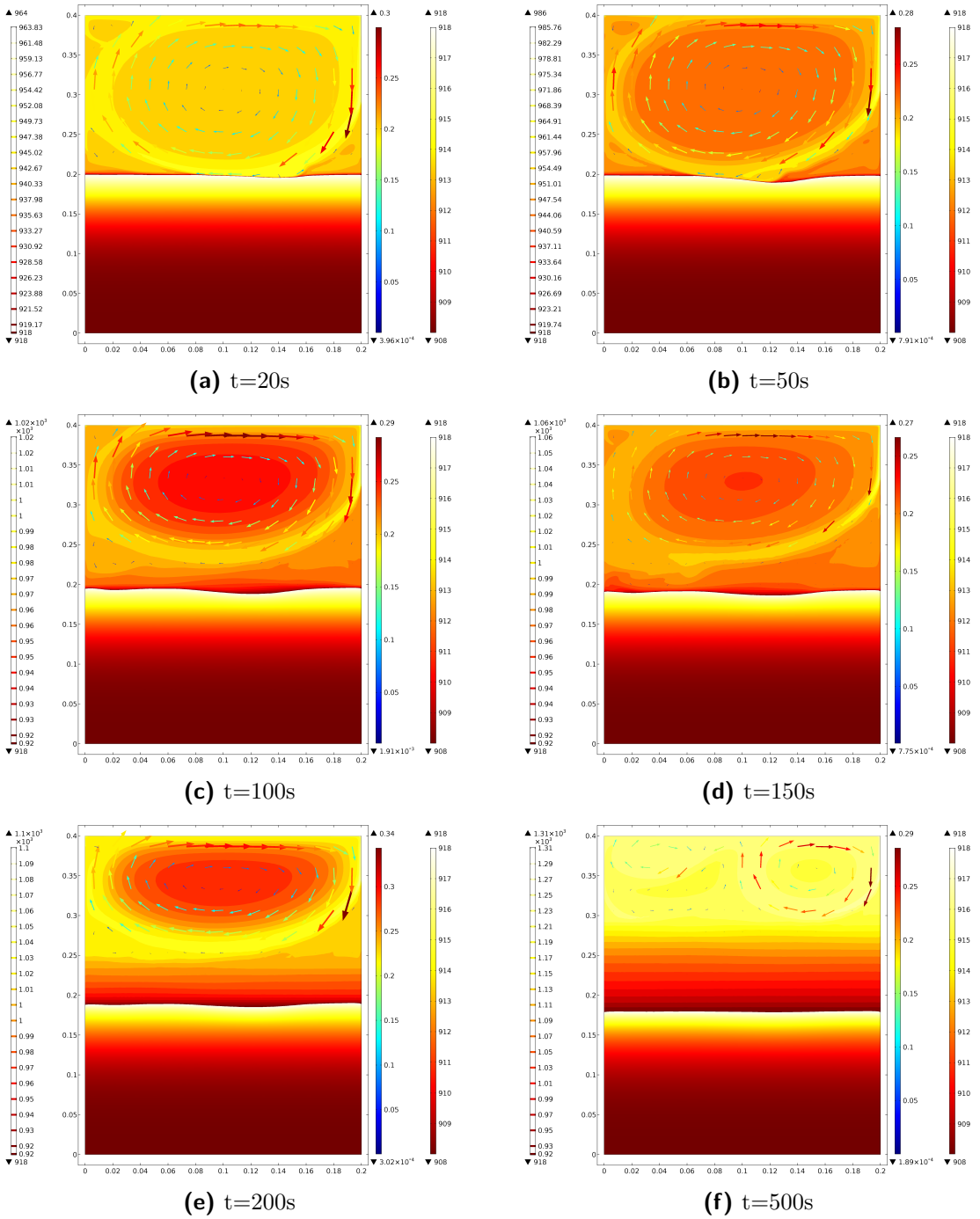

(a) t=20s **(b)** t=50s **(c)** t=100s **(d)** t=150s **(e)** t=200s **(f)** t=500s

Figure 26: Time snapshots of the melting due to temperature increase at the moving wall. Parameter Setting : Re =60,000 , Ri = 0.085, D=B= 0.2m
. Note the change in scale for temperature labels for cavity and freeze plug.

end of the cavity does not rise as quickly as rest of the cavity. This creates a large local temperature difference near DSE. As understood in point (i) in section(3.1.1), the fluid flow is initiated along the side wall of the cavity. Further, due to the boundary condition of increasing $T(t)_\infty$, the temperature along this side wall increases. Due to this local increase in temperature difference, causes an increase in local buoyancy force (and hence high Ri), which cause stratification of the flow along the DSE. Due to the reduced penetration depth, it prevents further distribution of the temperature due convection near the interface.

The following effects on the heat flux (Φ) at the interface is shown in figure (27).For the time being, the focus will be on heat flux evaluated from triangular mesh indicated by legend Mesh B in figure(27) and dotted line. It can observed that the initial peaks of heat flux correspond to the presence of the fluid flow near the interface region. This peak value increases for t= 20s to t=50s, despite decrease in velocity as observed previously. This is due that fact temperature near the interface increases from 940 K to 958 K. This was the effect, which was expected from lid driven cavity for improving the melting time when compared to the case of conduction. However the heat flux later reduces due to stratification. On the side of the interface, in absence of fluid flow, the magnitude of the heat flux is considerably lower. As time progress, due to stratification, a considerable drop in the peak heat flux can be seen.

In summary

$$T(t)\uparrow \implies Ri_{local}\uparrow \implies |\vec{u}|_{local}\downarrow \implies \Phi_l\downarrow \implies v_n\downarrow$$

Thus, now it is of interest to find what would be the best condition suitable for melting. For this purpose, the temperature at the moving wall will be assumed to be constant.

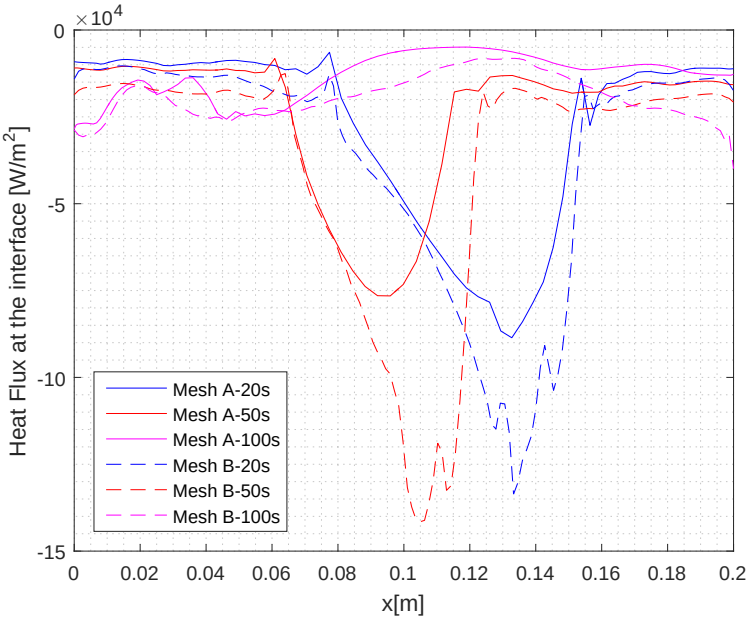

Figure 27: The above graph shows the heat flux values at the interface for time t= 20s, 50s and 100s as f(x) for quadrilateral and triangular meshes.

Further, in figure (27), it can be observed that for time t=20s and 50s, Mesh B, produces a sharp dip near the peak heat flux value (at x $\backsim$ 0.15) , which is less sharp in Mesh A. It should be highlighted here again that Mesh B, for the cavity region uses a boundary layer mesh incorporates rectangular elements near the wall boundary. But for the freeze plug region it uses triangular mesh everywhere which is the difference between the two types of meshes at the interface. Thus, this motivates us to choose a mixed mesh setting, Mesh C, as shown in figure (22c) for square cavity.

5.2.2 Effect of Geometry

In this section, first the melting simulation of a square cavity of D=B= 0.2 m will be put forth. Once the melting in square cavity is completely understood, a comparison of the

steady state solution obtained from different configuration will be compared with square cavity. Following this,the progression of melting for different aspect ratio can be evaluated.

Square Cavity

It was proposed in the previous section that use of mesh C, will bring an improvement in evaluation of heat flux at the interface. This can be clearly observed in figure(28a & 28b). This is due to the fact that the mesh in freeze plug domain is now mapped with 150 nodes using quadrilateral elements, which is also used for boundary layer mesh in the cavity. Thus, the number of nodes at the interface are equal to achieve a grid independent result for the heat flux.

However, unfortunately mesh C possess a different kind of problem. Using the same solver and the tolerance setting, the Mesh C, the solver crashes down after time t= 490s due to inverted mesh elements(A.3.4) while for Mesh B the solver is stable for the total time of simulation of t=600 secs. Thus, the time averaged of heat flux shown in figure(28b) is up to time t=450s using time step of 10s. It can be concluded that comsol's recommendation of using quadrilateral mesh for mesh translation does not seem to work for this particular case.

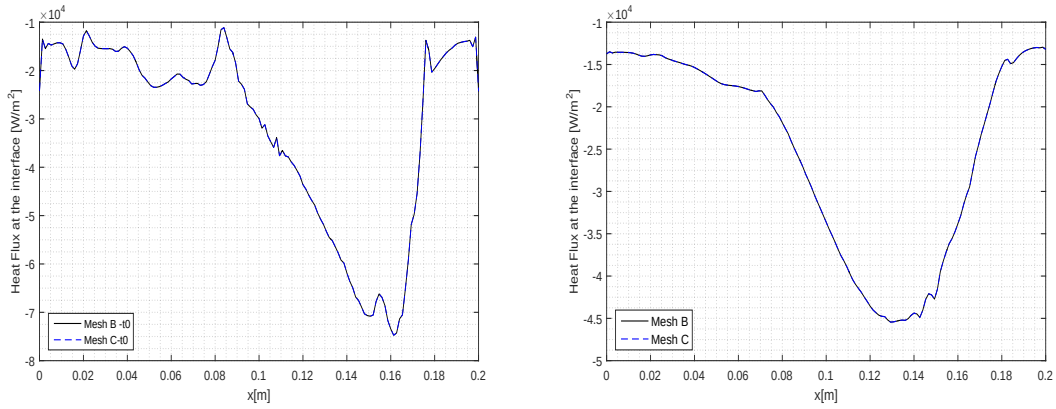

(a) t=0 **(b)** time averaged

Figure 28: In figure(28a), heat flux is evaluated for Mesh B and Mesh C at time t= 0. In figure(28b), heat flux is time averaged at each on the node at the interface for Mesh B and Mesh C. Parameter Setting : Re =40,000 , Ri = 0.19, D=B= 0.2m

In figure (29a & 29b), the development of melting can be visualized. The material from the freeze plug is removed like erosion due to fluid flow from above. Throughout the simulation, the melting is maximum occurs in between the DSE and USE. It can be also observed that the melting near the corners of the cavity (y $\approx$ 0.18 at t= 600s in figure (29b) is very low. Thus the corner of freeze plug still does not melt as fast as it is intended too. A special feature in the flow profile can be observed in figure(29a). Due to the curvature of melting, the flow separation near USE region is closer the side walls of the cavity. In figure(29a), the flow separation is caused at x $\backsim$ 0.08m while in figure(29b), this is shifted to x $\backsim$ 0.04m. It can also be observed that the magnitude of velocity, above the interface, has increased slightly. Unfortunately the magnitude of heat flux is still not large enough to cause faster melting.

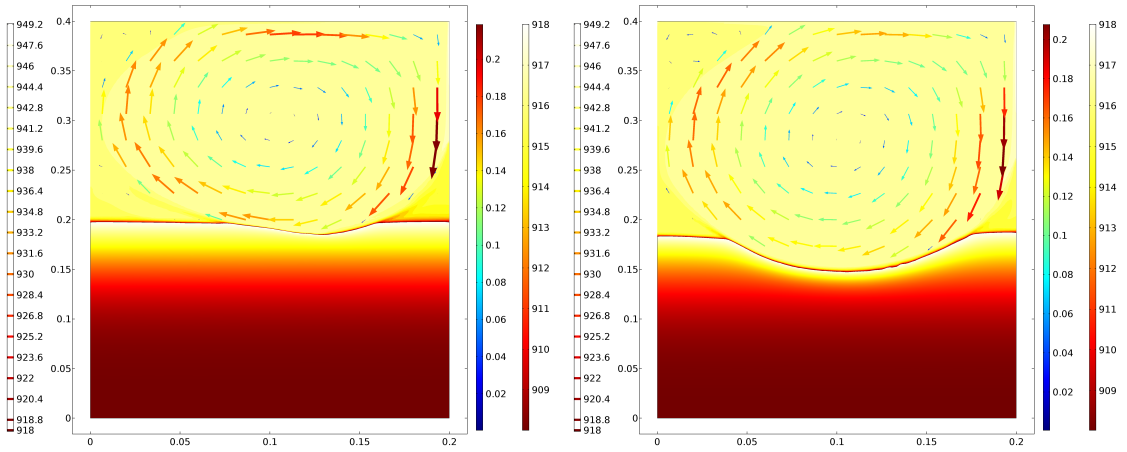

(a) t= 100 s **(b)** t= 600 s

Figure 29: Development of melting: time snapshot at t=100s and t=600s for square cavity A=1 D=B=0.2m. Note the change in scale for temperature labels for cavity and freeze plug.

In figure(30a & 30b), the values of the time averaged total heat flux at the interface and heat flux due to temperature gradient in the freeze plug is plotted respectively. This value is collected at time step Δt =10s for every node along the interface and then mean is evaluated. Figure (30b) is presented here only to gain more insight about Φ_l.

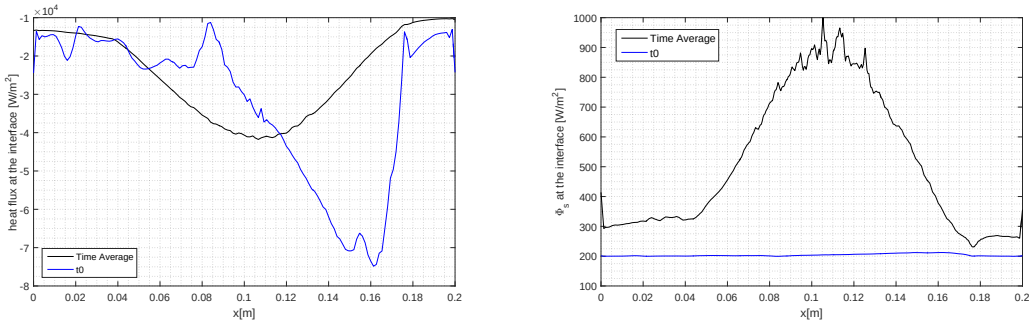

(a) Heat flux at the interface (Φ) **(b)** Heat flux in the freeze plug (Φ_s)

Figure 30: Comparison of time averaged heat flux (total heat flux in figure(30a) and heat flux from the freeze plug figure(30b)) with respect to respective heat flux at time t=0.

Thus, figure(30a) will be discussed in which following observations can be made:

- The peak value of the heat flux decreases from $\Phi = 7.5 \cdot 10^4$ [W/m^2] to $\Phi \approx 4 \cdot 10^4$ [W/m^2]. This is partly due to the fact maximum heat flux in freeze plug also increases as shown in the figure(30b). The magnitude of the heat flux indicates that the rate at which the freeze plug is being melted, is faster than the conduction mechanism inside the plug. But the more dominating effect for this can be observed in figure(29b). At the interface layer, in region $0.04 < x < 0.016$, the temperature drop is indicated by the presence of thin layer of red colour. Due to this, Φ_l also decreases significantly. Hence, as the melting progresses, there is evolution of temperature gradient at the liquid interface, which is not overcome by the presence of fluid flow. The contribution to the total heat flux comes from conductive, convective and turbulent heat flux. In the mixing length, the boundary layer, within which viscous effect dominate and the

heat transport is driven by conduction, is governed by fluid flow. The thickness of this boundary is determined by:

$$y = \frac{y^+ \nu}{u_\tau}$$

$$y^+ = B - \frac{1}{\kappa}\left(ln|4 \cdot \kappa| - 1\right) = 5.2 - \frac{1}{0.41}\left(ln|4 \cdot 0.41| - 1\right) = 6.23$$

$u_\tau = 0.012$m/s at t=0 at the center on the interface. Therefore,

$$y = \frac{6.23 \cdot 2.7 \cdot 10^{-6}}{0.012} = 0.0014m$$

This thickness is very close to the depth over which temperature distribution influenced in melting driven by conduction (refer to the figure(14) in chapter[2]). For a high Prandtl number ($LiF-ThF_4$ is 16.975), the thermal sub-layer is much closer to the wall than the momentum sub-layer thickness. Thus, the algebraic yplus turbulence model does not take the affect of thermal boundary layer into account.

- A shift in the peak value of $(\Phi_l - \Phi_s)$ can be observed such that it moves from x= 0.16 to x $\backsim$ 0.125. It can also be the seen the time averaged heat flux curve becomes boarder. This is in accordance the progression of melting which shown in figure (29a & 29b). This is due to the curvature of melting and the corresponding change in the flow near the DSE and USE region.
- A third observation can be made for the heat flux at the extremes. Between, 0<x< 0.04, it remains close to the initial condition. In figure (29b), it can be seen that in the same region Φ_s increases, which implies that the Φ_l value must also increase.

Thus, it can be concluded that an increase in heat flux in the freeze plug (Φ_s) and decrease in total heat flux Φ during the melting process, increases the time taken to melt. Due to lower magnitude of heat flux near the corners of the cavity, corners of the freeze plug melt slowly.

Root Cause Analysis

An important aspect in all the heat flux graphs previously presented (27, ,29a, 29b, 30a & 30b), is the presence of intermittently fluctuating values of heat flux. In particular this can be seen in (29b) between 0.8<x<0.14.

A root cause analysis was performed in order to pin point where the problem could be. A schematic of such root cause analysis is depicted in figure(31)

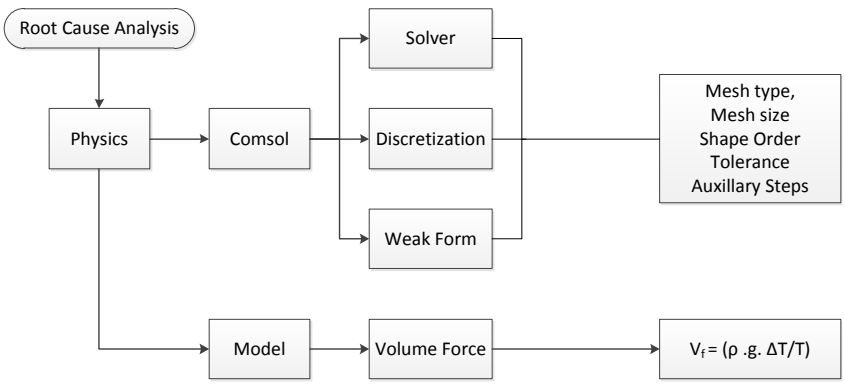

Figure 31: Root-Cause Analysis performed to determine the cause of spikes in the heat flux values.

The possible cause for this could be either model induced or comsol induced. According to physics, a dirichlet boundary condition is imposed at $T = T_m$, while due to fluid flow above, the temperature very near to the wall is $T \approx T_\infty$. This creates an extremely high temperature gradient, in the y direction, over very small distance. Further, the curve appears to have sharp point only at certain points in the interface. Here, a step by step analysis will be performed in order to check if this behaviour originates from comsol. According to [7], a large gradient introduced by applying a Dirichlet boundary condition, which results in a steep gradient near the boundary can cause numerical issues. But this could be overcome if the cell Peclet, defined below, is less than 1:

$$Pe = \frac{|\vec{u}|h}{2D} < 1$$

where, D is the diffusion coefficient of the transport equation, and h is the size of the mesh. This condition is not satisfied near the interface boundary, where Pe $\approx$ 210.8. The number of mesh required to satisfy this criteria would be:

$$h < \frac{2\mu}{|\vec{u}|} \implies h < \frac{2 \cdot 2.7 * 10^{-9}}{0.2} \implies h < 2.7 \cdot 10^{-8}$$

This is an extremely impractical mesh size. Thus, the solution to this issue is partly addressed by introducing stabilization methods in comsol as put forth in [7]. The other part can be controlled changing the parameters of mesh and solver by a trial and error an approach.

It was found that the following steps are not the solution for this:

- These spikes are present in all the type of Mesh A, Mesh B and Mesh C distribution (28a). Thus this cannot be due to the use of triangular or quadrilateral mesh elements.
- This is also could not be improved due to the resolution of the mesh. The number of mesh elements for Mesh A configuration was increased up to 300 nodes at the interface but this problem still exists.
- Increasing the tolerance setting to evaluate the heat flux from 10^{-3} to 10^{-4} for an improvement in the solution was also in vain.
- Third parameter which was changed was the order of polynomial used for discretization of velocity, pressure and temperature. The default order of discretization in COMSOL is linear (order =1) for all three variables. This implies that the shape functions which is used to describe the temperature distribution could show local fluctuations due to high gradients. This was changed to third order for velocity, second order for pressure and third order for temperature. Since an improvement could not be made using more number of mesh elements and changing the order of elements, these oscillation are not due to weak formulation.
- In order to decrease the convective effects which governs the Peclet number as mentioned above, Reynolds number is modified by auxiliary step for the simulation. Here, the initial solution is guessed for Re = 10,000 and then with a step 10,000 increased up to 60,000.
- Finally, the last iteration was performed to reduce non linearity in NS equation and mesh size requirement, was through viscosity ramp up. Similarly to above approach, initially the flow is solved for fluid with kinematic viscosity $10^3 \cdot \nu$ and then gradually reducing it in steps of 500, 250, 100, 50 and 1.

The above iterations might imply that these may results of numerical oscillations may not be improved by due to COMSOL. The percentage variation density due to extremely high temperature gradient, in the over small distance in y direction, can be evaluated as:

$$\frac{\rho(T)-\rho_0}{\rho_0} = (\beta\Delta T)\cdot 100 = \beta(T_\infty - T_m)\cdot 100 = 2.82\%$$

The density variation due the temperature in the simulation is taken into account only in form of buoyancy force. Thus, a possible source of local fluctuations could be due to the Boussinesq approximation in the model:

$$V_f = \rho_0 g\beta\Delta T$$

This approximation in only valid when the perturbation in temperatures are small [53]. Thus due to large ΔT, near the boundary, a large volume force is experienced which could effect the mean flow equation (27), leading to spikes in the numerical solution.

Having been unable to improve the heat flux distribution, a work around this was tried to be implemented. These spikes in the heat flux values causes discontinuity in the curvature of the deformation which eventually leads failure in meshes. Comsol offers a tuning parameter with the help of which the curvature of the mesh can be made smoother. This is given :

$$\frac{\partial X}{\partial t}.n = v_0 + \delta_0|v_0|hH$$

where X represent material coordinate of the point in comsol, v_0 is the prescribed mesh velocity given by equation(7), δ_0 is tuning parameter, h is the size of the mesh and H is surface curvature of the mesh. The default tuning parameter of 0.5 was chosen. The time step used during the simulation was 0.05 which is extremely low. Thus, in further simulations, Mesh B type is be used since this allows mesh deformation for the required time of simulation when compared to Mesh C. The time of simulation is lower when compared to implementing boundary smoothing.

Based on figure (23 & 15b), it could be said that, since the velocity profile evaluated by comsol is consistence with the literature results, the heat flux estimate by above results, must be of correct orders of magnitude. Thus, the results derived from these would still represent true picture about the flow and the melting of the plug.

5.2.3 Steady State

In section, effect of different varying cavity size (i.e diameter and depth) will be studied. Using the understanding of the melting in square cavity, the effect of geometry can be established from the flow profiles. The flow influence of velocity profile on the magnitude of heat flux graphs evaluated at the interface for different configuration using equation (28).

$$\frac{\partial\overline{\rho T}}{\partial t} + \underbrace{\overline{u_i}\frac{\partial\overline{\rho T}}{\partial x_i}}_{\text{convective transport}} = \frac{\partial}{\partial x_i}\left[\underbrace{\frac{\mu}{Pr}\frac{\partial\overline{\rho T}}{\partial x_i}}_{\text{conductive transport}} - \underbrace{\overline{\rho u_i' T'}}_{\text{turbulent transport}}\right]$$

In this equation it was established that the temperature distribution depends on the conductive transport, convective transport and turbulent transport. Temperature distribution near the interface will determine the magnitude of heat flux. This will directly help in comparing the melting time due equation (7).

$$\rho_s v_n \Delta H_{fus} = \Phi_l \cdot \hat{n} - \Phi_s \cdot \hat{n}$$

Figures (32a, 32b & 32c) represent square cavity (A=1) with a variation in diameter(B) of 0.2 m, 0.25m and 0.3m. The figure (32e & 32g) represents extremities of rectangular configurations (depth(D)) with dimensions D=0.2m, B= 0.3m and D=0.3m, B= 0.2m respectively. Besides these, figures (32d, 32f & 32h), represent the heat flux at the interface (for corresponding configurations) against normalized distance. Thus, $x - \overline{x} = 0$ would correspond to the centers of the interface, -0.5 is left end while 0.5 is the right end of the interface. The highest value of Ri is 0.644 which is obtained for the configuration of A=1 , D= 0.3 , B=0.3.

The heat flux graphs for the parameter varied can be understood based on the corresponding flow profiles and temperature distribution shown besides it.

Initially A =1 (Square cavity) will be studied from figure (32d). At the center of the cavity corresponding to $((x - \overline{x}) = 0)$, the following relationship holds true:

$$\Phi_{B=0.2} \gg \Phi_{B=0.25} \gg \Phi_{B=0.3}$$

This happens because from the figures (32a, 32b & 32c), at this region, it can be observed[3] that the magnitude of the velocity decreases:

$$|\vec{u}|_{B=0.2} > |\vec{u}|_{B=0.25} > |\vec{u}|_{B=0.3}$$

This means that the convective transport of energy reduces near the bottom of the cavity. This is also reflected in the as one moves towards USE $(-0.5 < (x - \overline{x}) < 0)$. Thus, increasing the size of the cavity decreases the magnitude of the peak heat flux. As we move towards the DSE $((x - \overline{x}) > 0.3)$, the above relationship for becomes:

$$\Phi_{A=1} > \Phi_{A=0.8} \approx \Phi_{A=0.67}$$

Further this magnitude is equivalent on the both end sides of the cavity. This is due to the fact that, near the flow separated region at DSE and USE, the magnitude of temperature is lower near the corners than the rest of the interface as the size of the cavity is increased.

From these, it can concluded that the melting will progress even slower if the size of the cavity increased keeping the aspect ratio constant.

Now, the affect of increasing diameter can be studied using (figure 32f). At the center of the cavity, the following relationship holds true

$$\Phi_{A=1} > \Phi_{A=0.8} \approx \Phi_{A=0.67}$$

This is because of the fact that increasing the diameter of the cavity leads to the formation of counter rotating eddies (in B>0.2m). Further it can be observed that the peak heat flux values which corresponds to the strength of the primary circulation remains the same. As we move towards the DSE $(x - \overline{x} > 0)$, the above relationship for the peak heat flux becomes:

$$\Phi_{A=1} \approx \Phi_{A=0.8} \approx \Phi_{A=0.67}$$

Thus increasing the diameter does not decrease the peak heat flux but distribution of heat flux over the interface becomes narrower. The above mathematical relationship is also true for the corner near the DSE. Thus it implies that the formation of the secondary eddy does not contribute in increasing the heat flux near the corners of the cavity.

[3] Be aware that there is a change in scale for the velocity profile in each of the figure despite the colour code being the same.

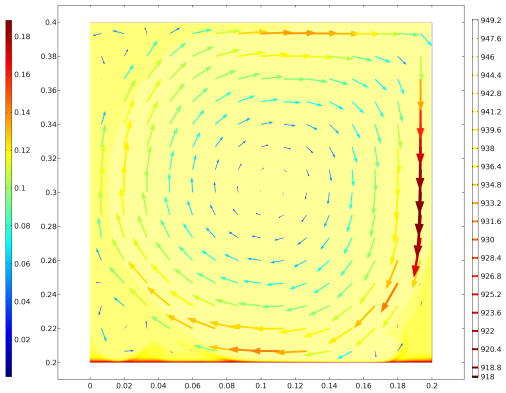

(a) A=1, B=D= 0.2

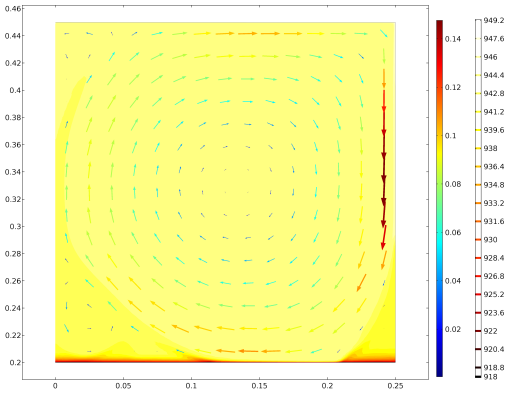

(b) A= 1 , B=D= 0.25

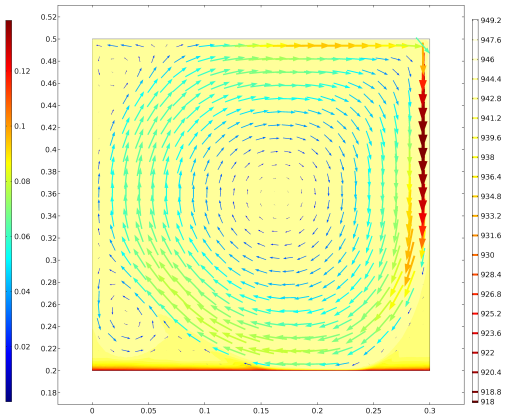

(c) A= 1, B=D= 0.3

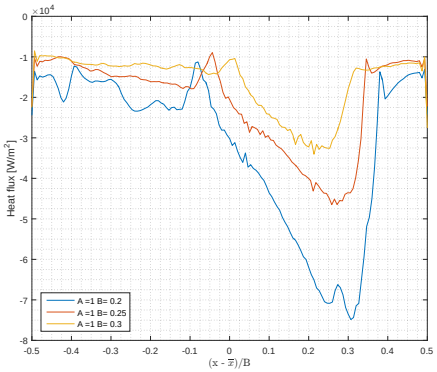

(d) Φ for A =1

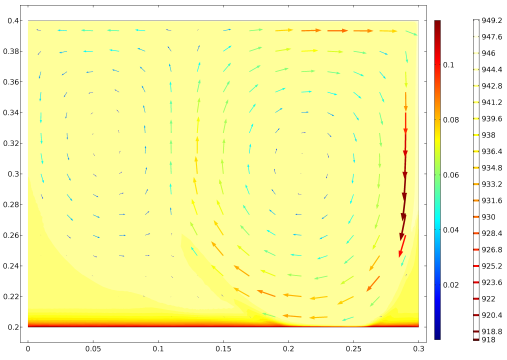

(e) A= 0.67 , B= 0.3 D= 0.2

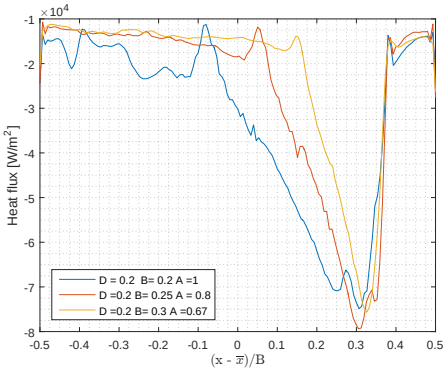

(f) Φ for constant D, change in B

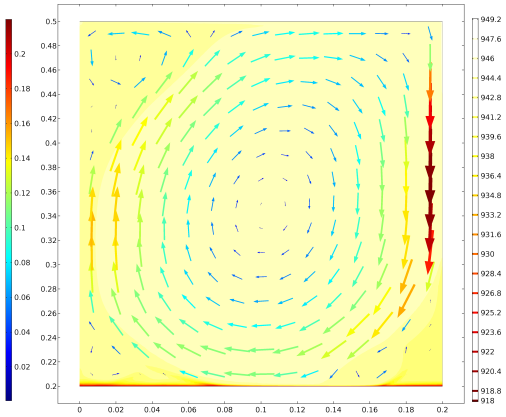

(g) A= 0.15 , B= 0.2 D= 0.3

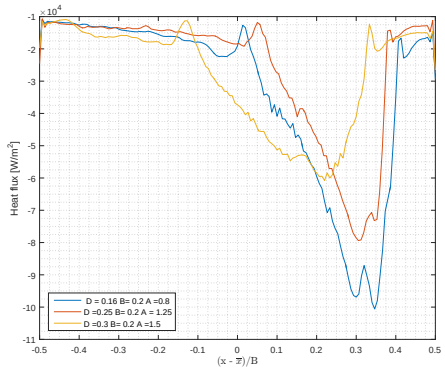

(h) Φ for constant B, change in D

Figure 32: Initial condition inside the cavity for melting considering different dimensions. This correspond to time t= 2000s for step 1.

Now, the focus will shift to studying the effect of increasing the depth of the cavity using (figure 32h). It is clear from the graph that:

$$D \uparrow \implies \Phi \downarrow$$

This is due to the fact that magnitude of velocity near the interface decreases and thus reduces the strength of convective flux.

$$|\vec{u}|_{D=0.2} > |\vec{u}|_{D=0.3}$$

Further, it is observed that increasing the depth causes a shift the peak of the heat flux curve towards the center of the cavity. As we move towards the DSE and USE, the following relation holds :

$$\Phi_{A=0.28} \approx \Phi_{A=1.25} \approx \Phi_{A=1.5}$$

As understood from the melting simulation of a square cavity, the most important region in fluid flow which governs the melting is the DSE and USE. These region influence the heat flux value the most. From the above figures it can be observed that different configuration exhibit different temperature distribution specifically near the interface region but not positively. It can be concluded that unless the depth of the cavity is reduced, i.e. the plug is placed closer to the core, the melting will progress slower in different geometric configuration when compared to square cavity due to decrease in magnitude of heat flux. Further changing the geometrical aspects of the cavity, does not contribute to increase in the heat flux near the corner which implies that the corner melting problem will persist.

5.2.4 Effect of Temperature Distribution

In figure (33b), isothermal contours for freeze plug is plotted at time t=0 for case 2 (Case 2 is explained in section (4.5)). In this case, the isothermal contours are semi circular in nature due to cooling from the sides while in figure (33a), for case 1, they are linear because a lower temperature is maintained at the bottom wall. For case 2, the temperature of the freeze plug decrease from T_{sub} to $T \approx 400$ K as one moves away from the center to the side walls ($\implies \Phi(x)_s \uparrow$). Since the boundary conditions for the cavity remain the same, the initial conditions inside the cavity is not affected ($\implies \Phi_l$ remains the same).

In figure (34a & 34b), it can be observed that the velocity profile near the DSE remains the same in both the cases. But, a difference in the upstream eddy near the left hand side wall can be observed. At y=0.3m the magnitude of the fluid velocity is much lower for case 2 when compared to case 1. But this change does not affect the melting of plug. As shown in graph (35), the magnitude of the heat flux, for both the case is highest near to the center of the cavity. Thus the melting near the center of the plug in not greatly affected.

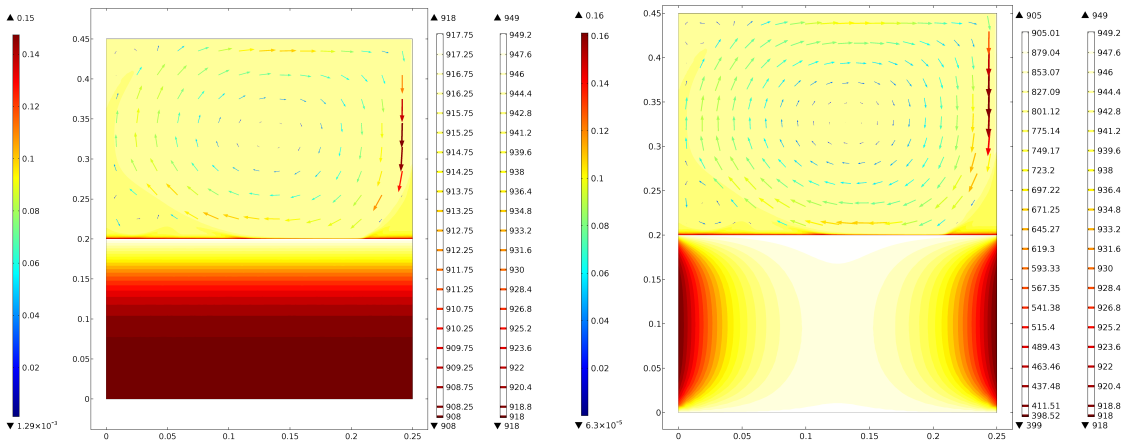

(a) Case 1 **(b)** Case 2

Figure 33: In fig(33a & 33b), the initial condition of temperature distribution is cavity and freeze plug and the velocity profile in cavity is shown.

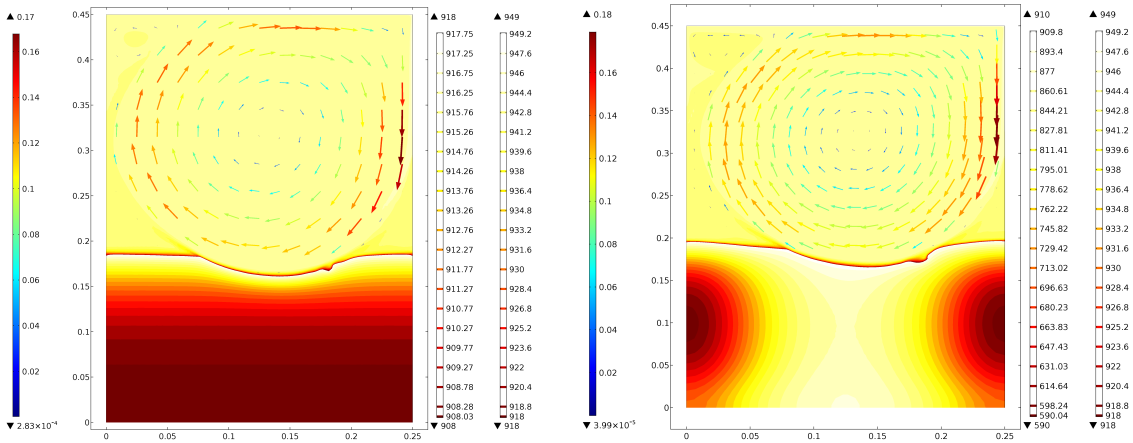

(a) Case 1 **(b)** Case 2

Figure 34: In fig(34a & 34b), the temperature distribution inside the cavity and the freeze plug and the velocity profile in cavity is shown along-with the melted freeze plug at t= 600s. Note the change in scale for temperature labels for cavity and freeze plug.

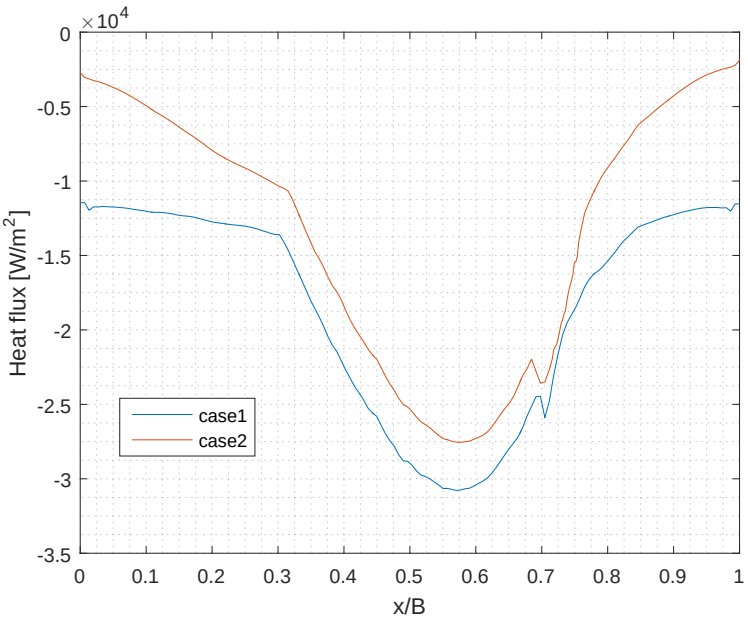

Figure 35: The above graph shows the time averaged heat flux values as a function of non dimensional distance 'x/B' for the two different temperature distribution cases considered.

From figure (34b), it can be concluded that the melting of the plug, as one moves away from the center of the interface, is considerably lower when compared with figure (34a). The magnitude of this heat flux is close to half the value when compared with figure (27) at time t= 600s (when the melting is driven by conduction). Thus, when the plug is initially cooled from sides due to the temperature distribution near the side walls, it cause significant increase Φ_s which drastically slows down the melting process.

In summary

$$h\Delta T|_{\text{side walls}} \implies \Phi_s \uparrow \implies \Phi_l - \Phi_s \downarrow \implies v_n \downarrow$$

Thus, in order that Φ_s not slower the process of melting, an higher thermal conductivity of the freeze plug material is required than CsCl. This would reduce the difference between the heat flux near the side walls shown in figure (35). One such criteria could be as follows:

$$\lambda_s > \lambda_{\text{eff}} (= \lambda_l + \lambda_T)$$

where λ_T is the turbulent conductivity. In comsol this turbulent conductivity is evaluated as [36]

$$\lambda_T = \frac{\mu_T C_p}{Pr_T}$$

In comsol, when using a RANS model, an effective thermal conductivity variable is available for post processing [36], which is defined as

$$\text{ht.k_eff} = \lambda + \lambda_T$$

using this, λ_{eff}, is evaluated as root mean square value :

$$\lambda_{\text{eff}} = \sqrt{\left(\text{ht.k_effyx}^2 + \text{ht.k_effyy}^2\right)}$$

The lowest value of λ_{eff}, near the interface amounts to $21.41[\text{W/m} \cdot \text{K}]$

$$\lambda_s > \lambda_{\text{eff}}$$

Thus, CsCl could be substituted with Magnesium (based on figure(19) in section(3.2)), who's thermal conductivity is 156 [W/m · K] [31]. This would also provide a solution to criteria (iii) put forth for the material selection. It is possible to have an estimation for heat flux required to melt the plug of 0.2m in 600s using Mg as a material:

$$\Phi = \rho_s \Delta H_{fus} \frac{l}{t} = 6 \cdot 10^8 \cdot \frac{0.2}{600} = 2 \cdot 10^5$$

However, a major drawback is that since the T_m is slightly higher than CsCl, Φ_l would decrease and thus cause slower melting. Hence, from the current simulation results, this would still not meet the requirements of melting.

6 CONCLUSION AND RECOMMENDATION

This thesis work began with the introduction of the safety scenarios. These safety scenarios provide with an input data of velocity, temperature and response time values in order to design the system.

The main research question put forth in this thesis was:

Is the concept of freeze plug melting based on decay heat, feasible?

Here, the feasibility was governed by the function freeze plug is expected to perform, i.e melt fast enough (t < 600s) in an emergency situation. The melting time [1] is governed by the energy content of the freeze plug material [J/m^3] ($\rho_s \cdot \Delta H_{fus}$), the heat flux input from the liquid layer Φ_l and the length of the plug (l).

The method adopted to model the melting process is by using a deformed geometry method in COMSOL. In chapter 2, the implementation was verified with an analytical solution. In the analytical problem, the melting of the plug is governed purely by conduction. Two major conclusions drawn from this chapter were: 1) the melting of the freeze plug is affected by very local temperature differences near the interface and 2) The melting due to conduction progresses slower due to decrease Φ_l. Thus, in order to drive faster melting, it is important to maintain a constant Φ_l at the interface. This is pursued by melting the plug with the help of driven cavity flow by placing the plug eccentric to the reactor core.

The features of the driven cavity flow is governed by bulk Richardson Ri$_b$ [2] (refer to equation (19)). A high Ri value indicates thermal stratification i.e. the penetration of flow field inside cavity is reduced. Thus, a compromise is needed between a high heat flux, indicated by $(T_\infty - T_m)$ (temperature difference the reactor core and the melting temperature of the material), and a lower Ri value (i.e a large forced convection). In the equations of Ri number and the melting (7 & 19), parameters T_m, ρ_s and ΔH_{fus} can be controlled by the selection of material. An initial iteration is performed by choosing CsCl since it provides: 1) a lower value of Ri (0.08 at Re $= 6 \cdot 10^6$) and 2) a sufficiently large $(T_\infty - T_m)$ value and a low value of $\rho_s \cdot \Delta H_{fus}$. (refer to section (3.2))

The fluid flow in the lid driven cavity is in turbulent regime with Re $\approx 6 \cdot 10^6$. The turbulence model thus selected is Algebraic yPlus due to its simplicity in implementation (refer to section (4.2)). This model shows a very good correlation with more complex turbulence models such as SA and SST for isothermal lid driven cavity flows (refer to section (5.1.1)).

Based on the results of melting due to driven cavity flow (refer to section (5.2)), some of the major short-comings of the proposed design are as follows:

- An increase in heat flux in the freeze plug (Φ_s) during the melting process increases the time taken to melt due to low thermal conductivity of the freeze plug material. This can be improved by choosing Mg as material(see figure(19) in the section 3.2). This would also provide a solution to criteria (iii) put forth for the material selection.

[1] $\rho_s v_n \Delta H_{fus} = \Phi_l \cdot \hat{n} - \Phi_s \cdot \hat{n}$

[2] $\mathrm{Ri}_b = \frac{gD^3}{B^2 U_{lid}^2} \beta (T_\infty - T_m)$

However, for Mg, the energy content ($\rho_s \cdot \Delta H_{fus}$) would increase and since the T_m is slightly higher than CsCl, Φ_l would decrease and thus cause slower melting. Hence, from the current simulation results, this would still not meet the requirements of melting of 600s.

- The effect of temperature rise in reactor core causes further slowdown in melting of the freeze plug due to thermal stratification ($T_\infty \uparrow$).
- Another drawback of process is that the corners of the freeze plug melt slowly. The fundamental feature of cavity flow is that near the corners, vortices are formed. The velocity of the fluid in this region is much lower when compared to the primary recirculation. Hence, this decreases the input heat flux Φ_l required to melt the plug in the corners, drastically.
- The heat flux value predicted by the model, is not sufficient to melt the freeze plug. It is possible to have an estimation for heat flux required to melt the plug of 0.2m in 600s using Mg as a material:

$$\Phi = \rho_s \Delta H_{fus} \frac{l}{t} = 6 \cdot 10^8 \cdot \frac{0.2}{600} = 2 \cdot 10^5$$

The maximum time averaged heat flux predicted for the model for case 2 (in the section (5.2.4)) is $2.5 \cdot 10^4$. This is an order of magnitude lower.

Clearly, melting of the freeze plug using CsCl was not achieved within 10 minutes. The feasibility of the design, within the response time, is driven by two factors 1) The order of magnitude of the heat flux required from the reactor side should be greater than $2 \cdot 10^5$ [W/m^2] through out the melting process and 2) the ability to melt the corners should be improved. These requirements could be too stringent for building a robust system as a safety component.

6.1 RECOMMENDATION

In recommendation, the author would to propose a different concept. In the current MSFR, there are two functions that the current freeze plug (or any other similar design) should satisfy:

i It should stop the flow of the fuel-salt mixture to the drain tank during the normal operating conditions

ii It has to passively respond to changes which occur in the reactor core (for situations such as failure of components or power outage) such that the fuel-salt mixture can be drained.

Thus the framework of designing a flow control valve could be modified to: A system which responds to changes in the intensive thermodynamic variable (for example T, p, ρ etc) in the reactor core. This system could be a mechanical valve which operates without any external excitation (i.e system would have passive response).

Based on author's experience and understanding, a flow control valve which is used in automotive engine system could be a potential alternative. The thermodynamic variable to which this valve responds is temperature (T). The working principle of this valve is

as follows: converting volume expansion of a material in closed enclosure into a pressure force in order to move enclosure and open the valve. Such a system is shown in figure(36b). This flow control valve is in open position. A material with high expansion coefficient is filled inside a metal cylinder as shown in the figure. This metal chamber also has a push rod inside which used as guide for displacement. The initial position of valve (due to the initial internal pressure) is maintained by the spring force. Due to increase in the external temperature, i.e. when there is a fluid flow of higher temperature than T_∞ near the interface as shown in figure(36a), a volume change of material should occur inside the cylinder. This would increase the pressure inside the metal cylinder. Thus, the metal cylinder slides along the housing and the push rod compressing the spring. This leads to opening of the valve and the fluid can flow towards the drain tank. Once the material cools down, due to the restoring force of the spring, the valve returns to the close position [49].

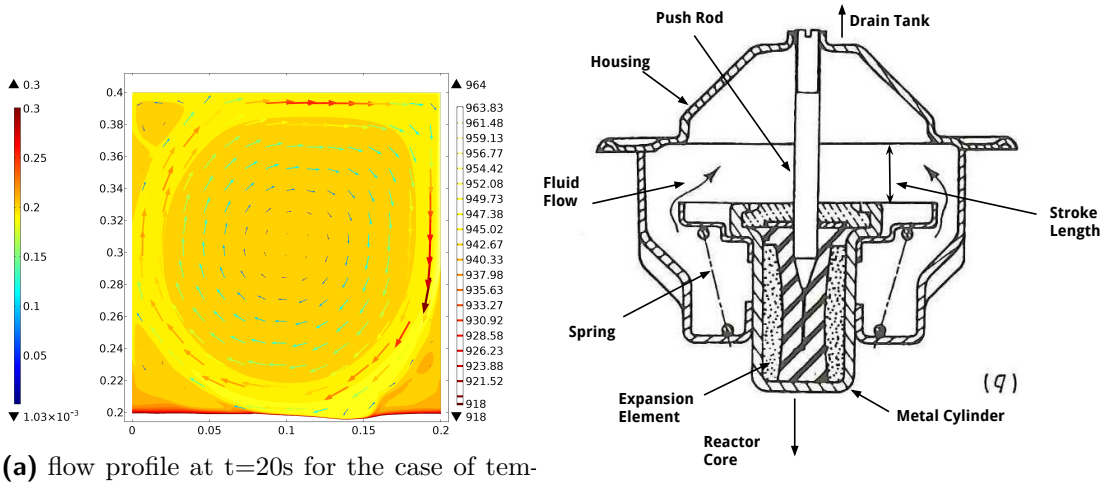

(a) flow profile at t=20s for the case of temperature increase

(b) Valve Position: Open

Figure 36: Temperature response based expansion valve. Adopted from [49]

This system takes flow characteristics and the temperature of fluid in the cavity as the input for design (as an example, a flow field from temperature rise case is shown in 36a). The response time of this system is dependent on the rate of temperature rise and the thermal expansion coefficient of the material. This adheres to the fact that the safety system should respond to temperature changes as fast as possible. This response is now governed by the flow over the metal cylinder. Therefore, the design is no longer dependent on the flow near the corners of the cavity. Moreover the required expansion of the material can be achieved over lesser temperature range and the process is less energy intensive than melting.

A APPENDIX:

A.1 MATERIAL PROPERTIES

Table 3: Properties of Material within temperature range of 600-700 °C

Material	T_m[K]	(Δh_{fus}) [J/kg]	(ρ) kg/m^3	E $\cdot 10^8$[J/m^3]
LiCL	883	470500	1494,68	7,03
CsCl	918	121000	3988	4,825
CsBr	911	111000	2986	3,314
CsI	905	96000	4510	4,329
[b]MgI	906	93000	4430	4,119
[b]$Sr(NO_3)_2$	918	231000	2986	6,89
NaF – NaBr 27-73	915	360000	4440	15,98
LiF NaF 60-40	925	816000	2500	20,4
[a]KF(55)-(45)KCl	878	407000	2198,295	8,94
[b](24) LiF (76)NaCl	953	476900	2213,972	10,55
LiF(32.5)-NaF(38.3)-CaF2(26.5)	888	636000	2660,022	16,92
LiF(52)- NaF(35)-CaF2(13)	888	640000	2630	16,83
Li(46)–NaF(44)–MgF2 (10)	905	858000	2610	22,39
NaCl(38.5)–23NaBr–38.5Na2MoO4	885	168000	3238,262	5,44
KBr(65)–35K2MoO4	898	90500	2584,559	2,34
Li2SO4(82)–11.44CaSO4–6.56CaMoO4	953	207000	2504,32	5,2
LiF(33.4)–49.9NaF2–17.1MgF2	923	860000	2820	24,3
LiF(46)–44NaF–10MgF2	905	858000	2240	19,22
Al	933	400000	2730	10,92
Mg	922	368000	1590	5,85
aMn(92,3)-Al (7.7)	929	235154,827	7210	16,95
NiAl3	915	279605,802	5099,636382	14,26

A.2 WALL FUNCTIONS

The turbulence models, $k-\omega$ and $k-\epsilon$, instead of resolving the flow near the wall, use analytical expression derived from fully developed flow over flat plate and then use this to model for the variables k, ω ϵ and ν_T. There are two main reasons for using wall functions: Firstly, in a wall bounded flows, a large number of grid points are required to evaluate to resolve the flow near the wall [19]. Secondly, turbulence models are invalid near the wall region where Reynolds number are low and only stress exerted on the wall is by viscous effects.[28, 11]. It is because at the walls, fluid velocity is zero, which implies both mean and fluctuations are set to zero.

$$\tau_{ij} = -\rho\overline{u'v'} = 0 \quad \because \bar{u} = 0, \quad u' = 0 \quad \bar{v} = 0, \quad v' = 0$$

A.2.1 Law of the Wall

The hypothesis of the law of the wall put forth is that, under many different flow conditions, the form of solution between the wall and the logarithmic layer can used be by appropriate scaling of the variables. Fig(37) shows the horizontal velocity distribution as a f(y) for a fully developed turbulent region of a fluid flow parallel to the wall. The regions are divided into three distinct layers: viscous layer, buffer layer and log-law layer. Let δ^+ be the non-dimensional perpendicular distance from the wall. For this flow, the balance of shear stress at the wall as :

$$(\mu + \mu_T)\frac{dU}{dy} = \tau_w = \mu\frac{\partial u}{\partial y} = \rho u_\tau^2 \tag{39}$$

where u_τ is the friction velocity. It is used to scale the velocity of fluid. This equation states that the sum of viscous and the turbulent shear stress is equal to the wall shear stress. The convective term in the momentum equation is considered to be negligible. Other non-dimensional parameters for further description are :

$$u^+ = \frac{u}{u_\tau} \quad y^+ = \frac{yu_\tau}{\nu} \quad \nu_T^+ = \frac{\nu_T}{\nu} \tag{40}$$

here, the subscript T denotes turbulence. Since u_τ is interpreted as velocity, y^+ can be interpreted as local Reynolds number, such that y is the vertical distance from the wall.

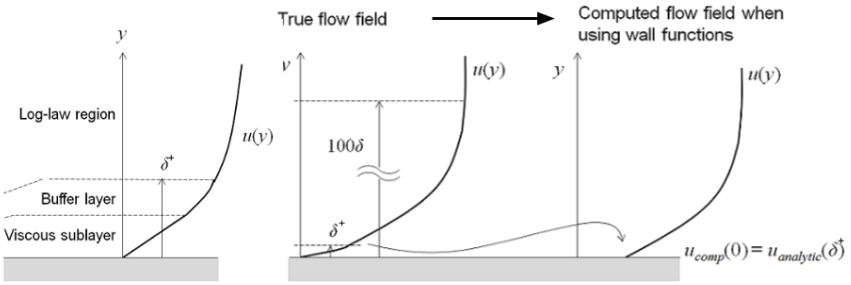

Figure 37: Wall function approximation of turbulence models using analytical expression developed for turbulence over flat plate. Adopted from [6]

Viscous Sublayer: In this layer, since the flow is dominated by very low Reynolds number $\nu_T^+ << 1$, and then eq.(39) reduces to

$$U \propto y$$

Thus, in this layer velocity is proportional to the normal distance from the wall. This can be observed in the figure (37) by a linear curve. The range of y^+ for the viscous layer is found to be $0 < y^+ < 5$.

Buffer layer: This is the layer which connects the viscous sub-layer to the log layer, were the flow is partially turbulent. The range of y^+ for the buffer layer is $5 < y^+ < 30$

Log-Law Layer: This layer corresponds to the region where the viscous stress is negligible when compared to Reynolds stress $\nu_T^+ >> 1$. Thus eq.(39) can be reduced as:

$$U \approx \frac{u_\tau}{\kappa} ln|y| + B$$

where κ is the von Karman constant and B is also a constant. This is known as the "law of wall". The range of y^+ for the logarithmic layer is $30 < y^+ < 300$

Thus, when COMSOL uses wall functions, the first computational domain is placed in the logarithmic layer at a distance δ_w. The viscous sub-layer is ignored and the solution is merged is shown in the the figure(37). Here, $\delta_w \equiv y$, is evaluated using set of equations given below:

$$y^+ = \frac{u_\tau y}{\nu} \tag{41}$$

$$u_\tau = \frac{|u|}{\frac{1}{\kappa} ln|y^+| + B} \tag{42}$$

It solves the above two equation iteratively until $u_\tau = 11.06 or y^+ < 20$ [29] which indicates the outer region of the viscous sublayer. The conditions for k and ϵ are:

$$\nabla.k = 0 \qquad \epsilon = \frac{u_\tau^3}{\kappa y}$$

And equation (39) is modelled as same.

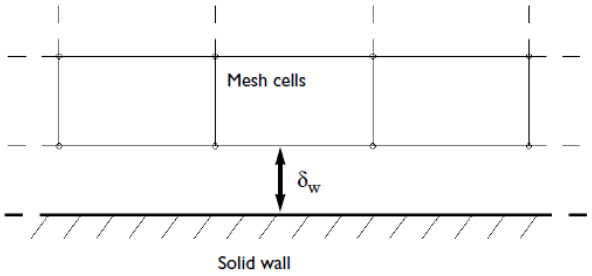

Figure 38: Computational domain joining wall and the logarithmic layer at distance δ_w

Now, in order to understand the influence of turbulence models on calculating the heat flux near the wall, it is important to understand thermal wall functions.

A.2.2 Thermal Wall Functions:

Since wall functions for the fluid flow are already understood, thermal wall function are easy to interpret. Heat transport in the thermal sub-layer is governed by conduction, while log-law holds true for the region where turbulent effects dominate [2, 30]. Thus similar to momentum transport postulate, in the law of thermal wall it is postulated that the heat flux at the wall can be evaluated as sum of diffusive heat flux and turbulent heat flux :

$$q_w = \frac{d}{dy}\left[\left(\frac{\mu}{Pr} + \frac{\mu_T}{Pr_T}\right)\frac{d\overline{T}}{dy}\right] \tag{43}$$

where Pr_T is the turbulent Prandtl number which is defined as :

$$Pr_T = \frac{\nu_T}{\alpha_T} = \frac{\overline{-u'v'}/(\frac{\partial \overline{u}}{\partial y})}{\overline{-t'v'}/(\frac{\partial \overline{T}}{\partial y})}$$

Thus, if $Pr_T \equiv 1$, then both the governing mechanism of turbulent momentum transport and turbulent heat transport would be similar. Introducing normalized variables :

$$y^+ = \frac{y u_\tau}{\nu}$$

$$T^+ = \rho C_p u_\tau \frac{T_w - \overline{T}}{q_w}$$

the following can obtained:

$$T^+ = \int_0^{y^+} \frac{dy^+}{(1/Pr) + \nu_T Pr_T/\nu}$$

Similarly, extremely close to the wall in the viscous layer, heat transfer can be purely conductive while far away turbulent effects dominate. Thus the law of thermal wall resembles:

$$T^+ \equiv Pr \cdot y^+$$

$$T^+ \equiv \frac{1}{\kappa_t} \cdot ln|y^+| + B_t$$

There is a small finite difference between the actual wall and computational domain, and this is ignored in computation. For thermal simulation in COMSOL, this is modeled as a thin isolation layer at the wall. If a prescribed wall temperature T_w is defined then the effective heat flux across the wall, with a fluid temperature T_f is defined as :

$$q_w = \rho C_p C_\mu^{\frac{1}{4}} k_w^{\frac{1}{4}} \frac{T_w - T_f}{T^+} \tag{44}$$

here, T^+ is given by :

$$T^+ = \begin{cases} Pr \cdot y^+ & y^+ < y_1^+ \\ 15 \cdot Pr^{2/3} - \frac{500}{(y^+)^2} & y_1^+ \leq y^+ \leq y_2^+ \\ \frac{Pr_T}{\kappa} \cdot ln|y^+| + B_t & y^+ \geq y_2^+ \end{cases} \tag{45}$$

$$y_1^+ = \frac{10}{Pr^{10/3}}$$

$$y_2^+ = 10\sqrt{10 \cdot \frac{\kappa}{Pr_T}}$$

$$B_t = 15 \cdot Pr^{2/3} - \frac{Pr_T}{2\kappa}\left(1 + ln(1000 \cdot \frac{\kappa}{Pr_T})\right)$$

The turbulent heat flux, in comsol, is modelled as :

$$\Phi_{T_c} = \frac{\mu_T C_p}{Pr_T} \frac{\partial \overline{T}}{\partial x_j}$$

For a high Prandtl number, the thermal sub-layer is much closer to the wall than the momentum sub-layer thickness. This implies that the thickness of the conduction layer just above the interface, is lower as the Prandtl number of the fluid increases. The Pr of $LiF-ThF_4$ is 16.975, which is $\gg 1$. This implies that the application of this wall function becomes debatable. Comsol only modifies the constants B_t and κ_t and formulation of Pr_T provided in Kays Crawford relation [52] to take into account the high Pr number of fluids.

A.3 IMPLEMENTATION IN COMSOL

This section explains which method was choosen to model the melting problem. Then it will be followed by how this method is implemented in comsol. Finally, this will be concluded by setting the parameters for method and solver in comsol.

A.3.1 Selection of Method

The different possibilities of implementing phase change phenomena in COMSOL is as follows:

i By using "Heat transfer with Phase Change" in the Heat transfer module.

ii By using Deformed Geometry/Moving Mesh option from the mathematical module of COMSOL

iii By using Moving Interface (i.e Level Set Method or Phase Field Method) option from the mathematical module of COMSOL

iv By using PDE Interface from the Mathematical module of COMSOL

In the default phase change model, COMSOL utilizes "Apparent heat capacity" formulation. In this method, the latent heat is included as an additional term in the heat capacity. The fundamental equations for this method is as follows :

$$\frac{\partial(\rho C_p T)}{\partial t} + u.\nabla(\rho C_p T) = \nabla.\lambda\nabla T + S$$

$$H = \theta \int_{T_ref}^{T} \rho_s C_{ps} dT + (1-\theta) \int_{T_ref}^{T} \rho_l C_{p_l} dT + \rho_l C_{p_l} \Delta H_{fus}$$

$$C_p = \frac{\partial H}{\partial T}$$

A transition temperature interval ΔT can be defined between phase 1 and phase 2. During the phase change transition, the material phase is modeled by function,θ, which represents the fraction of phase before transition. This θ is an Heaviside function such that :

$$\theta = \begin{cases} 1 & \left[T_{pc} - \frac{\Delta T}{2}\right] \leqslant 0 \\ 0 & \left[T_{pc} - \frac{\Delta T}{2}\right] \geqslant 0 \end{cases}$$

where T_{pc} represents that temperature of phase change. Thus, in this method,the transition of a "phase" is treated like a concentration: it varies between 0 and 1, and the material properties, between the phase transition, are varying as $f(\theta)$, for example, density is modelled as :

$$\rho = \theta(T)\rho_s + (1-\theta(T))\rho_l$$

This methods was primarily developed for modelling casting and solidification processes. It is inherently takes into account phase change over a finite temperature difference, hence robust in modelling eutectic materials than pure components [51]. As $\Delta T \to 0$, the changes in material properties are very large, which can observed from table (1) over relatively small mesh elements. This would require extremely fine mesh. It is also recommended by COMSOL to use moving mesh methods when there is a fluid flow in the liquid phase either due density variation or external excitation. Based on these arguments, modelling melting by change in geometry was chosen.

In options (ii),(iii) and (iv), it is possible to manually control the process of the phase change by implementing the equation(7). An extensive detail of mathematical formulation utilized in the moving interface form can be found in [17, 37]. In this formulation, it would be difficult to manipulate its mathematical variables in order to incorporate turbulent

heat flux in Φ_l as per equation(7). The most convenient way to implement this is using option(ii).

In COMSOL, there are two methods to model this [1] : 1) Deformed Geometry (DG) 2) Moving Mesh (M.M). In the M.M interface, when the material undergoes a change in shape/deformation, the total mass of the material is redistributed(in the solid domain). On the other hand, the D.G interface interprets the deformation as addition or removal of material.In order to model phase change correctly, the volume of solid that is melted should be removed from freeze plug. Hence, in this application, deformed geometry will be used.

A.3.2 ALE Method

Now, a brief overview is provided to understand how D.G method works. In comsol, the solutions of all the physical quantities is stored at a fixed set of mesh nodes (i.e mesh frame of reference). This also implies that the time derivative of a variable is computed with respect to the mesh nodes. Since this frame of reference is changing with time, it is difficult to track all the material properties with respect to moving frame (Lagrangian method). Thus, the material properties are defined with respect to a fixed frame of reference (Eulerian method). Thus, a mapping function is required for referencing the mesh frame with the fixed frame. The process is two ways, the governing equation(7) defines the mesh displacement, and then this displacement is remapped to fixed coordinate system [37, 42, 24]. A brief summary of the implementation of this method is as follows:

- In Comsol, mesh deformation is captured by arbitrary Lagrangian – Euler method (ALE). The basic principle of ALE method is to superimpose a moving frame of reference on a fixed frame of reference. It tracks the material properties and movement of mesh separately.

- The position of the moving frame of reference, at the previous time step, with the respect to the fixed frame of reference is known. After the frame is advanced through certain physical equation, it is remapped with respect to fixed frame reference. The transformation between the coordinates takes place via matrix inversion.

  $$x = f(g(h^{-1}(X_m, p)), t)$$

  where f, g and h are functions. g is the function which relates material coordinates and geometry coordinates. h is the function which relates mesh coordinates with geometry coordinates and f is the function which relates fixed frame of reference and material coordinates. Here, f is determined the by smoothing option selected to model the deformed. This is explained below. g is determined by the physical boundary condition imposed. Further, this inherently places a restriction on the time step and the extent to which deformation can occur. Larger deformation can cause failure in re transformation.

In the above expression $f()$ can be determined from various smoothing methods. These methods govern the distribution and the mapping of the meshes in the geometry. The two methods considered here are Laplace and Winslow. The mathematical expression that these two smoothing method use are as follows:

[1] It is preferable to start with conjugate heat transfer physics for fluid flow and heat transfer to interact with each other. If the material properties of fluid are a $f(T)$, then it is necessary to have "non-isothermal flow" option active in the multi-physics node.

Laplace Smoothing:

$$\frac{\partial^2}{\partial X^2}\left(\frac{\partial x}{\partial t}\right)+\frac{\partial^2}{\partial Y^2}\left(\frac{\partial x}{\partial t}\right)=0$$

Winslow Smoothing:

$$\frac{\partial^2}{\partial x^2}\left(\frac{\partial X}{\partial t}\right)+\frac{\partial^2}{\partial y^2}\left(\frac{\partial X}{\partial t}\right)=0$$

Here, x and y correspond to spatial frame of reference while X and Y correspond to material frame of reference. Thus, both the method solve the Laplace form of equation. According to the [42, 24] Laplace method is more prone to inverted mesh elements but it is computationally inexpensive solve while Winslow methods are computationally more expensive.

A.3.3 Weak Form

For understanding the implementation of weak formulation, consider a steady state conduction equation without heat source:

$$\lambda\frac{\partial^2 T}{\partial x^2}=0$$

The above expression can be re-written as:

$$\lambda\frac{\partial \Phi}{\partial x}=0 \text{ where } \Phi=\frac{\partial T}{\partial x}$$

Instead of solving this differential form, weak form of solution converts it into integral form. The main principle behind weak form is: If the equation is satisfied in the small sub domain and then it could be summed up to satisfied in the entire domain.

$$\sum_{m=1}^{m=n}\left[\int_{x_m-dx}^{x_m+dx}\lambda\frac{\partial \Phi}{\partial x}dx\right]=0$$

This means, the average of heat flux over small domain is zero. This equation could be written for the entire domain in order to retrieve the initial differential equation. However, the contribution of each sub domain is represented by a test functions ($T\tilde{(x)}$):

$$\lambda\int_{x=0}^{x=B}\frac{\partial \Phi(x)}{\partial x}\tilde{T}(x)dx=0$$

The order of the above integral equation in T is 2. The order of the different equation is reduced using chain rule of integral as follows:

$$\lambda\left[\Phi(x)\tilde{T}(x)\big|_{x=0}-\Phi(x)\tilde{T}(x)\big|_{x=B}-\int_{x=0}^{x=B}\Phi(x)\frac{\partial \tilde{T}(x)}{\partial x}dx\right]=0$$

The value of $\Phi(x=0)$ and $\Phi(x=B)$ are obtained from boundary conditions. The boundary condition to this equation can be of the type: Neumann ($\Phi=0$) or Dirichlet ($T=T_m$). Dirichlet boundary condition can also be interpreted as a condition which is imposed on inward and outward Φ such that a desired temperature is maintained. Suppose that at $x=0$, $\Phi=\Phi(0)$ and at $x=B$, $T=T_m$, then the above equation can be rewritten as:

$$\lambda\left[\Phi(0)\tilde{T}_1-\Lambda\tilde{T}_2-\tilde{\Lambda}\left(\tilde{T}_2-T_m\right)-\int_{x=0}^{x=B}\Phi(x)\frac{\partial \tilde{T}(x)}{\partial x}dx\right]=0$$

where, Λ is as unknown flux required to impose the Dirichlet condition and $\tilde{\Lambda}$ is it corresponding test function while $\tilde{T}_1$ & $\tilde{T}_2$ are corresponding test functions at the boundary. The above equation can be re-written as :

$$\lambda \int_{x=0}^{x=B} \Phi(x) \frac{\partial \tilde{T}(x)}{\partial x} dx = \Phi(0)\tilde{T}_1 - \Lambda\tilde{T}_2 - \tilde{\Lambda}\left(\tilde{T}_2 - T_m\right)$$

Now, the let the solution of T(x) in space be represented as :

$$T(x) = a_1\psi_1(x) + a_2\psi_2(x) + ...a_n\psi_n(x)$$

where n is the number of nodal points and a is the coefficient of the of the function $\psi(x)$. $\psi(x)$ is could be linear, quadratic or a higher order polynomial function to represent the shape of the solution of $T(x)$ between the node points. Substituting this expression, it can be obtained:

$$\lambda \left[\int_{x=0}^{x=B} a_1 \frac{\partial \psi_1(x)}{\partial x} \frac{\partial \tilde{T}(x)}{\partial x} dx + a_2 \int_{x=0}^{x=B} \frac{\partial \psi_2(x)}{\partial x} \frac{\partial \tilde{T}(x)}{\partial x} dx + ... \right.$$
$$\left. a_n \int_{x=0}^{x=B} \frac{\partial \psi_n(x)}{\partial x} \frac{\partial \tilde{T}(x)}{\partial x} dx \right] = \Phi(0)\tilde{T}_1 - \Lambda\tilde{T}_2 - \tilde{\Lambda}\left(a_n - T_m\right)$$

There are n+1 unknowns in the above equation which are the coefficients of the shape function and the heat flux Λ at the boundary. Hence, n+1 set of equations are required. Here, $\psi(x)$ is also local function representing the contribution of temperature in the sub domain, which in principle, is equivalent to the idea of test function $\tilde{T}(x)$. Hence, by substituting $\psi_1(x)$ as the first test function, the first equation from required set of equations can be obtained:

$$\lambda \left[\int_{x=0}^{x=B} a_1 \frac{\partial \psi_1(x)}{\partial x} \frac{\partial \psi_1(x)}{\partial x} dx + a_2 \int_{x=0}^{x=B} \frac{\partial \psi_2(x)}{\partial x} \frac{\partial \psi_1(x)}{\partial x} dx + ... \right.$$
$$\left. a_n \int_{x=0}^{x=B} \frac{\partial \psi_n(x)}{\partial x} \frac{\partial \psi_1(x)}{\partial x} dx \right] = \Phi(0)\psi_1(x=0) - \Lambda\psi_1(x=B) - \tilde{\Lambda}\left(a_n - T_m\right)$$

Each of this basis function can only contribute to its neighbouring terms. If, it is assumed that this basis function is linear, then following property can be used :

$$\int_{x=0}^{x=B} \frac{\partial \psi_1(x)}{\partial x} \frac{\partial \psi_1(x)}{\partial x} dx = 1$$

$$\int_{x=0}^{x=B} \frac{\partial \psi_2(x)}{\partial x} \frac{\partial \psi_1(x)}{\partial x} dx = -1$$

and rest of the terms will be zero. So, the first equation would be :

$$\lambda\left[a_1 - a_2\right] = \Phi(0)\psi_1(x=0)$$

Contribution of $\tilde{\Lambda}$ at the boundary x=0 , must be zero. Collecting all such terms by substituting $\psi_2(x), \psi_3(x)...\psi_n(x)$ as test functions, a system of linear equations can be obtained. It can be condensed into a matrix representation of the form :

$$A \cdot B = C$$

where C is the column matrix of the boundary condition, A is an nxn matrix, with coefficients of a_1, a_2 .. a_n and B is the solution one seeks. At the boundary x=B gives the solution of Λ, which is the heat flux at that boundary.

A.3.4 Parameter Study

This section describes selection of certain option available under deformed geometry node and the mesh setting require for simulation of deformed meshes. The commonly occurring warning or error which lead to an end of the simulation was " inverted mesh elements near the coordinates.. " This indicates the breakdown of mesh such that it is wrapped "inside-out" leading to zero area (2D) or zero volume in 3D. This cause a zero determinant for the jacobian matrix which maps local coordinates to global coordinates. According to COMSOL [37], as such, occurrence of inverted mesh element doesn't pose a threat if the solution converges but it was observed that it caused breakdown in iterative solvers. Thus, the parameter mentioned below will adjusted so as to avoid this, and run the simulation in the smallest possible time frame.

Some of the important parameters which can controlled in order to achieve convergence are explained below :

i Geometry shape order (GSO): It defines the order of polynomial used for representing the geometry shape of the meshes. Geometry shape order of 1 implies linear mesh while < 2 indicates high- order curved elements. More curved the mesh elements are, easier it is to get inverted mesh warnings. In all the simulation, thus GSO is set to 1.

ii It is recommend to start with mesh that is uniform is distribution. This could be tricky to achieve in when a parametric study of check the effect of geometric dimensions is performed. The mesh size can be adjusted by changing the maximum element size. Otherwise, according to the manual, quad mesh and mapped meshes tend to perform better than triangular meshes.

iii Use Automatic Remeshing: This is a very powerful tool to implement changes in the mesh during the simulation. If the mesh distortion becomes too large such that the quality of the mesh deteriorates, it is possible to instruct COMSOL make an new mesh in the existing deformed state. This option can be enabled by checking the automatic remeshing box in the study extension. This feature acts like an if condition, with the control parameter of mesh quality. The quality of mesh can be governed by it's maximum distortion (comp1.dg.I1isoMax)$<$ 1.5, because it is of interest to prevent inverted meshes.

In order to avoid the use of automatic remeshing (because it adds a further complexity to the solver), the inverted meshing will avoided by setting the mesh size, solver settings and smoothing method. The smoothing method chosen is winslow. The effect of mesh size is presented in the results section.

A.3.5 Solver Settings

Very minute details of comsol solver are not discussed, but it is important to understand how comsol computes it solutions, to achieve reduction in simulations time and hence faster convergence. Even this is an extremely detailed study, hence only some fundamental understanding will be establish. Stationary solver which is used to obtain a steady state solution is a non linear solver. It uses a version of damped Newton Raphson algorithm to solve coupled physics [37]. Suppose one could write the discretized form of the equations as $f(U) = 0$, where f(U) is the "residual vector" and U is the solution vector. Residual vector is vector which represents the physics to be solved at each node. The system starts with

the initial guess U_0 and forms a linearized model using U0 as the linearization point. The linearized model is represented as:

$$f'(U_0)\delta U = -f(U_0)$$

where $f'(U_0)$ is the Jacobian matrix. It solves the discretized form of this model for the Newton step δU using the selected linear system solver. It then computes the new iteration

$$U_1 = U_0 + \lambda\delta U$$

where $\lambda(0 \leqslant \lambda \geqslant 1)$ is the damping factor. Next the modified Newton correction estimates the error ϵ for the new iteration U_1 by solving:

$$f'(U_0)\epsilon = -f(U_1).$$

If the relative error corresponding to ϵ is larger than the relative error in the previous iteration, the algorithm reduces the damping factor λ and recomputes U_1. Thus the algorithm iterates until the relative error is less than in the previous iteration or until the minimum damping factor is achieved. Thus we can sense that the solver can fail if the initial conditions are poor or it will take much more number of iterations to converge the solution. This is available in the log data.

By trial and error, the range of damping factor could be between 0.7 to 1 for solving the physics used in this thesis. In most of the simulation, it was set to 1. Further in the solver settings, the criteria to stop the iterations are based on tolerances. The tolerance factor is set to 1e-1. Tolerance factor indicates the factor by which the relative tolerance is multiplied. Solving for higher tolerance could reduce fluctuations in the solutions, especially for time dependent study, but it also decreases the time steps and thus slower to converge. Further "update on every iteration" option is chosen for jacobian

BIBLIOGRAPHY

[1] A Abhat. "Low temperature latent heat thermal energy storage: heat storage materials". In: *Solar energy* 30.4 (1983), pp. 313–332.

[2] Jonas Bredberg. "On the wall boundary condition for turbulence models". In: *Chalmers University of Technology, Department of Thermo and Fluid Dynamics. Internal Report 00/4. G oteborg* (2000).

[3] Stanley Cantor et al. "Physical properties of molten-salt reactor fuel, coolant, and flush salts". In: *ORNL-TM-2316 (August 1968)* (1968), p. 14.

[4] Elisa Capelli. *Thermodynamic characterization of salt components for Molten Salt Reactor fuel*. Delft University of Technology, 2016.

[5] N Cohen et al. "Sheared stably stratified turbulence and large-scale waves in a lid driven cavity". In: *Physics of Fluids (1994-present)* 26.10 (2014), p. 105106.

[6] *COMSOL Blog*. 2013. URL: https://www.COMSOL.com/blogs/which-turbulence-model-should-choose-cfd-application/.

[7] *COMSOL Blog*. 2013. URL: https://www.COMSOL.nl/blogs/understanding-stabilization-methods/.

[8] Badawy M Elsheikh. "Safety assessment of molten salt reactors in comparison with light water reactors". In: *Journal of Radiation Research and Applied Sciences* 6.2 (2013), pp. 63–70.

[9] Ercan Erturk. "Discussions on driven cavity flow". In: *International Journal for Numerical Methods in Fluids* 60.3 (2009), pp. 275–294.

[10] Ercan Erturk, Thomas C Corke, and Cihan Gökçöl. "Numerical solutions of 2-D steady incompressible driven cavity flow at high Reynolds numbers". In: *International Journal for Numerical Methods in Fluids* 48.7 (2005), pp. 747–774.

[11] Prof. Glenn Flierl and Prof. Raffaele Ferrari. *Chapter 16 : Boundary Layer Turbulence*. MIT Open CourseWare, 2007.

[12] LLW Frima et al. "Burnup in a Molten Salt Fast Reactor". In: *Delft University of Technology* (2013).

[13] KJ Hsieh and FS Lien. "Numerical modeling of buoyancy-driven turbulent flows in enclosures". In: *International Journal of Heat and Fluid Flow* 25.4 (2004), pp. 659–670.

[14] Reima Iwatsu, Jae Min Hyun, and Kunio Kuwahara. "Mixed convection in a driven cavity with a stable vertical temperature gradient". In: *International Journal of Heat and Mass Transfer* 36.6 (1993), pp. 1601–1608.

[15] LPBM Janssen and MMCG Warmoeskerken. *Transport phenomena data companion*. VSSD Delft, The Netherlands, 2006.

[16] George J Janz. *Molten salts handbook*. Elsevier, 2013.

[17] E Javierre et al. “A comparison of numerical models for one-dimensional Stefan problems”. In: *Journal of Computational and Applied Mathematics* 192.2 (2006), pp. 445–459.

[18] Serp Jérôme et al. “The molten salt reactor (MSR) in generation IV: Overview and perspectives”. In: *Progress in Nuclear Energy* 77 (2014), pp. 308–319.

[19] Georgi Kalitzin et al. “Near-wall behavior of RANS turbulence models and implications for wall functions”. In: *Journal of Computational Physics* 204.1 (2005), pp. 265–291.

[20] Jos van Kan, A Segal, and Fred Vermolen. *Numerical methods in scientific computing*. VSSD, 2005.

[21] Murat M Kenisarin. “High-temperature phase change materials for thermal energy storage”. In: *Renewable and Sustainable Energy Reviews* 14.3 (2010), pp. 955–970.

[22] Sasa Kenjeres. *Numerical modelling of complex buoyancy-driven flows*. TU Delft, Delft University of Technology, 1999.

[23] K.huffman. “Fukushima Daiichi Accident- Technical Causal Factor Analysis”. In: (2012).

[24] EM Knobbe. “A FEM-ALE approach for continuous domains with arbitrary moving boundaries”. In: *European congress on computational methods in applied sciences and engineering ECCOMAS*. 2004.

[25] JR Koseff and RL Street. “Circulation structure in a stratified cavity flow”. In: *Journal of Hydraulic Engineering* 111.2 (1985), pp. 334–354.

[26] JR Koseff and RL Street. “On end wall effects in a lid-driven cavity flow”. In: *Journal of fluids engineering* 106.4 (1984), pp. 385–389.

[27] JR Koseff and RL Street. “Visualization studies of a shear driven three-dimensional recirculating flow”. In: *Journal of Fluids Engineering* 106.1 (1984), pp. 21–27.

[28] Dmitri Kuzmin, Otto Mierka, and Stefan Turek. “On the implementation of the κ-ε turbulence model in incompressible flow solvers based on a finite element discretisation”. In: *International Journal of Computing Science and Mathematics* 1.2-4 (2007), pp. 193–206.

[29] Dmitri Kuzmin and Stefan Turek. “Multidimensional FEM-TVD paradigm for convectiondominated flows”. In: *University of Dortmund*. Citeseer. 2004.

[30] David Lacasse, Eric Turgeon, and Dominique Pelletier. “On the judicious use of the k–ε model, wall functions and adaptivity”. In: *International Journal of Thermal Sciences* 43.10 (2004), pp. 925–938.

[31] Sanghyun Lee et al. “Thermal conductivity of magnesium alloys in the temperature range from- 125 C to 400 C”. In: *International Journal of Thermophysics* 34.12 (2013), pp. 2343–2350.

[32] Xiaobo Li et al. “Metallic Composites Phase-Change Materials for High-Temperature Thermal Energy Storage”. In: *ASME 2013 7th International Conference on Energy Sustainability collocated with the ASME 2013 Heat Transfer Summer Conference and the ASME 2013 11th International Conference on Fuel Cell Science, Engineering and Technology*. American Society of Mechanical Engineers. 2013, V001T11A014–V001T11A014.

[33] Erik van der Linden. “Coupled neutronics and computational fluid dynamics for the molten salt fast reactor”. In: *Delft University of Technology* (2012).

[34] Chien Liu. *Introduction to the Weak Form*. 2014. URL: https://www.COMSOL.nl/blogs/brief-introduction-weak-form/.

[35] Chiara Margheritis, Giorgio Flor, and Cesare Sinistri. "Miscibility gaps in fused salts". In: *Zeitschrift für Naturforschung A* 28.8 (1973), pp. 1329–1334.

[36] COMSOL Multiphysics. "COMSOL Multiphysics CFD Module User guide, Version: COMSOL 5.2". In: (2015).

[37] COMSOL Multiphysics. "COMSOL Multiphysics Reference Manual, Version: COMSOL 5.2". In: (2015).

[38] TG Myers et al. "A cubic heat balance integral method for one-dimensional melting of a finite thickness layer". In: *International Journal of Heat and Mass Transfer* 50.25 (2007), pp. 5305–5317.

[39] Hakop J Nagapetyan. "Application of Wray-Agarwal Model to Turbulent Flow in a 2D Lid-Driven Cavity and a 3D Lid-Driven Box". In: (2015).

[40] M Necati Ozisik. *Heat conduction*. John Wiley & Sons, 1993.

[41] Shia-Hui Peng and Lars Davidson. "Computation of turbulent buoyant flows in enclosures with low-Reynolds-number k-ω models". In: *International Journal of heat and fluid flow* 20.2 (1999), pp. 172–184.

[42] Antti Pohjoranta and Robert Tenno. "Implementing surfactant mass balance in 2D FEM–ALE models". In: *Engineering with Computers* 27.2 (2011), pp. 165–175.

[43] MM Rahman, T Siikonen, and RK Agarwal. "Improved low-Reynolds-number one-equation turbulence model". In: *AIAA journal* 49.4 (2011), pp. 735–747.

[44] M Richardson. "DEVELOPMENT OF FREEZE VALVE FOR USE IN THE MSRE". In: (1962).

[45] RC Robertson. *MSRE DESIGN AND OPERATIONS REPORT. PART I. DESCRIPTION OF REACTOR DESIGN*. Tech. rep. Oak Ridge National Lab., Tenn., 1965.

[46] Prof. Donald Sadoway. *Introduction to Solid State Chemistry, Lecture No: 10 Phase Equilibria and Phase Diagrams*. MIT Open CourseWare, 1993.

[47] DB Sirdeshmukh and K Srinivas. "Physical properties of mixed crystals of alkali halides". In: *Journal of materials science* 21.12 (1986), pp. 4117–4130.

[48] Philipe R Spalart and Stephen R Allmaras. "A one equation turbulence model for aerodinamic flows." In: *AIAA journal* 94 (1992).

[49] John Turner. *Automotive sensors*. Momentum Press, 2009.

[50] JPM Van Der Meer. "Thermochemical investigation of molten fluoride salts for Generation IV nuclear applications-an equilibrium exercise". In: *Geologica Ultraiectina* 262 (2006).

[51] VR Voller, CR Swaminathan, and Brian G Thomas. "Fixed grid techniques for phase change problems: a review". In: *International Journal for Numerical Methods in Engineering* 30.4 (1990), pp. 875–898.

[52] B Weigand, JR Ferguson, and ME Crawford. "An extended Kays and Crawford turbulent Prandtl number model". In: *International journal of heat and mass transfer* 40.17 (1997), pp. 4191–4196.

[53] Jerry Westerweel, Bendiks J Boersma, and Frans TM Nieuwstadt. *Turbulence: Introduction to Theory and Applications of Turbulent Flows*. Springer, 2016.

[54] David C Wilcox. *Turbulence modeling for CFD*. Vol. 2. DCW industries La Canada, CA, 1998.

[55] *World Nuclear Association*. URL: http://www.world-nuclear.org/info/safety-and-security/safety-of-plants/fukushima-accident/.

[56] Ritsuo Yoshioka, Yoichiro Shimazu, and Koshi Mitachi. "Guidelines for MSR accident analysis". In: *Thorium Energy Conference*. 2012, pp. 1–42.